



VCU

Virginia Commonwealth University
VCU Scholars Compass

Theses and Dissertations


Graduate School

2020

Phenotype Extraction: Estimation and Biometrical Genetic Analysis of Individual Dynamics

Kevin L. McKee
Virginia Commonwealth University

Follow this and additional works at: <https://scholarscompass.vcu.edu/etd>

 Part of the [Applied Statistics Commons](#), [Longitudinal Data Analysis and Time Series Commons](#), [Quantitative Psychology Commons](#), and the [Statistical Models Commons](#)

© Kevin L. McKee, February 2020

Downloaded from

<https://scholarscompass.vcu.edu/etd/6166>

This Dissertation is brought to you for free and open access by the Graduate School at VCU Scholars Compass. It has been accepted for inclusion in Theses and Dissertations by an authorized administrator of VCU Scholars Compass. For more information, please contact libcompass@vcu.edu.

©Kevin L. McKee, February 2020

All Rights Reserved.

PHENOTYPE EXTRACTION: ESTIMATION AND BIOMETRICAL GENETIC
ANALYSIS OF INDIVIDUAL DYNAMICS

A Dissertation submitted in partial fulfillment of the requirements for the degree of
Doctor of Philosophy at Virginia Commonwealth University.

by

KEVIN L. MCKEE

August 2015 to May 2020

Director: Michael C. Neale,
Professor, Department of Psychiatry

Virginia Commonwealth University
Richmond, Virginia
February, 2020

Acknowledgements

My training and research would not have been possible without funding from the National Institute of Health (NIH) and the National Institute on Drug Abuse (NIDA). Special thanks goes to Drs. Michael Neale and Kenneth Kendler for procuring the necessary funds and granting me the protected time and autonomy for my professional development.

Dr. Neale has generously spent his time and resources on our innumerable meetings, in which all of the work of this dissertation was in some way collaboratively conceived and refined. Thanks to Drs. Michael Mason and Kelly Klump for including me on their projects and sharing their meticulously collected data, which have enabled us to test so many new ideas. Thanks to Dr. Steven Boker for introducing me and the behavioral genetics community to many fruitful ideas about dynamical systems that I have tried to develop further. Thanks to Drs. Michael Hunter, Robert Kirkpatrick, Joshua Pritikin, and Steven Aggen for teaching me a great deal of what I know about statistics and psychometrics. Thanks to Drs. Marvin Alexander Meredith and Ruth Clemo, who have been mentors to me since 2012, giving many incredible opportunities and insights that have helped clarify my scientific interests.

Thanks to Linnea for giving the unwavering love, companionship, and clarity of perspective that I have needed throughout this work. Thanks to Ryan for being my first mentor for so many creative pursuits throughout life, and to Mom and Dad for providing so much in support, opportunity, and patience, and everything else.

TABLE OF CONTENTS

Chapter	Page
Acknowledgements	i
Table of Contents	ii
List of Tables	iv
List of Figures	vii
Abstract	x
1 Introduction	1
1.1 Intrinsic Dynamics	3
1.2 Control Theory	6
1.3 Aims	10
2 Time Series Methods	12
2.1 General concepts	12
2.2 Time domain	13
2.2.1 Discrete Time, Discrete Space	14
2.2.2 Discrete Time, Continuous Space	15
2.2.3 Continuous Time, Discrete Space	17
2.2.4 Continuous Time, Continuous Space	19
2.2.5 Structural Equation Models of Change	21
2.2.6 State-Space Modeling	22
2.3 Frequency domain	24
3 Study I: Well-Behaved Physiological Sensor Data, Complex Nonlinear Model	27
3.1 Introduction	27
3.1.1 Model	31
3.1.2 Estimation	35
3.1.2.1 Optimal filtering	36
3.1.2.2 Estimation of feedback delay	37
3.1.2.3 Constrained interpolation of dynamic switching points	38
3.1.2.4 Optimization	41

3.1.2.5	Software	42
3.2	Simulations	43
3.2.1	Parameter sets	44
3.2.2	Sim 1: Noiseless series	44
3.2.3	Sim 2 Estimation from noisy data	47
3.3	Data Analysis	51
3.4	Discussion	57
3.4.1	Simulation	57
3.4.2	Experimental Data	61
3.4.3	Conclusions	67
4	Study II: Poorly-Behaved Psychometric Data, Simple Linear Model	68
4.1	Introduction	68
4.2	Methods	72
4.3	Results	79
4.4	Discussion	82
4.4.1	Conclusions	86
4.5	Appendix: Power Analysis	87
5	Study III: Considerations for Experience Sampling of Twin Pairs	89
5.1	Introduction	89
5.2	Models	92
5.3	Simulations	98
5.3.1	Simulation I: Sampling Distributions	98
5.3.2	Simulation II: Heritability	100
5.4	Application: Affect data	102
5.4.1	Model	104
5.4.2	Analyses	107
5.5	Results	108
5.6	Discussion	115
6	Hierarchical Modeling for Biometrical Genetic Analysis of Dynamics	121
6.1	Introduction	121
6.2	Power and Bias by Sample Size	122
6.3	Modeling Strategies	125
6.4	Application: Heart Rate	133
7	Discussion	135

7.1 Summary of Findings	135
7.2 Limitations	137
7.3 Future Directions	141
References	143
Appendix A AR(1) ACE Hierarchical Likelihood Model and simulation in OpenMx	165
Appendix B AR(1) ACE Bayesian Hierarchical Model in STAN	170
Appendix C Simulation script for Bayesian AR(1) ACE model	173
Vita	175

LIST OF TABLES

Table		Page
1	Parameters of the IPC model with units and descriptions.	34
2	Optimization bounds for all parameters	43
3	Parameter sets for generating simulated data	45
4	Parameter point estimates for simulated noiseless series. Downsampling rate in Hz is shown in the left column. See Table 3 for the true, data-generating parameter values of each set.	46
5	Simulation results: Means (μ) and standard deviations (σ) of estimated parameters over 100 iterations of simulation for six parameter sets. True values are given in Table 3, and parameter descriptions are given in Table 1.	48
6	Optimization boundaries [lower, upper] for each parameter, under each model.	54
7	Summary statistics, effects of age and vision accounting for height and mass, and person-level intraclass correlations of parameter estimates under each model. Bonferroni adjusted $\alpha = .0029$	55
8	Correlation matrix of affect states across the total sample.	74
9	Multiple Negative Binomial regression of substance use counts on: (a) only descriptive statistics of affect sum scores: mean (μ_{SS}) and standard deviation (σ_{SS}); (b) only model-based predictors: regulation (δ) and volatility (σ_w); (c) both descriptive and model-based statistics. β_0 is the intercept for each model.	81
10	Generalized R^2 values for models predicting with: (a) only descriptive statistics of affect sum scores (mean and standard deviation); (b) only model-based statistics (regulation and volatility); (c) all four predictors; and (c)-(a), the improvement to R^2 as a result of including the model-based predictors with descriptors.	82

11	Sampling covariance of VAR parameters from simulation. Correlations are given in bold in the upper triangle.	99
12	Estimated Hessian-based sampling covariance $\mathbb{E}[(\frac{1}{2}\mathbf{H})^{-1}]$. Correlations are given in bold in the upper triangle.	100
13	Estimated twin correlations True values were $r_{MZ} = .9$, $r_{DZ} = .6$	103
14	Number of individuals per number of unique responses on each item of the PANAS.	105
15	Contingency table of significant Likelihood Ratio Tests (LRT) by zygosity. A significant LRT indicates that the twin pair model fits significantly worse when cross-twin effects are constrained to zero.	111
16	Results of multiple regression of twin-pair LRs onto zygosity, data completeness, and cohabitation. LRs were computed from the difference of the $-2\ln(\hat{\mathcal{L}})$ of models in which twin effect parameters were freely estimated versus models in which they were constrained to zero. Zygosity (rG) was coded as $DZ = 0.5$ and $MZ = 1.0$	112
17	Descriptive statistics for the twin-specific phenotypic parameter estimates $\hat{\beta}$ and cross-twin effects γ and ρ . Excluding twin effects (CTFX) from the model slightly inflated effect sizes, as cross-twin regressions accounted for part of the time dependence.	113
18	Coefficients from multiple regression of cross-twin effect sizes (γ^2 and ρ) onto zygosity (rG) and cohabitation status. All cross-twin effects were significantly associated with zygosity at $p < .05$	114
19	Twin correlations for autoregressive effects $\hat{\beta}$ with and without bias adjustment.	115
20	Statistical power for a $\sigma_{A,\alpha}^2 = .8$ given within (T) and between (N) person sample sizes.	124
21	Biometrical genetic variance components of model parameters from two models of heart rate measures: independent and identically distributed (i.i.d.) and an AR(1) model. μ is mean heart rate, σ is the standard deviation, and β is the lag-1 autoregression coefficient from the AR(1) model.	134

LIST OF FIGURES

Figure	Page	
1	Equivalent representations of $\ddot{x}_t = \eta x_t + \zeta \dot{x}_t$ (left) and $\ddot{x}_t = \eta x_t + \zeta \dot{x}_t + \sigma \delta_t, \delta \sim N(0, 1)$ (right). Top: Phase portraits; Bottom: Time plots.	9
2	A time series $x_t = 0.8z_{t-1} + \epsilon_t$ with its autocorrelation and partial autocorrelation functions shown below.	16
3	Noiseless series with initial values $x_0 = 1, \dot{x}_0 = 0$	45
4	Examples of simulated series from six parameter sets.	49
5	Parameter recovery results for each parameter configuration. Black squares: data-generating value; Empty squares: Estimate mean; Triangles: Upper and lower std. dev.; Circles: Outliers; Crosses: Optimization boundaries.	50
6	Marginal distributions of the ISDDE parameter estimates. Solid lines are means and dashed lines are standard deviations, both trimmed for the 15 highest values.	56
7	Phase portraits of observed body tilt angle with estimated intermittent activation structures and vector fields. Horizontal axis: COM; Vertical axis: COM velocity. Shaded region: state where $P = D = 0$. (a) Estimated parameters match theoretical expectations showing two equilibria. (b) and (c) the nonlinear mechanisms deviate uniquely from theoretical purpose.	63

8	Phase portraits and time series from two models generated from the same vector of noise (scaled by σ_w). In (a) data were simulated from the ISDDE model with the theoretical priors. In (b) data were simulated from a 3-parameter SDE. The large ratio of derivative (B) to proportional (K) force results in non-equilibrium Langevin dynamics that may exhibit similar features to the ISDDE for limited periods of time. Characteristic features distinguish (a) from (b), such as sharp changes in velocity localized to quadrants II and IV, slow change in velocity associated with quadrants I and III, and higher density at two spatial equilibria	65
9	Path diagram of state-space twin model	95
10	Path model representation of the positive and negative affect twin state-space model with cross-twin effects.	106
11	Series of estimated latent states in one twin pair that showed statistical anomalies, likely due to a problematic lack of variation.	109
12	Bivariate distributions of estimated effects $\hat{\beta}$. The saturated model (Left) shows extreme correlation driven by outliers. The constrained model (Right) had fewer outliers. Pearson correlations are shown in the upper right triangles.	110
13	Bivariate distributions of estimated effects $\hat{\beta}$ from the saturated model after exclusion of outliers. The extreme correlations disappear and a relatively Gaussian distribution remains. Pearson correlations are shown in the upper right triangle.	111
14	Bias, variance, and statistical power for $\sigma_{A,\alpha}^2 = .8$ given within (T) and between (N) person sample sizes.	123
15	Simulation of hierarchical AR(1) processes ($N = 64, T = 1280$) with the autoregressive parameters distributed according to $\sigma_A^2 = .6, \sigma_C^2 = .3, \sigma_E^2 = .1$. 60 iterations were run. Blue letters represent data-generating parameter values. Estimates were obtained using Maximum Likelihood Estimation.	128

16	Resulting Bayesian posterior parameter distributions from simulated large-sample studies. The dotted red line is the mean of the posterior distribution, and the solid black line is the true data-generating value. . .	131
17	Simulation of hierarchical AR(1) processes($N = 150, T = 45$) with the autoregressive parameters distributed according to $\sigma_A^2 = .6, \sigma_C^2 = .3, \sigma_E^2 = .1$. 30 iterations were run. Blue letters represent data-generating parameter values.	133

Abstract

PHENOTYPE EXTRACTION: ESTIMATION AND BIOMETRICAL GENETIC ANALYSIS OF INDIVIDUAL DYNAMICS

By Kevin L. McKee

A Dissertation submitted in partial fulfillment of the requirements for the degree of
Doctor of Philosophy at Virginia Commonwealth University.

Virginia Commonwealth University, 2020.

Director: Michael C. Neale,
Professor, Department of Psychiatry

Within-person data can exhibit a virtually limitless variety of statistical patterns, but it can be difficult to distinguish meaningful features from statistical artifacts. Studies of complex traits have previously used genetic signals like twin-based heritability to distinguish between the two. This dissertation is a collection of studies applying state-space modeling to conceptualize and estimate novel phenotypic constructs for use in psychiatric research and further biometrical genetic analysis. The aims are to: (1) relate control theoretic concepts to health-related phenotypes; (2) design statistical models that formally define those phenotypes; (3) estimate individual phenotypic values from time series data; (4) consider hierarchical methods for biometrical genetic analysis of individual phenotypic variation.

CHAPTER 1

INTRODUCTION

This dissertation is a collection of studies that aimed to advance both the conceptualization and methodology of complex human traits with applications to psychiatric research. The title is a combination of two concepts. In signal processing, algorithms for *feature extraction* reduce voluminous data to set of statistical patterns or constructs that are fewer in number [1]. In human genetics, a *phenotype* is any human feature, whether social, behavioral, cognitive, or biological, that is determined to some degree by genetic factors.

Feature extraction most often refers to techniques of dimension reduction, but can also refer generally to structures obtained by classification and parametric modeling. Features can be extracted from either between or within-person data. In psychiatric research, most studies involve relatively abstract assessment of traits via questionnaires and structured interviews. Exploratory, data-driven techniques are then used to generate new cognitive and behavioral constructs from the responses. Exploratory factor analysis (EFA), a method of dimension reduction that decomposes observed data into latent variables and indicator residuals, has led to the five-factor model of personality [2], the two-dimensional circumplex models of affect [3, 4], the higher-order factors of disordered behaviors called *internalizing* and *externalizing*[5], and many others. Within-person data can be treated the same way. In the field of computer vision, facial recognition models commonly rely on principal components of facial structure, called “Eigenfaces” [6, 7]. Rather than identify each face as a pattern of thousands of relative pixel values or correlations, most identifying features can be

described with a linear combinations of the principal components. In functional magnetic resonance imaging (fMRI) of brain activity, Independent Component Analysis (ICA)[8] is used to reduce thousands of three-dimensional voxels, each with their own time course, to the time courses of anywhere between eight and fifty brain networks [9, 10].

When these methods are applied to data from human subjects in the context of Behavioral Genetics, they imply the existence of a phenotype that cannot be measured directly but has greater theoretical importance and utility than any of its particular indicators. The fact that data can be reduced to fewer dimensions does not, however, imply that the dimensions must represent something “real”. Without invoking the broader philosophical problems of ontology, we can proceed with our particular aims using a narrow definition that a psychological construct is real, or a “natural kind”, if it represents a set of functions that distinctly and reliably explain natural phenomena. In practice, determining whether a feature extraction model does “carve nature at its joints” in such a way is a question of theoretical validation. A latent variable might attain *construct validity*[11] if it is known to accurately measure or represent something with an intelligible, etiological role that corroborates or complements other empirical observations. A related idea is the *nomothetic span* of a variable: the frequency and strength of its network of associations with other variables and ability to account for individual differences [12]. More often, latent variables attain the weaker *criterion* validity, in which they are found to have reliable, statistical relationships to outcomes of interest. If found to predict outcomes at a later time, they may be considered to have *predictive* validity.

Where the development and validation of latent variable models concerns psychiatric disorders and complex traits generally, Biometrical Genetic modeling [13] enables another form of validation that falls under the category of nomothetic span.

The genetic signals of complex traits can be used to gauge their proximity to biological pathways, and to some extent, their reliability. Heritability, or the total percentage of variation in the population due to additive genetic factors, can be estimated from data in monozygotic (MZ) and dizygotic (DZ) twins, or from genotypic data using methods like Genome-wide Complex Trait Analysis (GCTA) [14]. In Hans Eysenck’s estimation of the heritability of Neuroticism [15], one of the five personality factors, he summarized the new form of biometrical genetic validation succinctly: “If the result shows that the factor is inherited to a more marked extent than any single test, it follows that we have succeeded in proving that the factor is no mere artefact, but has a certain degree of biological reality.” To determine the specific genetic mechanisms underlying variation in a phenotype, genome-wide association studies (GWAS) may be used to detect effects from Single Nucleotide Polymorphisms (SNP) throughout the genome [16]. When SNP-level associations to a complex trait can be found and reproduced, the functions of their associated genetic regions may give important insight into the trait’s biological architecture. Recent progress in GWAS of complex traits suggests that for more abstract phenotypes, and particularly psychiatric disorders [17, 18], SNP effects are typically so small and numerous that tens of thousands of study participants may be needed to detect them [19, 20]. For this reason, the costs of a GWAS are generally too large to justify for early studies of novel phenotypes. Detecting aggregate heritability by twin study or GCTA requires far fewer subjects and is thus a more accessible, general way to contrast the ontology of competing phenotypic definitions [21].

1.1 Intrinsic Dynamics

The major goals of psychological research concern interindividual variation to make nomothetic inferences. That is, we want knowledge of people in general. Many

psychological study designs involve intensive repeated measures, such as Ecological Momentary Assessment (EMA) [22], in which data reflecting subjective experiences are recorded on a daily or hourly basis (called active measurement), or experiments in which sensors continually sample physiological correlates of mental processes (passive measurement). These hierarchical data sets can become overwhelming to investigators, as it is not always clear how to incorporate such an abundance of within-person information into a between-person analysis.

The complexity of hierarchical data is simplified if within-person processes can be summarized by indices of temporally stable traits. An atheoretical first pass at simplifying the problem is to extract descriptive statistics such as the means and standard deviations of each individual's time series, but these are not always sufficiently reliable, predictive, or interpretable. Theoretical, model-based indices have the potential to access different kinds of information and posit more specific hypotheses. By definition, theoretical indices predicate their specificity on more *a priori* conjectures than exploratory, atheoretical descriptors. Consequently, if such conjectures are not accurate, they will tend to fail more completely than generic descriptors in terms of both reliability and prediction. It is exactly this property that makes them interesting, however, because both failures and successes can lead to the improvement of the underlying conjectures and a deeper theoretical understanding of the problem.

The kind of theoretical indices explored in this dissertation are commonly called *dynamics*, meaning the particular relations within and between entities that determine their motion over time. The study of dynamics has seen the most success in physics, from Newton's models of how bodies move and interact in space, to the random behavior of molecules in solution described by Langevin [23]. Recently, some authors have taken interest in a Newtonian view of psychology and called for the pursuit of intrinsic psychological dynamics [24, 25, 26]. This call more closely resembles

the practice in Econometrics of deriving “structural parameters” to develop more empirical theories of market fluctuation and clearer indices of the effects of changing economic policy. Econometrics was famously critiqued by Lucas[27] for producing only short-term predictive models, but nothing general or fundamental enough to evaluate changes in policy and the context of economic trends more broadly. Summers [28] went on to admonish the pursuit of structural parameters in Econometrics as a “scientific illusion” that has resulted in impressive mathematical techniques and a slightly broader vocabulary for economic theory, but no enduring empirical foundation. Within their criticisms, we find many relevant reasons to be skeptical of the same pursuit in Psychology. Human minds and markets exhibit a similar degree of complexity, importance of external context, and relative inadequacy of measurement strategies. Both can change to unprecedented states over time as a consequence of rare and unique events, rather than statistical regularities. Regarding economics, wars and natural disasters often lead to economic recessions with lasting changes in policy. Major technological advances, such as automobiles and computers, have irreversibly led to new kinds of demand and the obsolescence of old markets, and with that, large-scale changes in the overall standard of living. Analogously, single traumatic events can trigger lasting changes in personality. For example, Borderline Personality Disorder (BPD) seems to arise as a result of childhood exposure to violence and abuse [29]. Alternatively, acquisition of a new coping strategies and knowledge [30] or addiction to a new drug can alter one’s fundamental strategies for coping with daily stress. That complex systems can suddenly adapt and undergo lasting changes in state suggests that many readily apparent dynamics of functioning may be superficial and transient, whereas more trait-like mechanisms may have to be found deeper within the adaptation process itself.

As we will discuss in Chapter 2, the hunt for intrinsic, trait-like dynamics begins

with the problem that a time series can be parameterized in countless ways. Every model is predicated upon a set of theoretical assumptions and a set of parameters that potentially represent stable, ontologically convincing phenotypes. Eysenck’s reasoning [15] would seem to provide us with a generic criterion for comparing such models and evaluating their ontology. The generative role of the genome in human behavior and the differential magnitude of genetic signals by candidate phenotype should give the pursuit of intrinsic dynamics in psychology a stronger footing than has been possible in econometrics. Genetic signals have arguably served as a kind of ontological SONAR, with each theoretical conjecture sending a ping and receiving its reflection off the underlying biological landscape. Like SONAR, a particular signal is cryptic. Mapping must take place over many iterations, and interpretation must proceed by inference.

As genetic modeling of intrinsic dynamics no longer refers to variation on a latent variable, but rather variation in the parameters of a process, it is less clear what takes the place of “any single test” in Eysenck’s statement. Perhaps a model parameter earns some validity when its heritability is greater than any summary statistic of the subject time series. A more cautious criterion may be to only make relativistic comparisons of parameter heritability between competing models, much like the practice of comparing model fit statistics. In this way, we would choose a model with the highest chances of linking to known biological systems (such as particular SNPs) as its mechanisms and parameters are further elaborated and tested.

1.2 Control Theory

How do we begin to conceptualize intrinsic dynamics in psychology? Human behavioral processes express tensions between intrinsic and extrinsic forces. Environmental changes force people to adapt, while periods of stability allow them to

optimize. These themes have in common the problem of *control*. In the health sciences, control is essential to defining and explaining disease states. Pathogens disrupt the regulatory functions of the body and lead to declines in health and functioning. In the DSM-5, functional impairment in work, interpersonal relations, or self-care is a key criterion for the diagnostic categories [31]. It follows that many concepts from *control theory* [32, 33] may be useful for conceptualizing behavioral and psychological health in terms of stability, variation, and response to disturbance.

Despite their utility in engineering, relevant technical concepts and methods from control theory are not as commonplace in studies of mental health. If we look to physiology more generally, there are many domains in which control schemes compete to best explain observable processes. In practice, they are implemented as *computational models*. A computational model attempts to describe the emergent properties of a process by way of its underlying mechanisms, often using simulation to compare its expectations with reality. In Chapter 3, we examine one such model in the field of human postural control to empirically evaluate its underlying theory. Computational modeling is less convenient in psychology and psychiatry, where observations can be clustered and associated with outcomes or latent dimensions, but the intractable complexity of cognitive processing and environmental context make it difficult to conceive of detailed, mechanistic theories for any particular behavior. We nonetheless attempt in Chapter 4 to apply an analogous procedure to time series of affect for a simple model of emotion control.

A number of concepts from the theory of control systems will be useful. First, a *feedback control* system is one that takes its own outputs at one time as inputs at a later time. A simple example would be a household thermostat, which activates the heating or cooling of a room when that room's temperature deviates too far from a set value. Specifically, a thermostat is said to use *negative feedback* to keep the

temperature close to that set value because the amount of heating or cooling applied is inversely related to the current temperature. A system with *positive feedback* would accelerate away from the set value, as higher temperatures invoke more heating. In either case, the thermostat is known as a simple *proportional* controller, as change in the state is proportional to its level. If a hot oven were suddenly opened, releasing a gust of hot air into a small kitchen, the thermostat would detect the sudden change in temperature and activate the air conditioning in response. In modeling terms, the oven is a *forcing function* that acts directly upon the temperature of the kitchen. If the oven is regarded as an *exogenous* force, external and circumstantial, then the HVAC system would be regarded as an *endogenous* force, or one that responds predictably and automatically by design.

In human experience, both external and internal forces on behavior are perpetual and numerous. The stresses of daily life originate from external responsibilities, social interactions, accidents, as well as the internal fluctuations of bodily needs, diseases, and hormones. These are met with regulatory responses that can also be internal or external. Social support networks, daily comforts, and habits of self-care reduce stress responses and create regularity in behavior and experience. To model the competing factors of stress and emotion control, we can think of the human mind as a control system undergoing continual, random perturbation. Figure 1 illustrates the path of a negative *proportional-derivative* feedback cycle over time, which includes negative feedbacks from both level and velocity. On the left, the state begins from a high point and, absent any external forces, surges down to its equilibrium point at zero. Imperfect adjustments cause the system to overshoot, but the negative feedback with velocity gradually reduces the error with each oscillation. In the graph on the right, continual, random disturbances drive the system back up to a nearly constant amplitude.

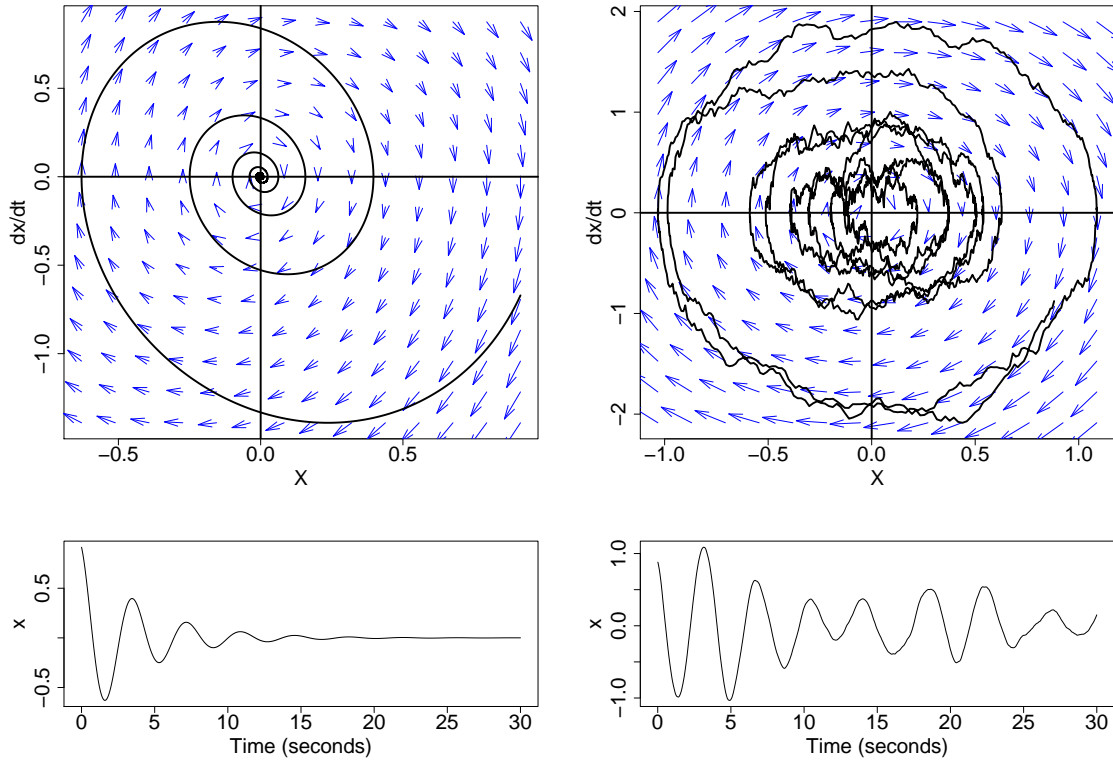


Fig. 1.: Equivalent representations of $\ddot{x}_t = \eta x_t + \zeta \dot{x}_t$ (left) and $\ddot{x}_t = \eta x_t + \zeta \dot{x}_t + \sigma \delta_t$, $\delta \sim N(0, 1)$ (right). Top: Phase portraits; Bottom: Time plots.

The phase plots, shown above the time series, are another way of representing the system with its predicted motion for any values of its current level and velocity. Like fitting regression lines to bivariate scatter plots, the vector field (in blue) can be approximately fit to stochastic series like the one shown on the right. The direction and magnitude of the predictive vectors is a function of the estimated dynamic coefficients. In this case, there are two: the proportional coefficient, or frequency, and the derivative coefficient, or damping. This damped linear oscillator model has many uses in engineering and physics, where frequency is generally determined by a spring constant or other accelerating force, while damping most often represents sources of friction that gradually dissipate energy. In representing stress and emotion

control, the distinction between proportional and derivative control may be harder to attribute to such specific mechanisms. Possibly, each kind of regulatory factor at play could be regarded as having precise and imprecise effects that more or less lead to overcompensation of stress, adding variously to the values of these two dynamics when taken in aggregate. Mainly, the damped linear oscillator is used here because it is easy to understand visually. The dynamics of more plausible control processes may not be possible to detect by visual inspection at all, instead requiring statistical deconvolution.

1.3 Aims

The aims of this dissertation are to: (1) relate control theoretic concepts to health-related phenotypes; (2) design statistical models that formally define those phenotypes; (3) estimate individual phenotypic values from time series data; (4) consider hierarchical methods for biometrical genetic analysis of individual phenotypic variation. The next chapter gives a brief overview of relevant statistical methods for modeling time series with interpretations in the context of cognitive and behavioral processes.

To explore the capabilities of within-person modeling, the third chapter examines a complex, theoretical model of postural sway fit to high quality physiological data. The study was published by *PLOS ONE* in September of 2019 [34]. Postural sway data were chosen because of the existence of high quality public data sets and several options for theoretical models, few of which had been validated using the strategies proposed.

The fourth chapter navigates the limitations and uncertainties inherent to psychometric data using a much simpler model of feedback control. That study was published in *Addictive Behaviors* in March of 2020 [35]. The chosen data represent a

typical, developmental Experience Sampling design with measurement bursts over a period of two years. It was chosen for analysis because the included affect data inherently present technical challenges for a dynamical systems analysis, such as irregular response intervals, noisy measurements, and high dimensionality.

The fifth chapter considers a similar study design, data set, and phenotypic model as the fourth chapter, but navigates a range of new, additional challenges that arise when individuals in the sample are dependent. Specifically, it considers the problem of obtaining truly individualized dynamics for twin studies when twins cohabit, share experiences, and influence one another throughout the study period.

The sixth chapter considers methods of hierarchical twin modeling to perform both feature extractions and biometrical genetic analyses simultaneously for maximum statistical accuracy. The seventh and final chapter discusses future applications and implications of hierarchical biometrical genetic analyses.

CHAPTER 2

TIME SERIES METHODS

The basic problem of time series analysis is in accounting for variation and serial dependence among observations of a process. By considering process models in the context of cognition and behavior, we can derive many new, generic phenotypic constructs. This chapter reviews many of the most common strategies and concepts for modeling behavioral time series. The content briefly summarized here is standard in many introductory textbooks; see [36, 37].

2.1 General concepts

A stochastic process is an indexed random variable, x_i , and a time series is a time-indexed random variable, $x(t)$ or x_t , $t \geq 0$, that implies a time-dependent process. A white noise process is a Gaussian, independent and identically distributed (i.i.d) variable that, while having no time dependence in itself, is a useful component of time series models. A single series is called a sample *realization* of the process. The *ensemble* is the set of all sample realizations. Take N as the number of sample realizations and T as the number of observations per realization. A process is *ergodic* if its statistical properties converge to the same values either when $T \rightarrow \infty, N = 1$ or when $N \rightarrow \infty, T < \infty$. Alternatively, a single sample realization will span the full sample space with $p \rightarrow 1.0$ as $T \rightarrow \infty$. Ergodicity holds primarily for simple, linear models and is a necessary property for models that aggregate over many individuals.

Another important concept is that of *stationarity*, or constancy over time. In a strictly stationary system, all moments of the distribution of x_t remain constant.

In n -th order weak stationarity, all moments up to order n are stationary. For example, it is common for models to assume second-order stationarity (also known as “wide-sense stationarity”) in which only means and variances are assumed to be constant. The assumption of stationarity may be more or less weak depending on the time frame and context of the series. For series representing short intervals recorded at high-frequency, such as sensor data, stationarity may be a plausible or necessary assumption because of *a priori* boundaries on the system imposed experimentally or by the physiology itself. For developmental studies, it may not make sense to assume certain degrees of stationarity when the time frame and subject matter concern irreversible and unbound processes of overall growth or decay. The kind of stationarity in question depends on the phenotype and its model. For instance, the height of an individual over a lifetime is first-order or mean-nonstationary, as it continually increases through early adulthood, then decreases slightly in late adulthood. Over a time frame restricted to middle adulthood, it may be considered mean stationary in that it is nearly a constant value. More complex traits, represented by dynamics in a model, may be subject to higher-order forms of nonstationarity. One example would be changes in lability or variance in emotional states over the course of adolescence, which may be of primary interest in a study of emotional maturation.

2.2 Time domain

In time-domain analysis, a series is described by relations between its values at different time lags up to lag L .

$$x_t = f(x_{t-l}, t), \quad l \in 1, 2, \dots, L \quad (2.1)$$

A Markov process is one in which future states, x_{t+l} , depend only on the current state x_t . The definition given by Wei [36] states: “The state of a system is defined

to be a minimum set of information from the present and past such that the future behavior of a system can be completely described by the knowledge of the present state and the future input.” Markov processes can be organized by whether time intervals are discrete and uniform, e.g., with $t \in [1, 2, 3, \dots, T]$, or continuous, with $t \in \mathbb{R}$ and potentially irregular intervals. Second, the sample space x may either be continuous or discrete. We will discuss a few examples of each kind of process in the sections to follow.

2.2.1 Discrete Time, Discrete Space

A discrete time, discrete sample space process can be described by a Markov chain. For every possible state of the system, there is a probability of either remaining the same or changing to a different state. The transitional probabilities can be described by a Markov matrix where columns contain probabilities summing to one. In the simplest case of two possible states, 0 and 1, we would have:

$$\begin{bmatrix} P(x = 0|x = 0) & 1 - P(x = 1|x = 0) \\ 1 - P(x = 0|x = 1) & P(x = 1|x = 1) \end{bmatrix} \quad (2.2)$$

This kind of model may be useful for time series of relatively sparse categorical data measured at regular intervals, such as monthly or annual occurrence of an episodic psychopathology. The diagonal elements describe the probability of staying in the same state, and the off-diagonals are the probability of switching. This kind of model is useful in general for describing regime change over time, as a state may represent more than just values on an observed variable. For example, states may represent distinct factor models, and hence the inter-correlations of many variables randomly change between two configurations.

2.2.2 Discrete Time, Continuous Space

Models of continuous variables, $x \in \mathbb{R}$, can assume continuous change from one discrete timepoint to the next. The basic descriptive statistics resemble those for cross-sectional continuous-variable analysis, such as the covariance and correlation. The Autocorrelation Function (ACF) describes the self-similarity over different time lags as the covariance of a variable with itself at some lag or lead k :

$$\gamma_k = Cov(X_t, X_{t-k}) = \mathbb{E}[(X_t - \mu)(X_{t-k} - \mu)]. \quad (2.3)$$

The autocorrelation is the standardized autocovariance:

$$\rho_k = \frac{Cov(X_t, X_{t-k})}{\sqrt{Var(X_t)}\sqrt{Var(X_{t-k})}}. \quad (2.4)$$

Assuming stationarity, $Var(X_t) = Var(X_{t-k})$, so $\rho_k = \frac{\gamma_k}{\gamma_0}$, where γ_0 is the variance of X .

The partial autocorrelation function (PACF) estimates the relationship of X_t, X_{t-k} accounting for intermediate lags:

$$P_k = Corr(X_t, X_{t-k} | X_{t-1}, \dots, X_{t-k+1}) \quad (2.5)$$

$$= \frac{\rho_k - \alpha_1 \rho_{k+1} - \dots - \alpha_{k+1} \rho_1}{1 - \alpha_1 \rho_1 - \dots - \alpha_{k-1} \rho_{k-1}} \quad (2.6)$$

Obtaining α_k is somewhat more involved, but can be computed using multiple regression. See Chapter 2 of [36] for details.

Figure 2 shows an autocorrelated processes with its ACF and PACF shown below. The PACF shows that it can be described by a partial autocorrelation of 0.8 with lag 1. No other lags are significant, conditional on the effect of lag 1. There is a false positive association with lag 18. These descriptive results aid in determining an appropriate linear model of the process.

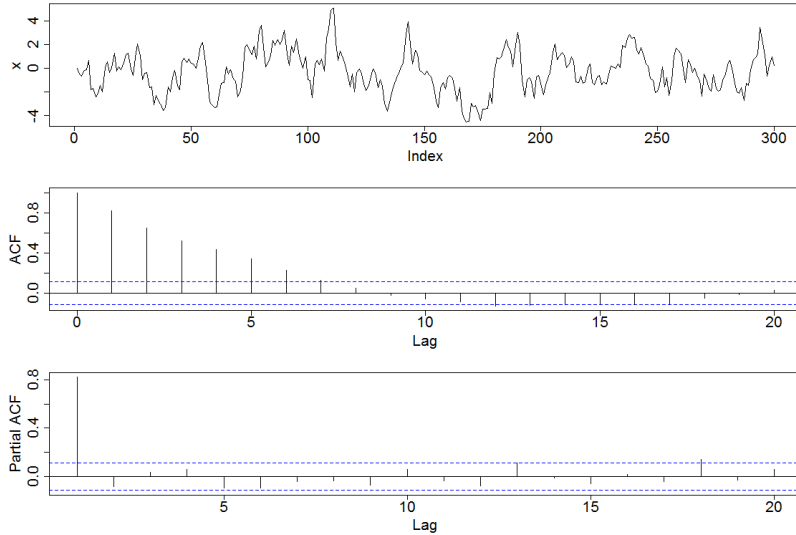


Fig. 2.: A time series $x_t = 0.8z_{t-1} + \epsilon_t$ with its autocorrelation and partial autocorrelation functions shown below.

An *autoregressive* process, denoted $AR(p)$, describes X_t as a linear combination of X_{t-i} for order p lags:

$$x_t = \mu + \sum_{i=1}^p \beta_i x_{t-i} + \epsilon_t, \quad \epsilon \sim N(0, 1). \quad (2.7)$$

The parameter, β_i , determines the degree of time dependence specific to each lag. ϵ_t is a white noise process contributing novel change at each step. In various contexts, ϵ may be referred to as the innovations, disturbances, process noise, or dynamic error.

An $AR(p)$ process has a decaying ACF and a discontinuous PACF. It is one of the most common models of the interplay between system history as a function of β and disturbances ϵ . When $\beta = 1$, the model describes a random walk, or the cumulative sum of a white noise variable. In developmental models, β represents the proportion of the phenotypic state's deviation from its mean at time t that is carried forward to time $t + 1$. In control models, $0 < \beta < 1$ results in an expected decay toward a mean value, and $-1 < \beta < 0$ results in discrete, decaying oscillations.

A moving average process MA(q) of order q is one in which the present state is a linear combination of previous disturbances:

$$x_t = \mu + \epsilon_t + \sum_{i=0}^q \alpha_i \epsilon_{t-i} \quad (2.8)$$

Each new disturbance has a temporary influence described by α up to lag q . Whereas the ACF of an AR process decays continuously to zero as the lag value increases, MA processes have a discontinuous ACF with associations only out to lag q . They can be understood conceptually as a finite impulse response process in which the effect of each disturbance vanishes completely after a fixed time interval.

These two models are often combined to create an Autoregressive Moving Average model, or ARMA(p, q):

$$x_t = \mu + \sum_{i=1}^p \beta_i x_{t-i} + \epsilon_t + \sum_{j=1}^q \alpha_j \epsilon_{t-j} \quad (2.9)$$

A further extension of the ARMA model is the Autoregressive Integrated Moving Average, or ARIMA(p, d, q). X_t is differenced up to order d and the differences are modeled as ARMA(p, q). ARIMA models are highly general because the differences of a mean-nonstationary series are often stationary, and mean-nonstationarity is common in a wide range of applications. A consequence of differencing is that estimated parameters will be more sensitive to noise, as variance due to the signal is being systematically subtracted out. Because of their generality, ARIMA models are often used with exploratory fitting processes with the goal of obtaining a highly predictive model without making theoretical assumptions.

2.2.3 Continuous Time, Discrete Space

When discrete variables such as binary indicators and counts of an event are recorded at irregular, real-valued times, we can model their occurrence as a Poisson

process. The Poisson distribution maps a given time interval to an expected number (k) of occurrences of an event.

$$P(X = k) = \frac{\lambda^k e^{-\lambda}}{k!} \quad (2.10)$$

where λ is the number of occurrences or rate in the form of a standardized interval, k/T , where T is the length of the time interval.

The Poisson distribution can be derived as a limiting case of the binomial distribution. To start, we assume that each new event is an independent Bernoulli trial at each new time $t \in 1, 2, \dots, T$ with probability of occurrence k . The Binomial distribution gives the expected number of occurrences k given T trials and probability of occurrence k :

$$P(X = k; T, p) = \frac{T!}{k!(T - k)!} p^k (1 - p)^{T - k} \quad (2.11)$$

The factorial term represents all possible combinations of occurrences across the T time points. To conceptualize this as a continuous time process, we can take $T \rightarrow \infty$ and $p \rightarrow 0$, making k a real-valued interval that maps to a probability density. A full proof of this is given by the Poisson Limit Theorem.

Take for instance binary indicators of substance use, stressful events, or accidents recorded in an EMA study with an event-contingent design. These variables may be recorded along with those of an ordinal or continuous sample space, such as affect. When recording the affect, the event indicators may be zero most of the time. When the event of interest occurs, a new report is submitted with the value of one. The model describes the distribution of the events across time. Along with binary indicators, the distribution accepts equally well a count of, for instance, the number of cigarettes smoked or alcoholic drinks consumed in the previous hour. In these models, zeros and missing data do not give different results- everything is zero

between individual instances or aggregated counts of the event.

Poisson regression and the related negative binomial regression are two ways of testing associations between such aggregate counts and their continuous covariates. The exponentiated parameters give expected counts of the event conditional on the value of the predictors. In Chapter 4, negative binomial regression is used to relate the total number of occasions of substance use to a parameter of emotion regulation.

2.2.4 Continuous Time, Continuous Space

When both the time intervals and the sample space belong to \mathbb{R} , a continuous time model may be used instead. These models take the form of stochastic differential equations (SDE). For brevity, we can use dot notation: $\frac{dx_t}{dt} =: \dot{x}_t$, $\frac{d^2x_t}{dt^2} =: \ddot{x}_t$, etc. A continuous-time random walk can be described by a process with a random first derivative:

$$\dot{x}_t = \delta_t, \quad \delta_t \sim N(0, 1) \tag{2.12}$$

This basic relation has been used to describe “Brownian motion” of molecules in a solution. The integral is called a “Wiener process”: A function that is everywhere continuous but nowhere differentiable. It is a random fractal, in that it exhibits statistical self-similarity at all scales. This property simplifies the problem of random intervals in that the expectations for x_{t+1} can always be computed the same way, regardless of Δt .

The AR(1) model in Equation 2.7 can equivalently be written for continuous time:

$$\dot{x}_t = \lambda x_t + \delta_t, \tag{2.13}$$

where $\lambda = \frac{\ln(\beta)}{\Delta t}$ or $\beta = e^{\lambda \Delta t}$, using the solution to a linear first-order ordinary

differential equation (ODE). Variation in time intervals is thus handled implicitly. The solution of an SDE is called a *diffusion process*, where diffusion refers to the stochastic component.

Differential equations can be characterized by their phase portraits, the bivariate plots of different derivatives. Take for instance the second order equation for damped oscillation described in Chapter 1:

$$\ddot{x}_t = \eta x_t + \zeta \dot{x}_t + \delta_t \tag{2.14}$$

When η is negative and $\eta + \zeta^2/4 < 0$, this equation produces oscillations of random amplitude. The sign of ζ determines whether the amplitude tends to grow or decay. A continuous time model will fit a vector field to the series that predicts its motion for any coordinate in the sample space, as was shown in Figure 1.

It is useful in many scenarios, regardless of whether time intervals are actually continuous or discrete, to use differential equation notation instead of equivalent discrete-time notations. When comparing the results of substantively similar studies with different measurement intervals, autoregressive models may be converted to differential equations for directly comparable parameter values. Many kinds of dynamical systems, and physical systems in particular, are also much more straight forward to describe with differential equations. A thrown baseball, measured at equal intervals, will be highly autocorrelated because each new position will be almost completely accounted for by the last known position. But it is not intuitive or convenient to analyze physical trajectories in terms of discrete variance transfers using an equation like 2.7, when the parabolic curve can be described by the relationship between forces of acceleration, velocity, and position instead. Similarly, the generic damped oscillator model may be described by a second-order autoregression, $y_t = \beta_1 y_{t-1} + \beta_2 y_{t-2} + \delta_t$ in which $\beta_1 > 0$, $\beta_2 < 0$, and $\beta_1 + \beta_2 < 1$. The most obvious topological features of

the series, damping and frequency, become a somewhat more obscure joint function of β_1 and β_2 , rather than being controlled primarily by separate parameters.

2.2.5 Structural Equation Models of Change

Biometrical genetic analyses of multi-indicator factors over time often use a combination of dimension reduction and structured linear modeling in the framework of Structural Equation Modeling (SEM) with latent variables [38]. SEM is a highly general way of specifying linear models that incorporates latent dimensions. It can be used to specify measurement models in which the unmeasured phenotype is inferred from the network of correlations among many observed indicators. The SEM algebra generalizes that of factor analysis, decomposing the expected covariance matrix of the observed variables into regressions onto a smaller set of latent dimensions:

$$\hat{\Sigma}(\mathbf{X}) = \mathbf{L}\mathbf{S}\mathbf{L}^T + \mathbf{U}, \quad (2.15)$$

where \mathbf{L} is a matrix of factor *loadings*, or the regression coefficients of observed variables X onto latent factors. \mathbf{S} is the covariance matrix of the latent factors, and \mathbf{U} is a diagonal matrix of residuals. Pre- and post-multiplication by $(\mathbf{I} - \mathbf{A})^{-1}$ allows us to specify unidirectional relations between latent factors in the \mathbf{A} matrix:

$$\hat{\Sigma}(\mathbf{X}) = \mathbf{L}(\mathbf{I} - \mathbf{A})^{-1}\mathbf{S}(\mathbf{I} - \mathbf{A})^{-1T}\mathbf{L}^T + \mathbf{U} \quad (2.16)$$

Time-series SEMs are often used in developmental studies with relatively few occasions of measurement, most often in the form of random-effects curve-fitting or between-persons autoregressive panels. In a Latent Growth Curve (LGC) [39], fixed factor loadings are used to define latent variables as terms of a polynomial trajectory that is allowed to vary across the sample. Autoregressive and cross-regressive panels [40, 41] are specified in “wide format”, where each of the T occasions is given a column

in each matrix. For AR models, most of the information that identifies the model comes from between-person variation per occasion. To estimate the autoregressive coefficients with sufficient statistical power, ergodicity must be assumed.

Continuous-time Ordinary Differential Equation models have been produced using SEM algebra as well. One such strategy, the Latent Differential Equation (LDE)[42], uses roughly the same specification as the LGC, but the rows of the data matrix are overlapping intervals of the series rather than independent persons. The dynamics are estimated as the linear relationships between the polynomial terms. The result is a deterministic differential equation model with measurement error that relies on local linear approximation of derivatives. So far, only a single specification, namely the damped linear oscillator, has been demonstrated, though multi-state [43], multi-timescale [44], and quasi-stochastic [45] generalizations have been developed.

2.2.6 State-Space Modeling

All of the Markovian models presented so far belong to the general class of State Space Models (SSM). SSMs, as an algebraic framework, can include any and all of the components of the above methods, modeling latent variables as continuous or discrete time processes according to particular dynamics. SSMs can be vectorized to allow multiple states as latent variables with multiple indicators:

$$\mathbf{x}_t = \mathbf{A}\mathbf{x}_{t-\Delta t} + \mathbf{B}\mathbf{u}_t + \mathbf{q}_t, \quad (2.17)$$

$$\mathbf{y}_t = \mathbf{C}\mathbf{x}_t + \mathbf{D}\mathbf{u}_t + \mathbf{r}_t. \quad (2.18)$$

The first line is the *state* equation that includes the dynamical specification, and the second line is the measurement model that relates the indicators to the states.

In equation 2.17, the \mathbf{A} matrix contains the auto and cross-regressive coefficients of the latent state, \mathbf{x}_t . \mathbf{B} contains the regression coefficients on potentially time-

varying covariates, or external forcing functions. \mathbf{q}_t is a Gaussian distributed white noise variable representing random disturbances to the state. In equation 2.18, the \mathbf{C} matrix contains the factor loadings, or coefficients that relate the indicators to the latent state. It is identical to matrix \mathbf{L} in equation 2.16. \mathbf{D} , similarly to \mathbf{B} , includes regression coefficients of \mathbf{y}_t onto time-varying covariates. Finally, \mathbf{r}_t is a Gaussian distributed white noise variable that represents measurement error, or additional random variation that does not influence the latent state.

The same models can be specified as differential equations in continuous time:

$$\dot{\mathbf{x}}_t = \mathbf{A}\mathbf{x}_t + \mathbf{B}\mathbf{u}_t + \mathbf{q}_t \quad (2.19)$$

$$\mathbf{y}_t = \mathbf{C}\mathbf{x}_t + \mathbf{D}\mathbf{u}_t + \mathbf{r}_t \quad (2.20)$$

For a discrete-time system with two latent states, six indicators, one time-varying covariate, we would have:

$$\begin{bmatrix} x_{1,t} \\ x_{2,t} \end{bmatrix} = \begin{bmatrix} \beta_{1,1} & \beta_{2,1} \\ \beta_{1,2} & \beta_{2,2} \end{bmatrix} \begin{bmatrix} x_{1,t-\Delta t} \\ x_{2,t-\Delta t} \end{bmatrix} + \begin{bmatrix} \alpha_1 \\ \alpha_2 \end{bmatrix} \begin{bmatrix} u_t \end{bmatrix} + \begin{bmatrix} q_{1,t} \\ q_{2,t} \end{bmatrix} \quad (2.21)$$

$$(2.22)$$

and

$$\begin{bmatrix} y_{1,t} \\ y_{2,t} \\ y_{3,t} \\ y_{4,t} \\ y_{5,t} \\ y_{6,t} \end{bmatrix} = \begin{bmatrix} \lambda_{1,1} & \lambda_{2,1} \\ \lambda_{1,2} & \lambda_{2,2} \\ \lambda_{1,3} & \lambda_{2,3} \\ \lambda_{1,4} & \lambda_{2,4} \\ \lambda_{1,5} & \lambda_{2,5} \\ \lambda_{1,6} & \lambda_{2,6} \end{bmatrix} \begin{bmatrix} x_{1,t} \\ x_{2,t} \end{bmatrix} + \begin{bmatrix} \gamma_1 \\ \gamma_2 \\ \gamma_3 \\ \gamma_4 \\ \gamma_5 \\ \gamma_6 \end{bmatrix} \begin{bmatrix} u_t \end{bmatrix} + \begin{bmatrix} r_{1,t} \\ r_{2,t} \\ r_{3,t} \\ r_{4,t} \\ r_{5,t} \\ r_{6,t} \end{bmatrix} \quad (2.23)$$

SSMs can be fit to data using the Kalman filter (KF)[46], a method of iteratively

estimating means of the latent state conditional on previous values of the observed indicators. The KF produces minimum-variance, unbiased estimates of the latent state and the likelihood of the data given a set of parameter values. By re-running the KF over iterations of optimization, maximum-likelihood estimates (MLE) of the parameter values can be determined.

2.3 Frequency domain

The other major category of time series analyses involves the *frequency domain*. Instead of considering the behavior of observations at each time t , we can transform the data to consider the magnitudes of different frequencies f that comprise the signal. A function $g(t)$ can be described as an infinite sum of sinusoids (f_i) with varying amplitudes, frequencies, and phases.

$$g(t) = \sum_{i=0}^{\infty} A_i \cos\left(\frac{\pi f_i t}{T}\right) + \sum_{i=1}^{\infty} B_i \sin\left(\frac{\pi f_i t}{T}\right) \quad (2.24)$$

Coefficients A_i and B_i can be found as the inner product of the function $g(t)$ with harmonic cosine and sine functions:

$$A_i = \frac{1}{T} \int_{-T}^T g(t) \cos\left(\frac{\pi f_i t}{T}\right) dt, \quad (2.25)$$

$$B_i = \frac{1}{T} \int_{-T}^T g(t) \sin\left(\frac{\pi f_i t}{T}\right) dt, \quad (2.26)$$

$$f_i \in 1, 2, \dots, \infty \quad (2.27)$$

while A_0 is simply the series mean. In the case where $g(t)$ is a discrete function, i.e., a series of observations in discrete time, we can make sense of these coefficients as the

covariances of the time series with sine and cosine functions of the same length:

$$A_i = \frac{1}{T} \sum_{t=-T}^T g(t) \cos\left(\frac{\pi f_i t}{T}\right), \quad (2.28)$$

$$B_i = \frac{1}{T} \sum_{t=-T}^T g(t) \sin\left(\frac{\pi f_i t}{T}\right), \quad (2.29)$$

$$f_i \in 1, 2, \dots, T. \quad (2.30)$$

A Fourier transform on discrete data can therefore be equivalently performed as a multiple linear regression of the time series onto the set of equal length sine and cosine series for all harmonic frequencies f_i . The above coefficients can be transformed to put the series in terms of harmonic frequencies with a particular amplitude α and phase ϕ , i.e., t offset of the first peak:

$$g(t) = \sum_{i=0}^T \alpha_i \cos(2\pi f_i t + \phi_i), \quad (2.31)$$

$$\alpha_i = \sqrt{A_i^2 + B_i^2}, \quad (2.32)$$

$$\phi_i = -\tan^{-1}\left(\frac{B_i}{A_i}\right) \quad (2.33)$$

α_i is thus the *amplitude spectrum* and ϕ_i is the *phase spectrum*. Either these, or the original coefficients A_i and B_i are all that are needed to reconstruct the original series from the frequencies.

By modifying the spectra and reconstructing the series, frequencies can be selectively filtered out. High-pass filtering tapers the amplitudes of only low frequencies to zero and can be used to remove mean-nonstationarity. Low-pass filtering tapers the amplitudes of high frequencies to zero and is one method of removing noise. This is because the spectrum of Gaussian white noise dominates the high frequency range. In most applications, measurement error or sensor noise also has a much lower vari-

ance than the signals of interest. Suppressing high frequencies can eliminate a greater proportion of error variance than the signal of interest, but it can also lead to artifacts and misleading smoothness.

The Fourier Transform has numerous other uses throughout signal processing, including data and image compression, edge detection, and analysis of the underlying structure of a series. In mathematics generally, it is commonly used to solve partial differential equations by reducing difficult systems to an infinite series of far simpler components. The Fourier Transform also has a number of non-sinusoidal generalizations, including Wavelet transforms[47], which serve many of the same purposes but with properties like localization of features.

Frequency-domain analyses are common in physiological studies, particularly EEG and fMRI where the activity of brain networks is characterized by rhythmic oscillations. Different frequencies, amplitudes, and synchronizations of electrophysiological activity in different regions of the brain appear to correspond respectively to the type, degree, and combination of different mental tasks. Frequency domain analyses also allow raw feeds of electrocardiogram (ECG) and respiration to be converted to series of heart rate and breaths-per-minute.

CHAPTER 3

STUDY I: WELL-BEHAVED PHYSIOLOGICAL SENSOR DATA, COMPLEX NONLINEAR MODEL

3.1 Introduction

Several previous studies have analyzed bodily sway patterns in quiet standing, and a variety of models have been proposed. In this study, we designed and tested a method of directly estimating the parameters of the Asai et al. [48] intermittent feedback control model of posture from experimental data. We begin with a brief review of prior models and the rationale for choosing a model of intermittent postural control (IPC). In the second section, we describe the current model in more detail and explain our framework for the estimation of its parameters. The third section describes simulation studies that tested the estimation capabilities of our framework when the data-generating parameters are known and the model is specified accurately. In the fourth section, we applied the model to experimental data and estimated sampling distributions for each parameter.

Observed trajectories of postural sway have largely been studied as a problem of stochastic behavior, though some studies have focused on its chaotic properties [49]. In this study, we too regarded postural sway as a random process subject to statistical analysis. The center of pressure (COP) on a force plate during quiet standing has been shown to exhibit the features of a bounded, random walk, or correlated noise [50]. Center of mass (COM) is one of the most common metrics of body sway but has to be inferred from other position and force metrics such as the COP [51]. For the small radius in which postural sway occurs, body tilt angle is nearly equivalent

to COM and has likewise been used to develop models of posture [48].

Many authors have observed that sway follows a two-frequency oscillation scheme, with fast oscillations of the COP around a drifting center point [52, 50, 53, 54]. Collins and De Luca [50] regarded these patterns as a combination of short-term, open-loop system with long-term closed-loop control. Alternatively, the “rambling and trembling” hypothesis suggests that short-term tremors result from corrective, closed-loop feedback that is activated with deviation of the COP from the ground projection of the COM, which is itself allowed to drift [54].

Broadly, more recent debate over the control scheme of human balance has focused on two kinds of models: continuous and intermittent feedback controllers. Continuous control is exerted through a proportional-integral-derivative (PID) or closed-loop system often characterized by a second order linear differential equation, sometimes including delayed proportional and derivative feedback. For instance, Maurer and Peterka [55] tested a PID inverted pendulum model that distinguishes passive, instantaneous feedback from sources such as ankle joint stiffness, from delayed, active feedback from the central nervous system and subsequent muscular response. Others have argued that human postural movement is better described by intermittent feedback mechanisms due to a smaller reliance on process noise, reproduction of cyclical behavior over multiple timescales, more efficient energy expenditure, and greater robustness to disturbances and instability caused by delays in neural signaling [56]. Simulations [57] and reinforcement learning [58] have been used to show that an upright pendulum, taken as a simple model of the standing human body, can exhibit stability and the observed slow oscillation patterns as a result of learned, time-delayed, intermittent feedback.

Intermittent activation models have taken multiple forms. Gawthrop and Wang [59] initially proposed clock-driven muscular feedback, but later considered event-

driven models [60]. Event-driven models are generally defined by a combination of stable and unstable manifolds in the phase space of the body’s position or angle. Gawthrop et al. [60] and Eurich and Milton [61] describe the behavior of systems with position-based thresholds that result in two stable equilibria. A model by Bottaro et al. [62] proposes boundary functions of both position and velocity that jointly determine probabilistic bursts of negative feedback. Asai et al. [48] reproduced a commonly observed double power-law structure in the PSD of sway [53] using similar control manifolds but with deterministic rules for sustained feedback activation. Their model requires only a simpler, Gaussian distribution of process noise with a smaller variance as compared to continuous PID models. Nomura et al. [63] showed that the same intermittent activation feedback model is capable of reproducing both chaotic and stochastic patterns that resemble human postural sway as a function of small hemodynamic perturbations, while continuous feedback models cannot.

A common method of estimating the parameters of each model is to simulate data that optimally resemble the experimental data. This is accomplished by varying parameters over iterations of simulation until resulting disparities on a set of key summary statistics have been minimized. Bottaro et al. [62] used the the Root Mean Square (RMS) of both the COP and COM series and each of its derivatives, unimodality of the series histogram, the length of largest oscillations calculated from zero crossings, and the PSD of the COP series. Maurer and Peterka [55] estimated parameters from observed data in a similar manner using mean velocity, RMS distance and velocity, spectral properties such as mean frequency, frequency dispersion, and total power. Asai et al. [48] used the double power law structure of the frequency spectrum as a criterion for the success of their model but did not demonstrate a direct empirical application. To obtain statistical information about estimated parameters, summary statistic methods have been combined with approximate Bayesian inference

[64]. This method was used to acquire empirical posterior distributions of five out of the eight parameters of interest [65].

While the simulation approach is flexible for a wide range of model specifications and levels of complexity, it risks overlooking attributes of the data that do not have specific effects on the chosen summary statistics. Bottaro et al. [62] notes, for instance, that “The intermittent nature of the control process cannot be detected by global descriptors of the sway patterns, like the PSD of the COP, because they cannot distinguish between asymptotic and bounded stability.” Furthermore, the amplitude spectrum is invariant to reversal of the signal, giving identical results for potentially different mechanisms of variation. This is problematic when the system includes discontinuous dynamics, such as a sharp impulse followed by a more gradual decay. An alternative approach that better accounts for fine-grained sequential dependence is to estimate the structural parameters directly from the data using Kalman filtering or other iterative techniques. No simulation or descriptive statistics are necessarily used, rather the structural parameters are estimated by minimizing an objective function such as the squared prediction error, or by maximizing the likelihood of the data according to an expected noise distribution. The results obtained by this approach can be sensitive to the exact predictive mechanisms specified in the model, and post-hoc analyses of the estimates can be highly informative about the types and degrees of misspecification. Direct estimation (sometimes called *exact* estimation by comparison [66]) may be particularly useful when the dynamic structure cannot be represented by any descriptive statistics with sufficient specificity. The Asai et al. [48] model of posture may present one such case in that it postulates dependence of the spectral power-law property upon nonlinear, physiological mechanisms of feedback control and their properties. Such properties include the delay in neural signaling, the sensitivity of feedback activation, and the strength of passive versus active corrective forces. Fur-

thermore, the process noise distribution of the Asai et al. [48] model is a Gaussian process and thus accords with the statistical assumptions of the Kalman filter. A drawback of direct estimation is that a misspecified model is not guaranteed to result in any interpretable or accurate parameter estimates if the parameters are highly dependent. If the parameter estimates deviate significantly from their theorized values, we may nonetheless analyze the behaviors they imply and draw general inferences.

The aim of this study was to validate and apply a method of directly estimating parameters for event-driven control with specific focus on the popular intermittent control model by Asai et al. [48]. Validation of this analytic strategy will set a foundation for estimating the parameters of alternative models and more comprehensive comparisons. Following the validation study, we estimated empirical values of each parameter from publicly available COM data [67] and compared our results with theoretically expected values from the literature. We included two previously demonstrated covariates in our analysis, visual feedback and age, to attempt to replicate previous findings as further evidence for the validity of the model.

3.1.1 Model

The intermittent postural control (IPC) model by Asai et al. [48] describes a tension between toppling torque due to gravity and a combination of active and passive resistance mechanisms. Passive resistance is proposed to come from leg stiffness and joint friction and is modeled with instantaneous relations between position, velocity, and acceleration. Active feedback control is proposed to arise from motor responses signaled by the central nervous system and is consequently delayed by about 190-210 ms [68].

The model is provided in terms of body tilt angle (θ) as follows:

$$I\ddot{\theta}_t = mgh\theta_t - T, \quad (3.1)$$

$$T = mghK\theta_t + B\dot{\theta}_t + mghf_P(\theta_{t-\tau}) + f_D(\dot{\theta}_{t-\tau}) + \sigma w_t, \quad w_t \sim N(0, 1), \quad (3.2)$$

where I is the rotational inertia, m is the body mass (kg), g is gravity ($\approx 9.81m/s^2$), and h is the height of the COM. T includes all the terms representing mechanisms of resistance to the angular toppling force. w_t is a Gaussian, independent and identically distributed random variable accounting for stochastic variation in acceleration, with standard deviation σ . The total passive forces may be written as $mgh(1 - K)\theta_t$, as K is the percentage of the gravitational acceleration counteracted by passive resistance. While a certain definition of B is not given, its effects are non-trivial and an interpretation may be taken from the common use of the second-order damped oscillator equation, in which the velocity coefficient represents negative feedback due to friction. In this case, it may be regarded as a measure of ankle and knee joint friction.

The active control terms, f_P and f_D , intermittently respond to θ on a time lag of $\tau \approx 200$ ms according to the conditions:

$$\text{if } \theta_{t-\tau}(s\dot{\theta}_{t-\tau} - \alpha\theta_{t-\tau}) > 0, \text{ and } \theta_{t-\tau}^2 + (s\dot{\theta}_{t-\tau})^2 > r^2 \begin{cases} f_P(\theta_{t-\tau}) = P\theta_{t-\tau} \\ f_D(\dot{\theta}_{t-\tau}) = D\dot{\theta}_{t-\tau} \end{cases} \quad (\text{Active}), \quad (3.3)$$

$$\text{otherwise } \begin{cases} f_P(\theta_{t-\tau}) = 0 \\ f_D(\dot{\theta}_{t-\tau}) = 0 \end{cases} \quad (\text{Inactive}) \quad (3.4)$$

The first condition represents a threshold dividing the saddle-type attractor of

the toppling acceleration into stable and unstable manifolds. The stable manifold briefly occurs when the tilt angle is moving toward zero, while the unstable manifold is characterized by falling away from zero. The angle of the dividing line is given by the slope parameter α . The second condition describes a radius (r) about the origin within which the tilt angle is too small to be detected or too stable for immediate correction (note that r has conventionally been used to denote the delay time interval in the delay differential equation literature. Here we have preferred τ for that purpose.). By converting the switching threshold slope α into the angle a as $\alpha = \frac{\sin(a\pi)}{\cos(a\pi)}$, we change the upper and lower estimation bounds from $[-\infty, \infty]$ to $[0, 1]$. This way, the parameter a represents the percentage of the phase space, not including the insensitivity radius, for which the active control parameters are non-zero.

The estimable parameters of the SDDE are summarized in Table 1. Many of the parameters have previously been estimated in a variety of ways, sometimes with highly varied results. Tietäväinen et al. [65] used the approximate Bayesian inference [64] with data simulation to estimate P , D , a , τ , and σ . Among these, the method failed to obtain precise distributions for D in both simulations and empirical application. It is also not clear whether fixing the other parameters to uncertain theoretical priors ($K = .8$, $B = 4$, and $r = .004$) results in biased estimates. Direct physiological measurements found the relative resistance to toppling torque at the ankle, K , to be as high as 91% on average [69] when the average magnitude of disturbance is small. Another study estimated relative resistance to be around 64% when disturbances were larger [70]. Conversely, the chosen value of r involves a conjecture about perceptual sensitivity that is specific to this model and has not been measured directly.

Tietäväinen et al. [65] obtained a value of τ around 300 ms, while other methods of assessment have produced estimates including 125 ms [71] and 200 ms [68]. Direct measurements of ankle response, however, found response to start at 30 ms with

Table 1.: Parameters of the IPC model with units and descriptions.

Fixed / Observed		Unit
I	Inertia	(kgm) ²
m	Body mass	(kg)
h	Distance of center of mass from the ankle	(m)
g	Acceleration from gravity	(m/s ²)
Estimated		
K	Intrinsic upright stiffness	% (of total Nm/rad)
B	Joint friction	Nms/rad
P	Active response force	Nm/rad
D	Active response damping	Nms/rad
a	Percentage of phase space active	%
r	Insensitivity radius	rad
τ	Feedback delay	s
σ	Process noise variance	Nm
ϵ	Measurement error variance	rad

maximal displacement around 120 ms [72]. If feedback delay is too long, then intermittent periods of acceleration due to gravity or muscle feedback will be consequently prolonged even as the state enters unstable regions of the phase space. One result is overcompensation for error, in which the fast oscillations found in sway are more amplified than would be the case with shorter delays. Alternatively, if the value of a is too high, then delayed feedback may bypass the unstable manifold and activate at inappropriate locations in the phase space, potentially amplifying slower oscillations over time. Long feedback delays can therefore contribute to instability, sway ampli-

fication, and higher risk of falling, but the exact kinds of error are determined by the joint behavior of several parameters, including a , r , and disturbance magnitude σ [48].

3.1.2 Estimation

The above equations represent a Stochastic Delay Differential Equation (SDDE). The Kalman-Bucy filter provides minimum-variance unbiased estimates of the state of a stochastic process when both measurement and process noise are present and can be used to estimate the parameters of continuous-time differential equations from noisy data [46]. However, two challenges arise when estimating the parameters of an SDDE, including the lag interval τ and the lagged position and velocity coefficients, P and D . First, interpolation of the lagged states must be used to allow a continuous domain of possible values for τ . Second, backward extrapolation must be used to estimate the unmeasured interval of lagged states preceding initial state \mathbf{x}_0 .

Last, we address problems that occur when the discrete switching conditions are toggled between measured instances. For most intervals between measures, the dynamics are linear and the prediction is exact, but state predictions that traverse the condition thresholds will systematically introduce bias to the linear dynamics unless the correct ratio of active and inactive dynamics within each traversal is estimated. We detail an algorithm to resolve this bias by adjusting the prediction according to each of the possible threshold-traversal scenarios.

3.1.2.1 Optimal filtering

The state-space equation for the time-lagged IPC system is given as

$$\dot{\mathbf{x}}_t = \mathbf{A}\mathbf{x}_t + \mathbf{A}_\tau\mathbf{x}_{t-\tau} + \mathbf{Q}, \quad (3.5)$$

$$\mathbf{y}_t = \mathbf{H}\mathbf{x}_t + \mu + \mathbf{R}, \quad (3.6)$$

where \mathbf{Q} is the process noise covariance matrix, \mathbf{H} is the measurement matrix, μ is the estimated origin about which the COM oscillates, and \mathbf{R} is the covariance matrix of measurement error. The contemporaneous and lagged state vectors are

$$\mathbf{x}_t = \begin{bmatrix} x_t \\ \dot{x}_t \end{bmatrix}, \quad \dot{\mathbf{x}}_t = \begin{bmatrix} \dot{x}_t \\ \ddot{x}_t \end{bmatrix}, \quad \mathbf{x}_{t-\tau} = \begin{bmatrix} x_{t-\tau} \\ \dot{x}_{t-\tau} \end{bmatrix},$$

and the state transition matrices are

$$\mathbf{A} = \begin{bmatrix} 0 & 1 \\ mgh(1-K)/I & -B/I \end{bmatrix}, \quad \mathbf{A}_\tau = \begin{bmatrix} 0 & 0 \\ -mghP/I & -D/I \end{bmatrix}, \quad \mathbf{Q} = \begin{bmatrix} 0 & 0 \\ 0 & \sigma^2 \end{bmatrix},$$

Matrix \mathbf{A} contains the parameters of the passive, instantaneous forces, while \mathbf{A}_τ contains the conditional parameters of active feedback. When the conditions given in Eq 3.3 evaluate to false, $\mathbf{A}_\tau = 0$.

The measurement matrices simply attribute the observed COM to the state position with estimated origin μ and measurement error variance ϵ :

$$\mathbf{H} = \begin{bmatrix} 1 & 0 \end{bmatrix} \quad \mathbf{R} = \begin{bmatrix} \epsilon \end{bmatrix}$$

The complete algebra for the prediction and correction steps of Kalman Filtering is excluded, as its derivation can be found in many resources [36] and remains largely unchanged for this model. However, the key difference in this case is that the prediction step is altered to include the delayed term. Using the following matrix

discretizations,

$$\mathbf{A}^d = e^{\mathbf{A}\Delta t}, \quad (3.7)$$

$$\mathbf{A}_\tau^d = \mathbf{A}^{-1}(\mathbf{A}^d - \mathbf{I})\mathbf{A}_\tau \quad (3.8)$$

$$\mathbf{Q}^d = \int_{\delta=0}^{\Delta t} e^{\mathbf{A}\delta} \mathbf{Q} e^{\mathbf{A}\delta\mathbf{T}} d\delta \quad (3.9)$$

we can then provide the prediction equations for the state mean and covariance as follows:

$$\hat{\mathbf{x}}_{t+\Delta t} = \mathbf{A}^d \bar{\mathbf{x}}_t + \mathbf{A}_\tau^d \bar{\mathbf{x}}_{t-\tau+\Delta t} \quad (3.10)$$

$$\hat{\mathbf{P}}_{t+\Delta t} = \mathbf{A}^d \bar{\mathbf{P}}_t \mathbf{A}^{d\mathbf{T}} + \mathbf{A}_\tau^d \bar{\mathbf{P}}_t \mathbf{A}_\tau^{d\mathbf{T}} + \mathbf{Q}^d \quad (3.11)$$

For stationary series with large number of observations, $\mathbf{P}_t \approx \mathbf{P}_\infty$. For convenience, we use \mathbf{P}_{t-1} as an approximation to $\mathbf{P}_{t-\tau}$. Note that Eq 3.8 does not work if $K = 1$, making \mathbf{A} singular. However, small, numerically viable deviations from $K = 1$ will not substantially impact solution topology. Point singularities will also not impede derivative-free optimization methods.

3.1.2.2 Estimation of feedback delay

Linear interpolation To obtain estimates of the state at time lags that do not fall on measurement instances, we use linear interpolation of the state:

$$\lambda = \frac{\tau}{\Delta t}, \quad (3.12)$$

$$\hat{\mathbf{x}}_{t-\tau} = \mathbf{x}_{i-\lfloor\lambda\rfloor} + (\mathbf{x}_{i-\lfloor\lambda\rfloor} - \mathbf{x}_{i-\lceil\lambda\rceil})(\lambda - \lfloor\lambda\rfloor), \quad (3.13)$$

λ is the conversion of the time delay to the number of measured occasions comprising that interval. The ceiling and floor functions thus give valid measurement indices and are used to give a combination of measurements falling to either side of λ , weighted

proportionally. If $\tau = 0$, then the second term of Eq 3.13 can be neglected.

Backward extrapolation of initial values By introducing an initial value parameter for acceleration, we can estimate a quadratic extrapolation backward from t_0 to $t_0 - \tau$, allowing the influence of lagged states and switching conditions to be respected within the first λ iterations of filtering:

$$\text{If } t \leq \tau \begin{cases} \hat{x}_{t-\tau} = x_0 + \dot{x}_0(t - \tau) + \ddot{x}_0(t - \tau)^2, \\ \hat{\dot{x}}_{t-\tau} = \dot{x}_0 + 2\ddot{x}_0(t - \tau), \end{cases} \quad (3.14)$$

3.1.2.3 Constrained interpolation of dynamic switching points

To avoid bias due to missing transitional information between measures that straddle the threshold of the conditions given by Eq 3.3, we explicitly detect each case, interpolate the state falling on the condition threshold, and predict its traversal in two steps. For convenience, take the shortened terms u and v as the delayed states leading up to, and away from the condition threshold:

$$\begin{aligned} u &:= x_{t-\tau}, & \dot{u} &:= s\dot{x}_{t-\tau} \\ v &:= x_{t-\tau+\Delta t}, & \dot{v} &:= s\dot{x}_{t-\tau+\Delta t}, \end{aligned} \quad (3.15)$$

Where s is the seconds constant, such that v, u, \dot{v} , and \dot{u} are measured in radians. For use later, we note here that the slope between the two points is $m = \frac{\dot{v}-\dot{u}}{v-u}$.

Conditions for switching off:

$$\text{If } [u(\dot{u} - \alpha u) > 0 \text{ and } u^2 + \dot{u}^2 > r^2] \text{ and } [v(\dot{v} - \alpha v) \leq 0 \text{ or } v^2 + \dot{v}^2 \leq r^2], \quad (3.16)$$

then A_τ is switching off. If this holds true, then the following conditions further apply:

$$\begin{aligned}
& \text{If } v^2 + \dot{v}^2 > r^2 \\
& \text{and } ![(v > 0 \text{ and } \dot{v} < 0 \text{ and } u < 0 \text{ and } \dot{u} < 0) \\
& \text{or } (v < 0 \text{ and } \dot{v} > 0 \text{ and } u > 0 \text{ and } \dot{u} > 0)], \tag{3.17}
\end{aligned}$$

then the lagged state is traversing the line $\dot{x} = \alpha x$ outside of the slack radius and not traversing $u = 0$. The interpolated point $(\hat{u}, \hat{\dot{u}})$ falls on the line, and is calculated as

$$\hat{u} = -\frac{mv - \dot{v}}{\alpha - m}, \quad \hat{\dot{u}} = m\hat{u} - mv + \dot{v}, \tag{3.18}$$

If $v^2 + \dot{v}^2 \leq r^2$, then the lagged state is traversing into the slack radius, and the interpolated point is

$$\hat{u} = \frac{r^2 + v^2 + 2mv\dot{v} - \dot{v}^2}{2(v + m\dot{v})}, \quad \hat{\dot{u}} = m\hat{u} - mv + \dot{v}, \tag{3.19}$$

In all other cases in which (3.16) holds true, u is traversing the axis at $u = 0$.

$$\hat{u} = 0, \quad \hat{\dot{u}} = -mv + \dot{v}, \tag{3.20}$$

Conditions for switching on: For cases where the delayed feedback is switching on, the roles of u and v are simply traded. The interpolated point is calculated identically under each set of conditions analogous to those for switching off.

$$\text{If } [u(\dot{u} - \alpha u) \leq 0 \text{ or } u^2 + \dot{u}^2 \leq r^2] \text{ and } [v(\dot{v} - \alpha v) > 0 \text{ and } v^2 + \dot{v}^2 > r^2], \tag{3.21}$$

then \mathbf{A}_τ is switching on. If this holds true, then the following conditions further apply:

$$\begin{aligned} &\text{If } v^2 + \dot{v}^2 < r^2 \\ &\text{and } ![(u > 0 \text{ and } \dot{u} < 0 \text{ and } v < 0 \text{ and } \dot{v} < 0) \\ &\text{or } (u < 0 \text{ and } \dot{u} > 0 \text{ and } v > 0 \text{ and } \dot{v} > 0)], \end{aligned} \quad (3.22)$$

then the lagged state is traversing the line $\dot{x} = \alpha x$ outside of the slack radius and not traversing $u = 0$, and the interpolated point is calculated as equation (3.18). If $u^2 + \dot{u}^2 \leq r^2$, then the lagged state is traversing the slack radius from within, and the interpolated point is calculated with equation (3.19). In all other cases in which equation (3.21) holds true, u is traversing the axis at $u = 0$ and the interpolated point is calculated as equation (3.20).

Prediction for threshold traversal: The time for u to reach the switching threshold, Δt^- , and the time to reach the next observation after the threshold, Δt^+ , can be calculated from the interpolated state at the threshold and its neighboring states, u and v :

$$\Delta t^- = \frac{\|\mathbf{u} - \hat{\mathbf{u}}\|}{\|\mathbf{v} - \mathbf{u}\|} \Delta t, \quad \Delta t^+ = \frac{\|\mathbf{v} - \hat{\mathbf{u}}\|}{\|\mathbf{v} - \mathbf{u}\|} \Delta t, \quad (3.23)$$

In the first step, \mathbf{A} , \mathbf{A}_τ , and \mathbf{Q} are discretized for the interval Δt^- , and the prediction is given as:

$$\hat{\mathbf{x}}_{t+\Delta t^-} = \mathbf{A}^d \bar{\mathbf{x}}_t + \mathbf{A}_\tau^d \mathbf{u} \quad (3.24)$$

$$\hat{\mathbf{P}}_{t+\Delta t^-} = \mathbf{A}^d \bar{\mathbf{P}}_t \mathbf{A}^{d\Gamma} + \mathbf{A}_\tau^d \mathbf{P}_t \mathbf{A}_\tau^{d\Gamma} + \mathbf{Q}^d. \quad (3.25)$$

In the second step, \mathbf{A} , \mathbf{A}_τ , and \mathbf{Q} are discretized for the interval Δt^+ , and the

prediction is computed from time $t + \Delta t^-$ as:

$$\hat{\mathbf{x}}_{t+\Delta t} = \mathbf{A}^d \hat{\mathbf{x}}_{t+\Delta t^-} + \mathbf{A}_\tau^d \hat{\mathbf{u}} \quad (3.26)$$

$$\hat{\mathbf{P}}_{t+\Delta t} = \mathbf{A}^d \hat{\mathbf{P}}_{t+\Delta t^-} \mathbf{A}^{dT} + \mathbf{A}_\tau^d \hat{\mathbf{P}}_{t+\Delta t^-} \mathbf{A}_\tau^{dT} + \mathbf{Q}^d. \quad (3.27)$$

For either step, $\mathbf{A}_\tau^d = 0$, depending on whether the active feedback is switching on or off.

3.1.2.4 Optimization

The toggling of active feedback is not a smooth process and results in discontinuities in the space of a cost function for fitting the model, though these are greatly mitigated by the interpolation measures described above. The complexity of the model nonetheless gives rise to multiple local solutions, and attempts to find optimal parameters using local methods such as gradient descent and Nelder-Mead reliably fail. Instead, we recommend using a method of global, derivative-free optimization such as Differential Evolution (DE) [73]. The optimization parameters that we chose are listed below.

- Strategy: DE / rand / 1 / bin with per-vector-dither
- Iterations = 15000
- Population size = 30
- Crossover Probability (CR) = .95
- F = .15
- Weighting of successful members (c) = 0
- Step tolerance: 500

- Relative tolerance: 1e-10

We chose a high crossover probability (CR) due to high dependence between parameters of the model and used simulations to confirm reasonable convergence given the chosen population size, iterations, and F value. DE does not require initial values for parameter estimation, but instead populates a region within explicit bounds. The bounds used here for simulation and data analysis are given in Table 2. Parameter bounds were generally restricted to potentially stable and theoretically meaningful ranges, such as for K , P , r , and τ . Theoretical interpretations of parameters B and D were less certain and were therefore allowed to vary beyond boundaries imposed under any particular physiological definition. τ was constrained to the extremes of the empirical distribution of neural delay given the results from Peterka [68]. Otherwise, bounds were made extreme enough to capture all reasonable possibilities without unnecessarily slowing convergence.

3.1.2.5 Software

All analyses used R statistical programming environment [74]. Differential Evolution was provided by the R package DEoptim [75]. The IPC model was implemented in C++ using R packages Rcpp [76] and RcppArmadillo [77], and compiled to the open-source R package `IPCmodel`. The package includes the following functions:

- `ipcModel()`: C++ Kalman Filter with delayed terms and switching conditions that returns a -2Log-likelihood value for optimization.
- `ipcSimulate()`: C++ numerical integrator that generates simulated data for the IPC model.
- `ipcMultiGroup()`: R wrapper for `ipcModel()` that incorporates physical constants, parameter algebras, and enables the estimation of both within and

Table 2.: Optimization bounds for all parameters

Par.	Domain
K	$[0, 1]$
B	$[-1000, 1000]$
P	$[0, 2]$
D	$[-1000, 1000]$
a	$[0, 1]$
r	$[0, 2]$
τ	$[0.15, 0.25]$
σ_w	$[0, 5]$
σ_ϵ	$[0, 1]$
$x_{0,i}$	$[-10, 10]$
$\dot{x}_{0,i}$	$[-50, 50]$
$\ddot{x}_{0,i}$	$[-100, 100]$
μ_i	$[-20, 20]$

between-series parameters.

- `kalmanIntegrate()`: C++ helper function that accepts continuous-time state-space matrices and returns discretized matrices for Kalman-Bucy filtering.

3.2 Simulations

Two simulations were used: the first to check model specification, and the second to evaluate the accuracy and precision of parameter estimates. The first simulation used noiseless (i.e. deterministic trajectories) with perfect measurement to check for systematic bias due to the estimation strategy. The second simulation used data

simulated to include both process and measurement noise according to the possible properties of real data recorded by a force plate. Solutions for both deterministic and noiseless simulations were generated in linearized steps of size 10^{-5} s then down-sampled according to the design of each simulation. This procedure ensured both numerical accuracy of solutions and simulated real world mapping of analogue processes to discrete measurements. The statistical properties of simulated series were expected to be invariant to downsampling due to the fractal property of continuous random walks (i.e., Wiener processes) where $\Delta t \sim N(0, \Delta t)$.

3.2.1 Parameter sets

Six sets of simulated parameters were defined to test the model’s estimation capability over a variety of possible behaviors and are shown in Table 3. The first set replicates the simulated data for Model 4 by Asai et al. [48] and is named accordingly. The second and third sets (“Low Noise” and “High Noise”) respectively decrease and increase the variance of process noise to examine its effect on other parameters. The fourth and fifth (“Active Control” and “Passive Control”) sets respectively increase and decrease the ratio of active to passive control, representing different plausible configurations for stability. The sixth set (“Rambling and Trembling”) represents a stationary random-walk series that diverges markedly from the underlying theory but is nonetheless a stable and plausible configuration.

3.2.2 Sim 1: Noiseless series

To test for improper model specification and systematic sources of bias, noiseless series were generated to span 20s, with a step size of 10^{-5} s, then downsampled to an observation every 0.01s and again to every 0.1s. The noiseless series used in the first simulation are shown in Figure 3. Only one series per set and per downsample

Table 3.: Parameter sets for generating simulated data

	K	B	P	D	a	r	τ	σ	ϵ
Asai et al.	0.80	4.00	0.25	10.00	0.62	0.40	0.20	0.20	1E-04
Low Noise	0.80	4.00	0.25	10.00	0.62	0.40	0.20	0.05	1E-04
High Noise	0.80	4.00	0.25	10.00	0.62	0.40	0.20	1.00	1E-04
Passive Control	0.95	4.00	0.15	10.00	0.50	0.70	0.20	0.20	1E-04
Active Control	0.75	4.00	0.70	120.00	0.80	0.20	0.20	0.20	1E-04
Rambling and Trembling	0.98	500.00	0.20	-50.00	0.45	0.05	0.20	2.00	1E-04

rate was used, as there were no sources of sampling error. To ensure that estimates converged to a high degree of precision, 3000 iterations of optimization were used.

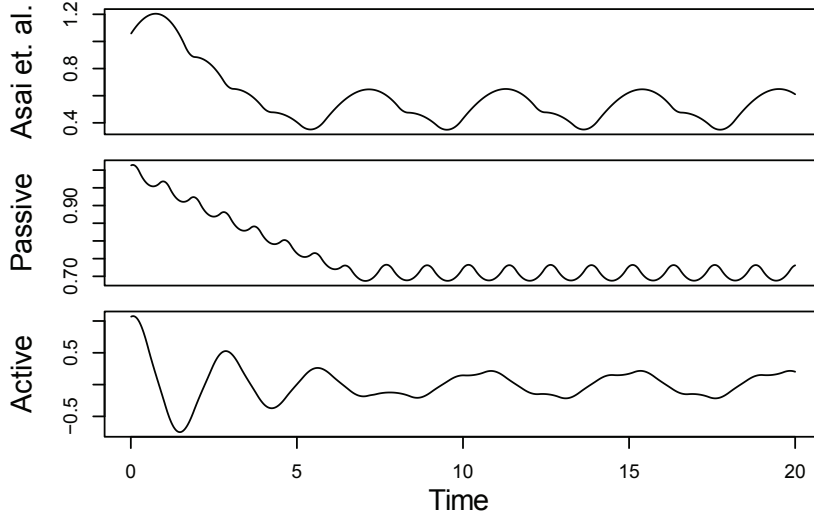


Fig. 3.: Noiseless series with initial values $x_0 = 1, \dot{x}_0 = 0$

Table 4 contains the parameter estimates for these simulations, with sampling rate shown to the left. Only the velocity coefficients B and D exhibited substantial bias all throughout, and the “High Active” set incurred the greatest bias over nearly all parameters. Most parameter estimates given 100Hz sampling were exact to at

Table 4.: Parameter point estimates for simulated noiseless series. Downsampling rate in Hz is shown in the left column. See Table 3 for the true, data-generating parameter values of each set.

Hz	Set	K	B	P	D	a	r	τ	σ
100	Asai et al.	0.80003	4.10640	0.24996	10.62579	0.62000	0.40000	0.20001	0.00000
	Passive Control	0.95000	4.08142	0.14998	10.46709	0.50000	0.70000	0.20000	0.00000
	Active Control	0.75086	4.09833	0.69372	122.07313	0.79987	0.19990	0.20020	0.00000
10	Asai et al.	0.80024	5.65678	0.24975	15.62635	0.62030	0.39914	0.20000	0.00000
	Passive Control	0.95001	5.40384	0.14939	19.03988	0.49999	0.70016	0.19978	0.00001
	Active Control	0.74853	4.17357	0.63636	140.82292	0.80120	0.19951	0.20097	0.00022

least 3-5 decimal places. Reducing sampling resolution by a factor of ten increased biases to parameters B and D by a factor of ten to fifteen, but much less so for K and P . The nonlinear parameters a , r , and τ exhibited the least bias for all sets.

The small biases to K , B , P , and D most likely occur as a result of the approximate, linear interpolation methods and inability to account for process noise before t_0 in the quadratic backward extrapolation. Biases may be further mitigated using polynomial interpolation of the lagged state. However, the exact accuracy of the estimated τ indicates that bias from linear interpolation is probably trivial in this case.

A second source of bias may be the limits of numerical precision. When no noise is present in the system, the state only occupies a small area of the phase space where certain values of B and D may have nearly unobservable effects on the solution. We show later that relatively unbiased estimates of B and D can indeed be obtained as a function of the other parameters, including the process noise variance σ .

3.2.3 Sim 2 Estimation from noisy data

To test the precision and accuracy of IPC parameter estimates given the dimensions and expected structure of the data from Santos et al. [67], one-hundred individuals were simulated for each parameter set in Table 3, with examples series shown in Figure 4. Each individual consisted of three trials, and each trial consisted of a 60s series downsampled to 100 Hz. The same parameters were estimated for all three trials, making for a total of 18,000 observations per individual model.

Figs 5a through 5f show the sampling variation and bias for each parameter set. Boxplots are grouped by common axis scale. Table 5 gives the means and standard deviations of each parameter for each set.

Variance and biases across all parameters were highly interdependent. Estimates of both process noise (σ) and measurement error were precise and close to their true values, indicating successful filtering of the state. The precision of active and passive control parameters depended on their true values and the resulting behavior of the process. For the Asai et al. replication and the sets with low and high process noise, most control parameters had only small bias and high precision, while others were less reliable under particular conditions. The greatest apparent contrast may be the insensitivity radius r , which was not estimable for the Rambling and Trembling set in which its true value was small, and much less reliable in the increased noise set where its value matched Asai et al.

The B and D parameters were the least reliable, and are possibly empirically unidentified without a sufficiently high process noise variance. This is evident from the increased noise set (Figure 5d) and the Rambling and Trembling set (Figure 5b). The active control set (Figure 5f) also showed successful estimation of the B parameter, and improvements in estimating D over the the Asai et al. set, low noise,

Table 5.: Simulation results: Means (μ) and standard deviations (σ) of estimated parameters over 100 iterations of simulation for six parameter sets. True values are given in Table 3, and parameter descriptions are given in Table 1.

Par.		Asai et al.	Low Noise	High Noise	Low Active	High Active	Ramb./Tremb.
K	μ	0.820	0.814	0.812	0.955	0.789	0.978
	σ	0.021	0.017	0.017	0.008	0.067	0.025
B	μ	15.654	22.278	4.203	9.811	6.350	504.441
	σ	10.727	13.743	9.631	6.922	4.743	28.426
P	μ	0.228	0.231	0.235	0.139	0.694	0.301
	σ	0.020	0.017	0.016	0.011	0.071	0.211
D	μ	-0.511	-3.337	11.039	7.556	101.869	-138.941
	σ	14.490	14.398	13.258	14.042	9.850	281.247
a	μ	0.621	0.623	0.620	0.505	0.813	0.481
	σ	0.006	0.005	0.004	0.008	0.016	0.072
r	μ	0.410	0.402	0.494	0.712	0.202	0.609
	σ	0.037	0.006	0.210	0.024	0.014	0.322
τ	μ	0.174	0.170	0.178	0.162	0.177	0.176
	σ	0.013	0.011	0.009	0.010	0.013	0.023
σ	μ	0.216	0.060	1.008	0.207	0.206	2.117
	σ	0.014	0.005	0.049	0.011	0.011	0.134
ϵ	μ	9.98E-05	1.00E-04	9.96E-05	1.00E-04	9.98E-05	9.99E-05
	σ	1.07E-06	1.16E-06	1.08E-06	1.04E-06	1.08E-06	1.15E-06

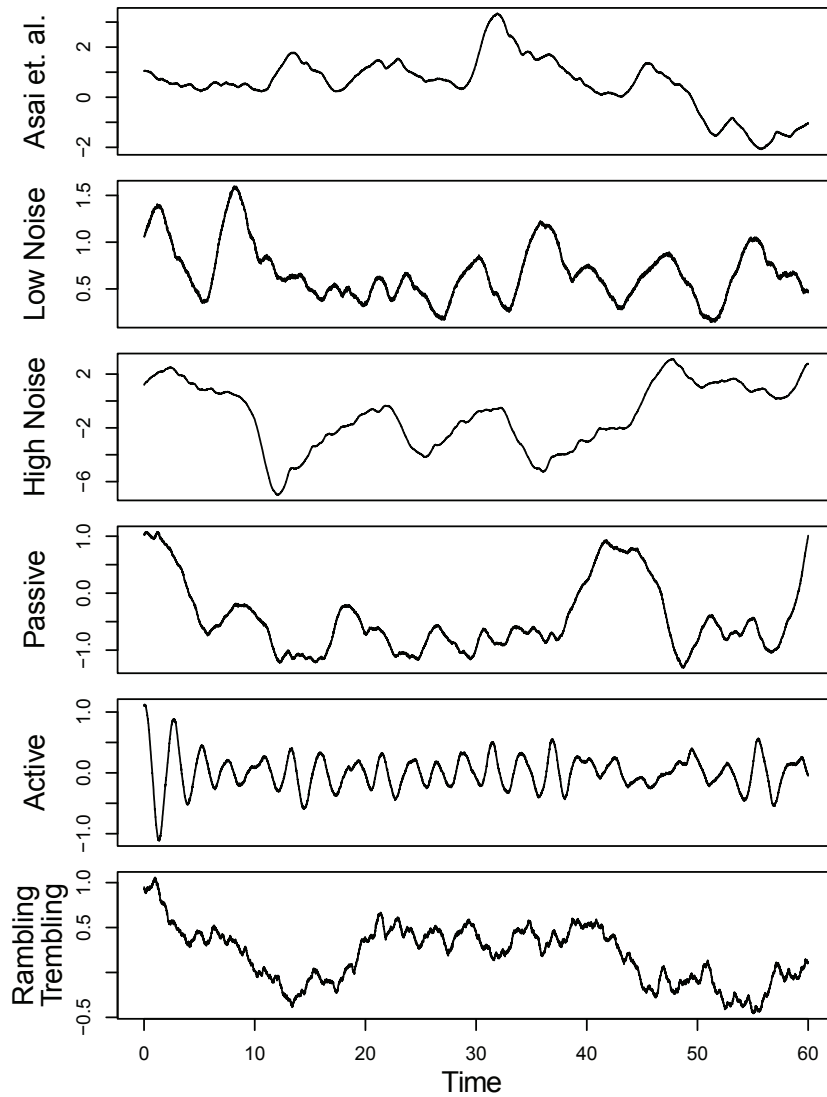
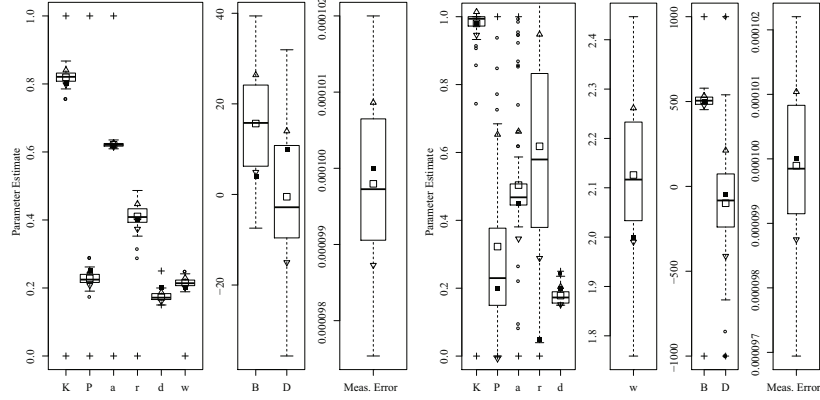


Fig. 4.: Examples of simulated series from six parameter sets.

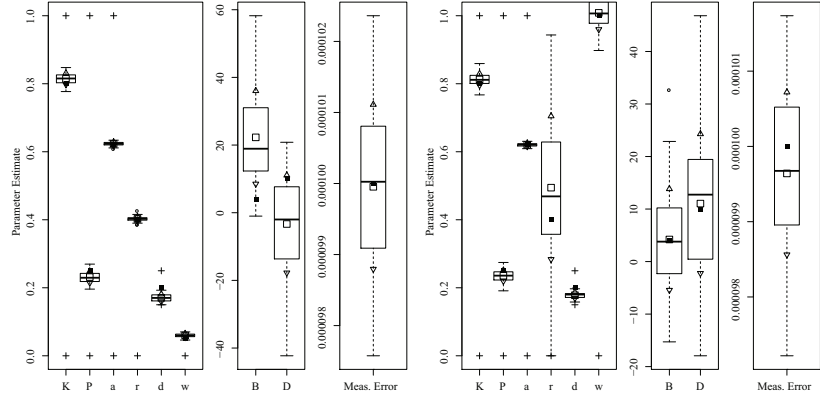
and passive control.

From the variation in results across sets, it can be inferred that a parameter can only be estimated reliably when the state occurs for a sufficient amount of time in the portions of the phase space for which that parameter has an influence. For instance, the insensitivity radius will not be estimable if the state tends to bypass it entirely. This may be due to a large variance of process noise, or for large values



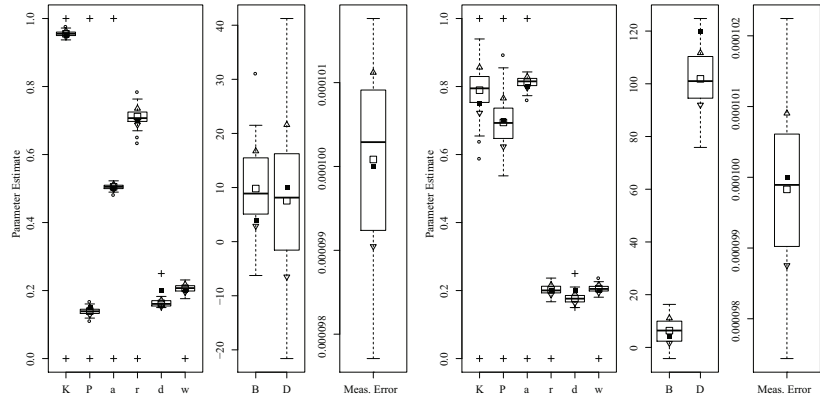
(a) Asai et al.

(b) Rambling and Trembling



(c) Low Noise

(d) High Noise



(e) Passive Control

(f) Active Control

Fig. 5.: Parameter recovery results for each parameter configuration. Black squares: data-generating value; Empty squares: Estimate mean; Triangles: Upper and lower std. dev.; Circles: Outliers; Crosses: Optimization boundaries.

of B that distort the saddle shape of the passive attractor space, causing an orbital path that never intersects the origin. Likewise B and D cannot be estimated reliably if the process does not frequently visit the extremes of the phase space where their influence is most apparent.

Empirical under-identification of some parameters is not necessarily problematic for the others, and does not imply the unreliable parameters should be fixed to some value or excluded. Two solutions to empirical under-identification are to increase the length and resolution of the sample to increase the chances of observing informative behavior, and perhaps to introduce small interventions or disturbances such that subjects express the full range of relevant dynamic behaviors.

Standing apart from the other parameters is the feedback delay τ . Despite perfect accuracy in the noiseless case, it tended to bias downwards when estimated from noisy data. It is unclear from our simulations why the bias occurs and whether it accounts for bias to other parameters. However, the estimates were not generally boundary cases, and the sampling variability was small. If the bias is consistent, the delay parameter should still be comparable between persons, with the caveat that the estimate is understated by 20-40ms.

3.3 Data Analysis

The IPC model was fit to empirical postural control data to 1) estimate the multivariate distributions of each parameter, 2) test for expected effects from age and visual feedback, 3) test the consistency of parameters within-person, 4) compare the proposed model to simpler alternatives. COM data were obtained from the data set published for public use by Santos et al. [67] and included 49 individuals at 100Hz for 60 seconds per trial. Three trials were conducted with eyes open, and three with eyes closed. Only trials tested with a rigid floor were used for our analyses. Height

and weight were provided for each individual and included as the constants h and m in the model, scaled to units of meters and kilograms respectively. Height was scaled by 0.51, the approximate ratio of vertical COM to total height in upright standing (calculated from Table 1, p.7 of [70]). By visual inspection of the sample, it was found that the first and last several seconds of many series contained large, sudden changes in position likely relating to movement during the initiation and termination of the trial period. To ensure that only the stationary dynamics of interest were modeled, 500 occasions were trimmed from the beginning and end of each series, leaving 5000 occasions or 50 seconds of data per trial, and 30,000 measurements in total per individual.

Models Three models were fit to each of three trials per individual to examine the statistical significance of the parameters involved in intermittent activation and delayed feedback. The models included, in descending order of complexity, the complete intermittent stochastic delay differential equation (ISDDE),

$$I\ddot{\theta}_t = mgh(1 - K)\theta_t + B\dot{\theta}_t + mghf_P(\theta_{t-\tau}) + f_D(\dot{\theta}_{t-\tau}) + \sigma w_t, \quad (3.28)$$

a stochastic delay differential equation (SDDE) with delayed feedback but no intermittent switching conditions,

$$I\ddot{\theta}_t = mgh(1 - K)\theta_t + B\dot{\theta}_t + mghP\theta_{t-\tau} + D\dot{\theta}_{t-\tau} + \sigma w_t, \quad (3.29)$$

and a stochastic differential equation (SDE) containing only instantaneous, continuous PID control terms:

$$I\ddot{\theta}_t = mgh(1 - K)\theta_t + B\dot{\theta}_t + \sigma w_t. \quad (3.30)$$

All models included trial-specific initial conditions $x_{0,i}$ and $\dot{x}_{0,i}$ and sway origins

μ_i for $i \in [1, 2, 3]$. The ISDDE and SDDE both included trial-specific estimation of $\ddot{x}_{0,i}$ for backward extrapolation. All models included measurement error variance σ_ϵ . Parameter boundaries, shown in Table 6 reflected both theoretical and analytic roles of each parameter. For example, B could not be less than zero in the ISDDE because it is conjectured to represent ankle stiffness, and stability is required to come from values of P and D in the given domains. In the SDE, stable solutions must rely on only instantaneous feedback with coefficients K and B . In the absence of other theoretical mechanisms, the same physiological interpretations of K and B could not be assumed and thus the same theoretical constraints were not applied.

Multiple regression was used to test the association between each parameter, visual feedback, and age, accounting for height and mass as covariates. Pearson correlation was used to estimate the correlation between parameter estimates during trials with eyes open and trials with eyes closed. Maximum likelihood estimation was used to fit each model, assuming the multivariate normality of measurement and process noise.

The estimated means $\hat{\mu}$, standard deviations $\hat{\sigma}$, and medians of each estimated parameter across all trials \times participants \times visual feedback conditions, are given in Table 7. The estimated individual-level intraclass correlations (ρ_{ICC}), effect sizes, and p -values for age and visual feedback are also given for each model. Measurement error estimates were generally small ($\sigma_\epsilon < 1e - 3$) and were omitted from the tables. Minor, trial-specific “nuisance” parameters including sway origins and initial values were also omitted. Mean sway origin was estimated to be 0.217, with a standard deviation of 0.11 and a median of 0.226.

The estimated parameters of the ISDDE fell within the expected domains. Several parameters of the ISDDE had outliers that substantially inflated estimates of their standard deviations. Trimmed standard deviations in which the highest 15 val-

Table 6.: Optimization boundaries [lower, upper] for each parameter, under each model.

Par.	ISDDE	SDDE	SDE
K	[0, 1]	[0, 1]	[-10, 10]
B	[0, 2000]	[0, 2000]	[-2000, 2000]
P	[0, 2]	[-2, 2]	
D	[-2000, 2000]	[-2000, 2000]	
a	[0, 1]		
r	[0, .1]		
τ	[0, 1]	[0, 1]	
σ	[0, 5]	[0, 5]	[0, 100]
ϵ	[0, .03]	[0, .03]	[0, 10]
x_0	[-5, 5]	[-5, 5]	[-5, 5]
\dot{x}_0	[-150, 150]	[-150, 150]	[-150, 150]
\ddot{x}_0	[-500, 500]	[-500, 500]	
Origin	[-1, 1]	[-1, 1]	[-1, 1]

ues were excluded are given in parentheses in Table 7. The marginal distributions of each parameter with these trimmed means and standard deviations are shown in Figure 6. B , P , D , and r in particular were skewed upward by outliers but otherwise had relatively precise distributions about their medians, with similar precision to those of the SDDE. K had consistent values around .91 to .93 in all three models. B was close to zero for most series but skewed upward by outliers as high as 80. In the SDE, B was allowed to take negative values but had a mean around 17. All values of B in the SDE were positive and greater than zero, with a minimum of .82. a was

Table 7.: Summary statistics, effects of age and vision accounting for height and mass, and person-level intraclass correlations of parameter estimates under each model. Bonferroni adjusted $\alpha = .0029$.

	$\hat{\mu}$	$\hat{\sigma}$ (Trimmed)	Median	β_{Vision}	CI	p	β_{Age}	CI	p	ρ_{RC}
ISDDE	K	0.920	0.021 (0.019)	0.920	0.002	(0, 0.004)	0.133	(1.9e-5, 1.3e-4)	*0.009	0.912
	B	3.057	10.223 (5.2)	0.000	1.019	(-1.314, 3.352)	0.393	(-0.144, -0.012)	*0.023	0.191
	P	0.174	0.272 (0.066)	0.116	0.048	(-0.015, 0.111)	0.132	(-0.004, 0)	0.074	-0.025
	D	154.789	160.153 (47)	131.123	-20.307	(-57.37, 16.76)	0.284	(-1.097, 1.011)	0.936	0.040
	a	0.730	0.259 (0.26)	0.853	-0.055	(-0.114, 0.004)	0.069	(-0.001, 0.003)	0.275	0.049
	r	0.002	0.003 (0.0017)	0.002	0	(-0.001, 0.001)	0.572	(-2.2e-5, 2.2e-5)	0.971	-0.112
	τ	0.302	0.124 (0.095)	0.284	0.018	(-0.01, 0.046)	0.212	(-0.002, 0)	*0.049	0.291
	σ_w	0.047	0.006 (4.2e-4)	0.046	-0.001	(-0.002, 0)	0.086	(0, 8e-6)	*0.033	0.490
SDDE	K	0.918	0.019	0.919	0	(-0.001, 0.001)	0.923	(4.6e-5, 1.2e-4)	**1e-5	0.999
	B	0.838	3.508	0.000	0.163	(-0.647, 0.973)	0.693	(-0.029, 0.017)	0.582	0.233
	P	0.162	0.071	0.146	-0.012	(-0.026, 0.002)	0.071	(0.001, 0.001)	**0.002	0.580
	D	68.818	53.280	50.384	-3.668	(-15.80, 8.47)	0.554	(-0.21, 0.48)	0.442	0.386
	τ	0.478	0.031	0.494	0.006	(-0.001, 0.013)	0.099	(-4e-4, -5e-5)	*0.015	0.034
	σ_w	0.047	0.006	0.046	-0.001	(-0.002, 0)	*0.044	(1e-6, 9e-6)	*0.012	0.494
SDE	K	0.931	0.020	0.930	0.004	(0.001, 0.007)	*0.007	(-5.8e-5, 9.4e-5)	0.641	0.804
	B	17.475	13.231	14.616	2.462	(-0.475, 5.399)	0.102	(-0.221, -0.053)	**0.001	0.608
	σ_w	0.048	0.006	0.048	-0.002	(-0.003, -0.001)	*0.011	(2e-6, 1e-5)	**0.002	0.544

*Significant at unadjusted $\alpha = .05$ **Significant at adjusted $\alpha = .0029$

generally high, representing active control over 75-85% of the phase space. Similarly, r was 50% smaller on average than values used in previous studies. τ had a median of 284 ms and was distributed between 200 to 400 ms. If the bias found in simulations is consistent and proportional, then the true median delay was closer to 240 ms. The SDDE estimated much longer delays on average at 470-490 ms but much lower values of D . Process noise standard deviation σ_w estimates were distributed identically between models.

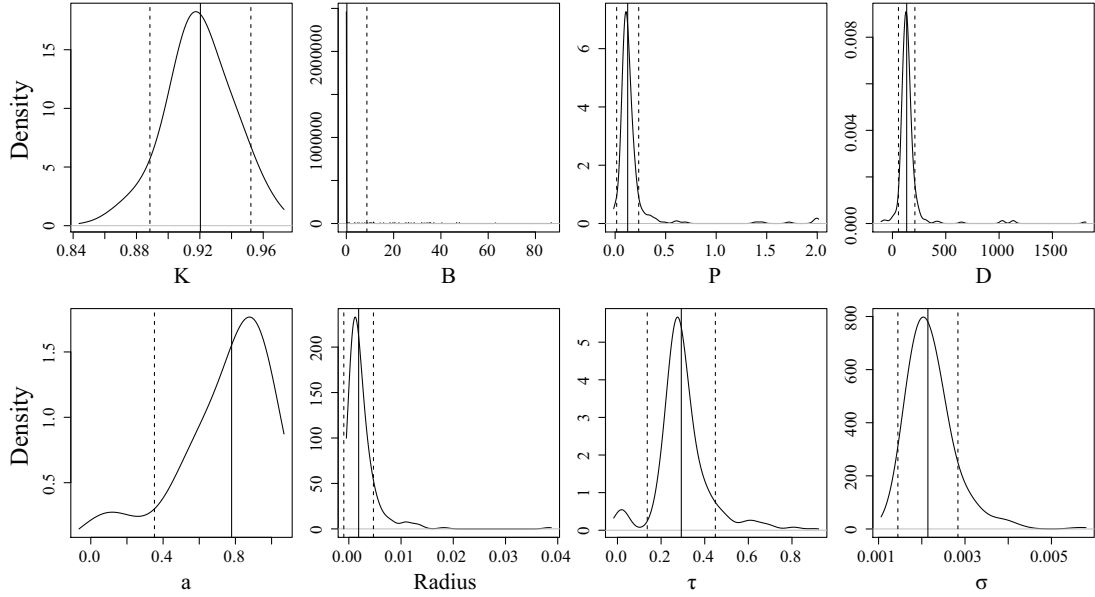


Fig. 6.: Marginal distributions of the ISDDE parameter estimates. Solid lines are means and dashed lines are standard deviations, both trimmed for the 15 highest values.

No significant effects of visual feedback were observed in the parameters of any of the three models. The lowest p -values were for a ($p = .069$) and σ_w ($p = .086$). Both the SDDE and SDE showed effects on σ with $p < .05$, the alpha level before adjusting for the 17 tests in total.

In the SDDE, both passive ankle stiffness K and active control coefficient P were

shown to significantly increase with age. The effects were detected given the adjusted alpha level, with $p < .0029$. Both B and σ_w in the SDE showed significant trends with age as well. Other non-significant effects with $p < .05$ were K and σ_w in both the ISDDE and SDDE, B in the ISDDE, and τ in the SDDE. Effect estimates of σ_w were consistent across models.

Overall, parameters tended to be more consistent within person for the simpler models. The highest intra-class correlation for all parameters in all models was K , with extreme reliability ($\rho = .999$) in the SDDE. σ generally correlated around .5 for each model. The ISDDE had the least consistent parameters with intraclass correlations near zero for P , D , a , and r . The SDDE and SDE intraclass correlations were moderate to high for all except feedback delay, τ , which was near zero.

Akaike’s Information Criterion (AIC) [78], as $-2 \ln(\hat{\mathcal{L}}) + 2k$ where k is the number of estimated parameters, was used to compare overall model fit for every individual. For each trial, the model with the lowest value of the AIC was selected as the best fitting option. In total, the ISDDE was selected for 227 trials, SDDE for 62, and SDE for 0. No significant associations were found between model selections over trials within person or by visual feedback condition.

3.4 Discussion

3.4.1 Simulation

Simulation studies were used to determine whether the parameters of the intermittent activation feedback control model proposed by Asai et al. [48] can be estimated using a Kalman Filtering-based framework with delayed proportional and derivative terms and discrete activation thresholds. The results of the simulations show that the parameters of the model can be estimated with relatively low bias and

high precision if the behaviors for which they are influential are sufficiently expressed in the data (i.e., empirically identified). Every parameter of the model was successfully recovered in at least one of the parameter configurations tested, though no single configuration of parameters resulted in a completely unbiased set. The set of results shown in Figure 5f comes close, with downward bias only to the active derivative controller. We can also see by comparing Figure 5d to Figures 5c and 5a that an increased variance of process noise allowed the identification of the B and D parameters, but with large standard errors. The derivative coefficients were likely biased and unreliable when the trajectories did not frequent the extremes of position and velocity where the directional effects of derivative terms could be distinguished from other sources. Figure 5b shows that with process noise of a standard deviation much greater than the insensitivity radius and a weak attraction to point equilibria ($K \approx 1$), the state is prone to drifting away from the origin where it will rarely traverse the insensitivity radius or switching boundary. If the data can be optimally explained without the use of the switching parameters, then they are said to be empirically unidentified. For this reason, both a and r do not contribute crucial information and converge to precise solutions when the data are optimally described by other parameter values characteristic of rambling and trembling. However, estimates of the derivative controllers B and D in that case were unbiased.

Across configurations, some iterations of model fitting resulted in negative values of B . In continual PID controllers, this would result in amplification and instability over time. In the ISDDE and SDDE, the stability of the system given a value of B depends on the corresponding values of P , D , and a , as the instantaneous proportional and derivative terms do not control the complete periodic behavior on their own. Negative values of B will promote further instability in the already unstable manifold of instantaneous feedback but will be counteracted when the state reaches the stable

manifold determined by active feedback. It is informative that solutions occasionally involved negative values of B that breach its theoretical interpretation as joint friction. Solutions that did estimate B and D accurately only did so when their true values were much larger than physically plausible, a priori values of joint friction. In simpler PID cases, estimates of damping tend to be far less reliable than, for instance, the proportional coefficients, so for these reasons together it may be inadvisable to rely on postural sway data and estimation approaches to specifically determine joint friction. Similar concerns may be directed toward the active feedback damping D , though the prior ISDDE literature does not assert as specific of a definition nor necessary theoretical boundaries.

Estimates of both process noise and measurement error were very close to their true values in every case, with only small upward bias proportional to the magnitude of the estimate for certain parameter sets (Figures 5a and 5b). The standard deviation of measurement error that we chose to simulate was $\sigma = .01$ cm, twenty times the error of the force plate used by Santos et al. [67] to obtain the data. The success of estimation despite greatly exaggerated sensor noise demonstrates the reliability of Kalman filtering and adequate technical specification of the model, and relieves researchers from the need to choose a preliminary noise reduction step such as spectral filtering. Instead, using the raw data and including measurement error in the model avoids removing fine-grained details of the signal represented in the domain of high frequencies typically suppressed by low-pass filtering.

The feedback delay, τ , was unbiased in noiseless simulations, and consistently biased downward in noisy simulations. It is not clear what causes the bias, but it did not appear to consistently induce bias in other parameters that depended on the correct lag interval, such as the active proportional and derivative controllers.

The results of our simulation demonstrate that the proposed method of direct,

statistical estimation by Kalman filter can recover the complete set of parameters for the model. Previous estimation methods only attempted to estimate five of the eight structural parameters [64, 65]. Among those attempted, the D parameter did not converge to its true value in simulation nor to a reliable, unimodal distribution in the empirical study. Despite this setback, no discussion was given of the role of empirical identification in determining D or other parameters, whereas we have demonstrated that the precision of estimates depends on their true values and interdependence. Additionally, the accuracy of their results rests on assumed values of K , B , and r . Due to the high degree of parameter dependence in univariate models such as this, error in one parameter is expected to propagate to other parameters in a compensatory manner. It is therefore preferable to jointly estimate all uncertain model parameters when possible.

The prior studies also did not account for measurement error. We determined that additional sources of sensor noise could be filtered simultaneously with estimation of the dynamic structure. If additive noise is Gaussian, then no preprocessing steps such as spectral filtering or downsampling should be needed and the risk of obscuring important, fine-grained topological features is greatly mitigated.

Computationally, the use of global optimization to maximize the likelihood function provided an efficient alternative to Bayesian MCMC methods as no data simulation procedures, prior distributions, or posterior sampling were required. An additional, unexplored benefit of maximum likelihood in this case is estimation of standard errors directly from the likelihood function. Because the model includes discrete thresholds, the likelihood function was stochastic and non-differentiable. This prevented the use of the Hessian matrix to calculate precision. However, future work may explore methods of smoothly approximating the marginal likelihood function, for instance by fitting splines to likelihood values retained from the optimization

procedure.

3.4.2 Experimental Data

The results of analyzing the empirical COM data show that the nonlinear mechanisms of feedback activation led to significant improvement in model fit over the simpler SDDE and SDE (i.e., delayed and instantaneous PID) models. It cannot be determined from statistical model comparisons alone whether the results validate the model-generating theory of posture control. To that end, we must compare the parameter estimates to their theoretical priors.

Overall, the distributions of parameters showed a feasible correspondence to the domains expected given the theory. K was consistently close to the 91% relative resistance found by Loram and Lakie [69] for all of the models tested, here showing resistance to 92% of the total gravitational toppling torque on average. Conversely, in the ISDDE and SDDE, B most often converged to zero and was not likely to play a critical role in the model behavior. Perhaps coincidentally, the mean of B was near its proposed value of 4 Nms/rad. It is possible that statistical power at the individual level was insufficient to identify small effects due to B , and the expected value would be recovered if it were estimated across the total data set. Active feedback was generally weaker than hypothesized but still sufficient for stability. Estimates of P were closer to .1 than the proposed .25 [48], likely due in part to the greater resistance to toppling forces from values of K closer to the high end of their theoretical distribution. D played a large role in the dynamics of active control and resulted in non-negligible damping in many individuals. Values of a and r reflected greater control sensitivity than expected. a values around 75% to 80% assign a larger share of the phase space to active feedback, while smaller values of r indicate less tolerance to falling at the origin of sway. The mean estimate of a was higher than found by

Tietäväinen et al. [65], which reported a control space closer to 64% in accordance with the analysis by Asai et al. [48]. We found a nearly identical distribution of the feedback delay, τ , to Tietäväinen et al. [65], ranging from 200 to 400 ms with a mean around 300 ms. Estimates of σ_w were an order of magnitude smaller than expected by Asai et al. [48], and about half of those found by Tietäväinen et al. [65].

A graphical vignette of these results is provided in Figure 7, which shows six raw data series with their respective intermittent activation conditions estimated by the model. The horizontal axis is the tilt angle and the vertical axis is the tilt angle's velocity. The shaded region represents behavior where P and D are equal to zero. In the unshaded region, all parameters are active with their non-zero values. Figure 7a shows two cases that resemble the theorized structure with combinations of stable and unstable manifolds in nearly equal proportion. In Figure 7b, the values of B and a are sufficiently large to minimize the influence of the unstable manifold. The result is behavior that closely resembles harmonic oscillation around a single equilibrium. The opposite trend is shown in Figure 7c, where the unstable manifold is not influential, but a high ratio of the derivative coefficients to proportional coefficients results in continual suppression of velocity. This pattern results in wandering oscillations without clear equilibria.

The optimal solution for the SDE model had a much larger, positive value for B than the other models while maintaining a theoretically plausible value of K less than 1. Furthermore, all values of B in the SDE were positive, as we might expect given that negative values would result in instability. When a linear system is strongly overdamped (in this case, a high value of B in the SDE, or either B or D in the SDDE) with relatively weak proportional feedback, as the SDE, then it exhibits non-equilibrium Langevin dynamics. These dynamics have conventionally described the random walk of a large molecule due to its collisions with a many smaller molecules

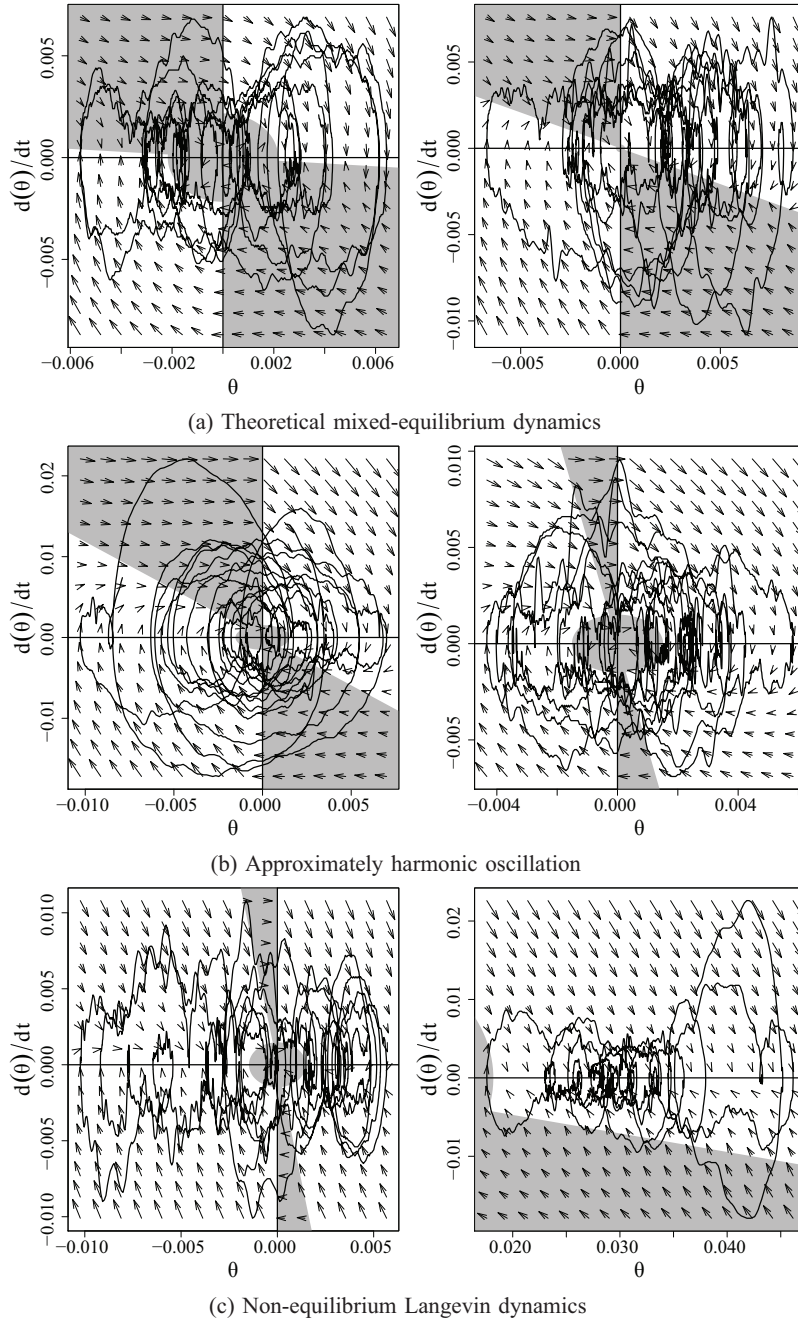


Fig. 7.: Phase portraits of observed body tilt angle with estimated intermittent activation structures and vector fields. Horizontal axis: COM; Vertical axis: COM velocity. Shaded region: state where $P = D = 0$. (a) Estimated parameters match theoretical expectations showing two equilibria. (b) and (c) the nonlinear mechanisms deviate uniquely from theoretical purpose.

in a solvent. The resulting trajectories can appear locally stationary by chance and exhibit short intervals of oscillation. Previous studies have modeled posture control in the context of Langevin dynamics [79, 80, 81, 82]. Our simplest model of COM movement, the SDE, resembled a model of COP proposed by Bosek et al. [79] that describes trajectories as a second order SDE with no proportional feedback and a large derivative coefficient B . Figure 8 shows how the theoretical model and Langevin dynamics differ markedly in their mechanistic parameterization and observed phase portraits, yet they share many notable features. In both, high-frequency oscillations move gradually across the sample space in a “rambling” pattern. By chance, the Langevin equation in Figure 8b can result in concentrated oscillations around a few apparent equilibria, but no equilibrium mechanism is present in the model. The parsimony of generating these patterns with only three parameters poses a challenge to the specificity of evidence for the theoretical ISDDE. Visual inspection of the complete results showed that trials ranged between the two extremes of theoretical misspecification, from harmonic oscillation to Langevin dynamics. The expected topology involves a mix of features from both, sometimes showing adherence to the principles of feedback switching with occasional deviations into Langevin-type random walk.

Regardless of the true form of the underlying process, we might expect that if the parameters represent underlying physiological mechanisms, they should exhibit some degree of trait-like stability within-person. The intraclass correlations in Table 7 show that the nonlinear switching parameters were generally unreliable within-person. The correlations for the remaining parameters increase as the model is simplified to the SDDE and SDE. The higher consistency of the simpler models’ parameters does not necessarily imply that they are more “real” than those of the ISDDE. It is expected that reliance on fewer parameters to explain the variance of sway results in

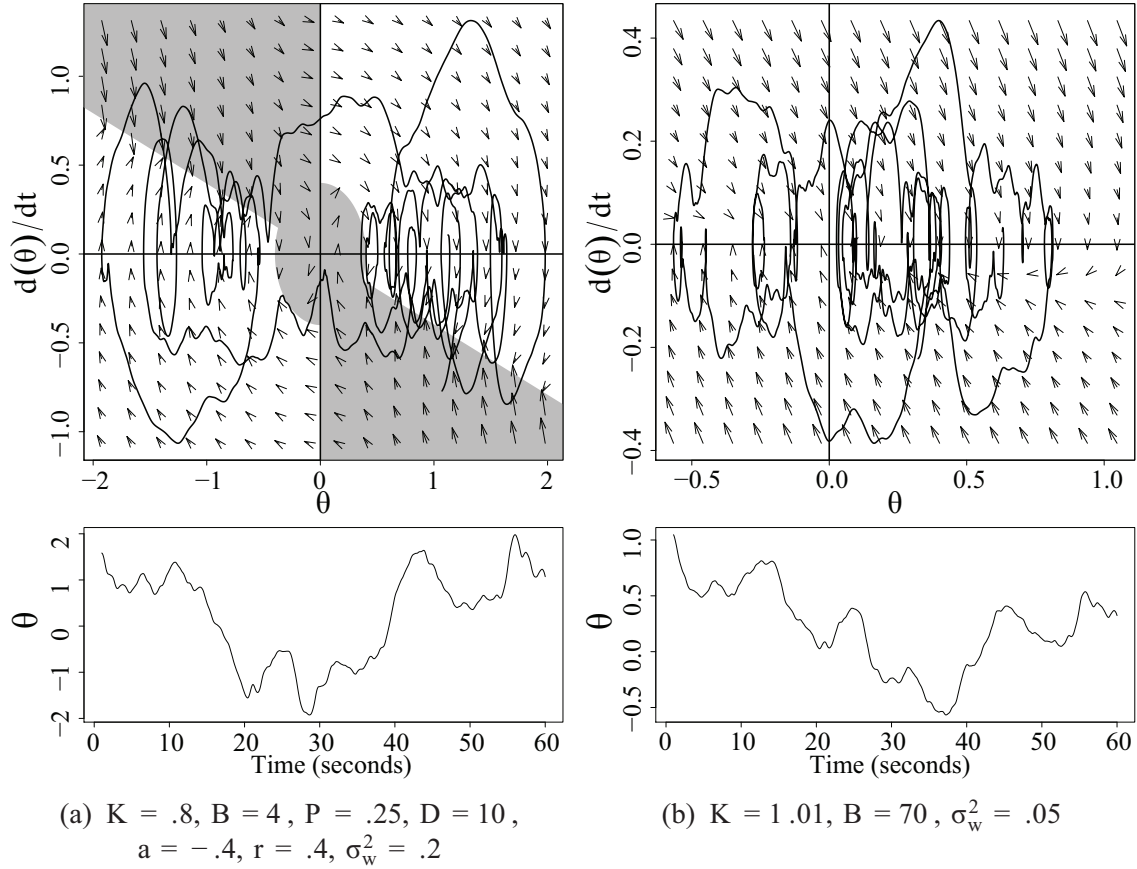


Fig. 8.: Phase portraits and time series from two models generated from the same vector of noise (scaled by σ_w). In (a) data were simulated from the ISDDE model with the theoretical priors. In (b) data were simulated from a 3-parameter SDE. The large ratio of derivative (B) to proportional (K) force results in non-equilibrium Langevin dynamics that may exhibit similar features to the ISDDE for limited periods of time. Characteristic features distinguish (a) from (b), such as sharp changes in velocity localized to quadrants II and IV, slow change in velocity associated with quadrants I and III, and higher density at two spatial equilibria

fewer competing configurations of those parameters. Any consistency of topological features within-person will be reflected in similarity of the model solutions. The lack of consistency in the more complex ISDDE is, however, a challenge to the trait-like

stability and actuality of its parameters.

Though no specific connections between visual feedback and the theoretical mechanisms of control were hypothesized for the present study, we expected one or more parameters to be significantly influenced over trials in which eyes were closed in correspondence with previously observed effects on summary statistics. By modeling center of pressure variation with Langevin dynamics, Bosek et al. [79] found that the process noise distribution was influenced by visual feedback. The same finding was replicated with further connections to Parkinson’s disease [80]. Vieira et al. [83] found associations of visual feedback with stabilogram measures of sway. All three models tested here had lower p -values for σ_w than for other parameters, suggesting that effects may be discernible given a larger sample or improvement in model specification.

Age has been previously associated with more general metrics of sway, such as path length [84], frequency band [83, 85] and mean velocity [85], though findings vary and few effects have been consistently reproduced in COP and COM data. Significant effects of age were observed in the present results, including ankle stiffness and active feedback force in the SDDE and process noise and ankle viscosity in the SDE. Interpretation of effects on the SDE is more difficult because the parameters of the SDE do not correspond to specific explanatory mechanisms in this case. The consistent positive associations of all models with noise magnitude σ_w with age may be linked to previously observed associations of stabilogram-based diffusion metrics with age [86]. The significant associations of ankle stiffness and active proportional feedback in the SDDE found here may reflect previously observed increases in stiffness and damping with age estimated from a simpler PID model [87].

Finally, the model concerns an abstract notion of body tilt angle, though there are many ways to represent this using the full kinematic data. For simplicity and

consistency with past studies, we chose to represent tilt angle by the COM. Preliminary tests using alternative measures included COP and the average angle of both ankle joints. The results were found to differ markedly from both our current results and those previously obtained with the COM, but a complete comparison of alternative measures is too complex to discuss here. We leave detailed examination of this question with regard to the feasibility of this model to future study.

3.4.3 Conclusions

We designed and implemented an Extended Kalman Filter-based estimation model of intermittent, delayed feedback control in postural sway and demonstrated that for a variety of stable configurations, parameters can be recovered accurately given adequate empirical identification. Application of the model to experimental data resulted in distributions of the parameters that correspond well to previous findings and suggest that physiologically informative and clinically useful attributes of human balance may be extracted directly from COM data. While the model replicates previous findings, the conjectured parameters of feedback activation were not reliable within-person or strongly associated with visual feedback and age. Further comparisons with alternative mechanistic theories and model parameterizations are warranted. Beyond postural control, the model stands as a framework for estimating parameters of stochastic delay differential equation models controlled by discrete activation thresholds.

CHAPTER 4

STUDY II: POORLY-BEHAVED PSYCHOMETRIC DATA, SIMPLE LINEAR MODEL

4.1 Introduction

Motivation to use psychoactive substances can arise both as a cause and a consequence of problems with emotion regulation. Data collected from psychological and behavioral time series designs, known as Ecological Momentary Assessment (EMA)[22] or Experience Sampling [88], present new opportunities to conceptualize emotion regulation in terms of variability in emotional states over time. Often, individual traits of emotion regulation are inferred from descriptive statistics, such as the means and standard deviations of repeated, within-person assessments of affect. Descriptive indices are simple to compute and can be used as general predictors, but they are difficult to interpret in terms of real-world concepts, saying little about the actual process of change in emotion over time. An alternative approach is to specify theoretical models that describe the structure of emotion variability in terms of its mechanisms. Indices with unambiguous, *a priori* interpretations can then be obtained as the statistical parameter estimates from such models. In the current study, we compared one such theoretical index of emotion variability to commonly used descriptive statistics for their capacity to predict substance use.

In psychiatric research, self-reported affect assessments have been used in many ways. As a general state-based assessment of subjective experiences, they can provide insight into the timing and valence of emotions linked to psychiatric symptoms and episodic behaviors. For instance, positive and negative affect have been studied

to differentiate between mood disorders [89] and as a means to identify distinctive features of anxiety and depression for the DSM-5 [90, 91]. Negative affect has been associated with both binge eating severity and its rate of comorbidity with depression [92]. A review of studies on smoking, stress and negative affect points to a general mediating or moderating role of negative affect in smoking initiation, maintenance, and relapse [93]. Smoking to cope with negative affect is associated with higher risk for regular, persistent use, and with greater difficulty quitting than occasional social smoking [94, 95].

With time-series of affect data, (i.e., frequently repeated measures), patterns of change can help to identify new, distinguishing features of psychiatric disorders. For instance, the mean and overall variability of negative affect are greater in patients with borderline personality disorder than healthy controls [96]. Intra-individual variability has been found to uniquely predict aspects of personality when compared to simple means [97, 98]. In clinical samples, the variability of momentary affect has been important to predicting and preventing behaviors and negative health outcomes, such as stress-induced binge eating [99, 100, 101], relapse to alcohol, [102, 103, 104] tobacco [105, 106] and other substance use, prodrome to manic and depressive episodes [107, 108], and suicide [109].

In this study, we conceptualize emotional variability in terms of feedback control and derive a measure of emotion regulation based on simple theoretical assumptions. Specifically, we assume that emotional states trend toward a mean or equilibrium value following stressful or joyful experiences. For short-term emotional stability, the rate at which emotions decay toward equilibrium, or their “offset”, must be sufficient to overcome perturbations from typical daily experiences [110]. Maintaining emotional homeostasis allows one to more easily predict and control one’s own behavior. Recovery from stress involves deactivation of flight or fight response and restfulness

associated with the parasympathetic nervous system [111, 112, 110] and a renewal of the capacity for healthy behaviors. Positive experiences, while desirable, nonetheless can lead to poor judgment if their effects accumulate unchecked, a scenario characterized by mania [113]. Mechanisms of emotion regulation likely vary individually by development and preference. Family and friends may serve as sources of regulatory feedback, providing social support and stable interpersonal roles [114, 115]. Intrinsic mechanisms of emotion regulation can include habits and tools of self-care, such as exercise, diet, structure and schedule, and cognitive-perceptual appraisal of experiences [116], all of which modulate the degree to which experiences disturb one from an equilibrium state and the time needed to recover.

The above concepts of emotional homeostasis, including equilibrium, disturbance, and rate of recovery, comprise the fundamental components of a feedback control system. The simplest case of linear feedback control subject to random perturbations can be formalized as a stochastic differential equation (SDE):

$$\frac{dx_t}{dt} = \lambda x_t + w_t, \quad w \sim N(0, \sigma_w), \quad (4.1)$$

where x_t is the state of affect at time t , λ is the coefficient of feedback, and w_t is a random, exogenous disturbance at each time. If λ has a negative value, then on average, deviations from equilibrium are counteracted proportional to their magnitude. Variability at time t is driven by random disturbances, w_t , leading to a continual flux between perturbations and regulation. Similar models have previously been used to characterize affect change and have been fit to empirical data [117, 118].

The regulation parameter in Equation 4.1, λ , is difficult to interpret in real-world terms. For a more intuitive index of emotion regulation, δ , we can define regulation as the percent recovery to equilibrium after a given time interval. This can be computed from λ in Equation 4.1 by considering an equivalent, discrete-time formulation as an

autoregressive model:

$$x_t = \beta x_{t-\Delta} + \sqrt{\Delta} w_t \quad (4.2)$$

$$\beta = e^{\lambda\Delta} \quad (4.3)$$

In this form, values of β from 0 to less than 1 characterize negative feedback or stabilization. In the current study, affect was assessed multiple times per day to study hourly variability. If we choose $\Delta = 1$ hour, then β is the percentage of deviation from equilibrium remaining from the previous hour. We can therefore take the effect size of emotion regulation as $1 - \beta$, interpreted as the expected percentage of recovery to equilibrium per hour given no further disturbances to affect. An alternative interpretation may be to take the average half-life of affect disturbances, given by $\frac{\ln(0.5)}{\beta}$. The former definition was chosen so that higher values represented stronger regulation.

In addition to the feedback coefficient λ , σ_w is the estimable standard deviation of exogenous disturbances. When the latent state describes affect or other subjective measures in the EMA context, such exogenous disturbances represent the distribution of unmeasured influences on the individual.

Together, the parameters λ and σ_w can be estimated from each individual's time series to obtain indices of emotion regulation and volatility or sensitivity, respectively. One potential benefit of theoretical indices such as these is that their underlying theory can be validated and improved through empirical applications. If the feedback control structure is an accurate representation of emotional processes, then associations between its indices and substance use can be expected to arise for several reasons, depending on the particular effects of each substance. Drugs such as nicotine [95, 119] and alcohol [104] may directly decrease average emotional volatility by

dulling emotional responses. Whether these drugs are used to reduce emotional sensitivity or increase emotion regulation response depends on their timing as preemptive or reactive to stress, respectively. Conversely, many stimulants are used specifically for their ability to induce or sustain mania-like symptoms, potentially undermining the goals of healthy regulation.

We hypothesized that our theoretical, model-based indices of emotion regulation would predict substance use independently from simpler descriptive statistics. We did not hypothesize about the degree to which descriptive statistics would associate with substance use, but included them in analyses as a benchmark for methodological improvement.

4.2 Methods

The available EMA data presented many technical, methodological challenges, and required multiple steps of processing. In this section, we detail the sample, our quality control criteria, a state-space affect model, and the second stage regression of substance use onto the estimated parameters from that model. Our analysis was organized as follows: 1) In each individual, data quality was first determined in terms of complete rows of data and the information content of responses; 2) If the quality control criteria were met, then affect indicators were aggregated into negative affect scores; 3) Descriptive statistics and state-space model parameters were estimated from the aggregate scores, and counts of reported use for each substance were summed; 4) After steps 1-3 were performed for all individuals, counts of usage for each substance were regressed on the descriptive statistics and state-space model parameters. Each of these steps is detailed in the sections that follow.

Participants This study utilizes data from the Social-Spatial Adolescent Study, a two-year longitudinal investigation of the interacting effects of peer networks, urban environment, and substance use [120]. Participants were recruited between November 2012 and February 2014. Most participants (72%) were recruited from an urban adolescent primary care clinic at Virginia Commonwealth University Medical Center, in Richmond, Virginia. Age-eligible (age 13 or 14) adolescents presenting to the clinic for routine or acute care were approached and invited to participate in this study by a research assistant. Other participants were recruited from a city health district satellite clinic, located within a subsidized housing development. These participants were recruited by referral to the study team from the primary Patient Advocate at the satellite clinic. Enrollment and data collection procedures were the same across sites. Chi-square tests revealed no significant differences in age, sex, or race of participants between the two recruitment sites. Race was not used because the sample was 86% African American and too small to estimate or control for any effects of demographic heterogeneity.

Ecological Momentary Assessment Moods All participants were given a smart phone for the period of the study, through which EMA surveys were delivered. EMA surveys were administered to each subject via text message with an embedded URL link 18 times over a four-day period every other month, over a period of two years. The 11-item survey asked participants to rate their current mood in terms of happiness, sadness, anger, worry, loneliness, and stress as well as feelings of safety, on a scale of 1 to 9 with 9 representing more intense feelings. Participants were asked questions about if they were using tobacco, alcohol, and marijuana with responses coded as yes = 1, and no = 0. Participants were encouraged to complete each of the surveys within an 8-minute window from when it was sent. Timestamps on each EMA survey were

collected to identify surveys that were answered within the prescribed time limit.

Dimension reduction It is common to aggregate information across affect items to simplify models and produce a small set of variables with maximal information content. For continuous state-space models, it is convenient to aggregate discrete, Likert-type variables to produce a sufficiently continuous sample space to be described by the differential equation model. If all response categories are used, then uniquely weighted combinations of the 7, 11-point affect items would produce an affect dimension with up to 11^7 possible values. In practice, most participants only use a small subset of the available response categories, making dimension reduction necessary.

Table 8 shows that all affect items were moderate to highly correlated across individuals and waves. Items “happy” and “safe” were positively correlated with each other and negatively correlated with all other items. The strong inter-correlations suggest that the indicators may be related to one or two underlying dimensions.

Table 8.: Correlation matrix of affect states across the total sample.

	happy	angry	safe	lonely	anxious	sad
angry	-0.47					
safe	0.35	-0.3				
lonely	-0.35	0.55	-0.29			
anxious	-0.34	0.58	-0.33	0.57		
sad	-0.43	0.67	-0.32	0.61	0.63	
stressed	-0.42	0.64	-0.32	0.59	0.66	0.68

When affect questionnaire items must be aggregated into a single dimension of affect, a common strategy is to sum the scores across all items for each measurement

occasion. To produce a methodological standard for comparison, we computed series of sum scores for each person along with their person-level means and standard deviations. Items “happy” and “safe” were first negatively coded, then all items were added together to produce a series of negative affect sum scores for each person.

To produce negative affect series for the state-space model, an alternative dimension reduction technique was used. Sum scores imply two untenable assumptions. First, that all items are equally important to the underlying dimension, and second, that no item-level variance is due to measurement error or other sources irrelevant to their collective underlying dimension. A standard alternative approach to aggregation is to produce scores from a factor model, or as an approximation, principal component analysis. These options weigh the items by their communality, or the inter-correlation of each with the other items. Scores representing the shared variance of the items are produced that exclude item-specific, residual variance. One rapid method of computing principal component scores is Singular Value Decomposition (SVD). SVD is given for $m \times n$ data matrix \mathbf{X} as $\mathbf{X} = \mathbf{U}\mathbf{\Sigma}\mathbf{V}^T$, where \mathbf{U} contains n length- m orthonormal columns of scores, \mathbf{V} is the $n \times n$ matrix of eigenvectors, and $\mathbf{\Sigma}$ is the $n \times n$ diagonal matrix of eigenvalues. The first column of \mathbf{U} provides a set of weighted composite scores that maximally account for the shared variance of the items. Subsequent columns account for diminishing proportions of the total variance of the items, and variance unique to particular items is relegated to the last columns in the \mathbf{U} matrix. Items “safe” and “happy” were automatically reverse coded by the SVD as a result of their negative correlations with the other items. Only a single variable maximally representing negative affect was of interest in this application, so only the first column of the \mathbf{U} matrix was used to represent affect principal component scores, and the others were discarded. Affect items were standardized and SVD was applied separately for each wave and for each person, allowing the respective

influence of each affect indicator to vary individually. This choice is analogous to relaxing the assumption of factor loading invariance in a factor analysis. The exact loading structure and its reliability were of less concern than the aggregation of available information across the items within each person’s time series.

Model The measurement intervals of each series were unequal, so a continuous-time state-space model (SSM) as shown in Equation 4.1 was used to model the reduced series of negative affect data as an SDE:

$$\dot{x}_t = \lambda(x_t - \mu_x) + w_t, \quad w_t \sim N(0, \sigma_w) \quad (4.4)$$

$$y_t = \mu_y + x_t + \epsilon_t, \quad \epsilon_t \sim N(0, \sigma_\epsilon) \quad (4.5)$$

The additional, second equation (4.5) relates observed measures y_t to the latent state by a constant mean μ_y and measurement error ϵ_t . Because affect indicator scores were standardized, the mean or equilibrium value of the state equation, μ_x was fixed to zero and the indicator means, μ_y , were subtracted out. Individual emotional resilience was calculated as $\delta = 1 - e^\lambda$, as described by Equations 4.2 and 4.3. Because as many as 18 repeated measures were taken over the course of each four day burst, we coded the time intervals to a scale of hours such that $\Delta = 1$ hour. δ is therefore interpreted as the expected percentage of emotional recovery to baseline over the course of 1 hour absent the effects of additional disturbances.

The SDE model was implemented using the Kalman filter [46], an optimal method of obtaining minimum-variance, unbiased estimates of latent states from noisy indicators and fitting time series models to data. Waves of negative affect SVD scores were aggregated in a multi-group manner within the state space model with the first observation of each wave beginning at hour 0. Maximum likelihood and the Nelder-Mead optimization algorithm [121] were used to estimate the parameters

in R [74]. Waves were far enough apart in time to be modeled independently with each starting over at time zero. Each parameter was estimated between-waves for sufficient statistical power. The first observation of each wave was used as the initial position of the latent state and the series variance as the initial state variance.

Cross-sectional Analysis The indices of emotion regulation, δ and σ_w , were estimated for each individual along with the means (μ_{SS}) and standard deviations (σ_{SS}) of negative affect sum scores. These within-person statistics were then used as the independent variables in a between-person analysis of aggregate counts of substance use. Total counts of nicotine, alcohol, and cannabis use were produced from the EMA data. Counts of each substance were overdispersed for a Poisson model, so they were regressed upon the extracted affect variables using multiple negative binomial regression. To estimate the uniqueness and contribution of the model-based predictors to the total explained variance of substance use, substance use counts were regressed onto: (a) only the mean and standard deviation of affect sum scores; (b) only the model-based predictors, emotion regulation and volatility; (c) predictors from both (a) and (b) combined. The magnitude and uniqueness of improvement in R^2 due to the model-based predictors was then quantified from comparisons of the three models. Nagelkerke’s generalized R^2 [122] was used for the negative binomial regressions with the recommended adjustment for discrete likelihood functions.

Preprocessing and quality control Data were preprocessed to ensure that only time series with the necessary quality requirements were used in the analysis. Statistics drawn from inadequate samples will be highly variable and add noise to any subsequent relationships with covariates. In two-step analyses such as this, uninformative or misleading response patterns may reduce statistical power of the final

analysis by reducing the estimable effect sizes, regardless of the number of people in the total sample. Data quality metrics included a minimum number of complete rows of data (6 per wave, 18 total per person) and a minimum amount of available affect information per wave. Many participants did not provide enough usable information, either using most affect items in a sparse, binary way, or entering only a single rating for all occasions. Data were frequently missing, so the amount of remaining data per wave was small and thus sensitive to bias introduced by interpolation. To avoid this risk, rows with missing data were simply excluded.

Variables with zero variance lead to singular matrices in computation of the model expectations and likelihood values. For integer-valued variables such as ordinal Likert scales, low variance is associated with only rarely using more than one response category. Such cases can produce erratic results and model-fitting errors in state-space models, which assume continuous variation in the sample space. If too few items were used in a nuanced way, for instance with no variability on some and binary responses on others, then the resulting SVD scores or other representations of the latent dimensions will be too coarse to model reliably. To address uninformative response patterns, Shannon entropy was used as a measure (in natural log units, or ‘nats’) of the available information content of each series. [123].

$$\mathbf{H}(x) = - \sum p_s \ln p_s, \quad s \in S. \quad (4.6)$$

S is the set of possible symbols s , or possible rating values in ordinal variable x . In the case of the ordinal affect items, ratings were integers $s \in \{1, \dots, 9\}$. A key property of entropy is that it is maximal when $P(s \in S)$ is uniformly distributed. Entropy also increases with the number of possible symbols in S . Setting a minimum requirement for the total entropy across the set of variables ensures that at a minimum, either a few ratings were used on several items or several ratings were used on a few items.

The entropy of a uniform distribution of 3 symbols is 1.1, so the total entropy for 7 of such items would be 7.7.

Simulations were used (See Appendix) to determine the statistical power resulting from values of N and T , given optimal $H(x)$. Only 67 participants had $\mathbf{H}(x) \geq 7.7$. Of the participants that qualified, the average number of completed affect reports was about 64. Assuming maximal $\mathbf{H}(x)$, the resulting sample would have only a 43% chance of detecting an effect of δ if the true parameters of the negative binomial model were a dispersion of .2 and mean δ effect of -3. Choosing a lower entropy threshold, $\mathbf{H}(x) = 6.0$ resulted in a potentially better balance of data quality with sample size ($N = 94$, $\mathbb{E}[T] = 65$), increasing our estimate of the maximum possible statistical power to 56%. Further decreases in the minimum $\mathbf{H}(x)$ were expected to add only highly noisy estimates of δ that no longer yield benefits to the statistical power. The complete set of data qualifications was therefore:

$$\sum_{i=1}^K \mathbf{H}_{\text{Wave}}(x_i) > 6.0, \quad T_{\text{Wave}} \geq 6, \quad T_{\text{Total}} \geq 18. \quad (4.7)$$

The quality control metrics, total entropy and total complete rows of data per person, were regressed on demographic variables sex, age, race, mean latitude, mean longitude to determine whether data quality control procedures may bias the results. No significant nor apparently trending associations were found, suggesting that the informativeness of response patterns was largely idiosyncratic with respect to the available data.

4.3 Results

Results of the negative binomial regressions are shown in Table 9. Emotion regulation δ and affect sum score means μ_{SS} were most consistently significant ($p < .05$) across models, both uniquely and conditional on use with other predictors. After

exponentiation, the significant effect sizes from the combined regression are interpreted as follows: Across participants, a 10% increase in emotion regulation rate corresponded to a 6 to 39% reduction in nicotine use, a 2 to 42% reduction in alcohol use, and a 2 to 34% reduction in cannabis use. A unit increase in mean negative affect sum score corresponded to a 7 to 31% increase in nicotine use, a 1 to 27% increase in alcohol use, and a 2 to 23% increase in cannabis use. Additionally, a unit standard deviation increase in negative affect sum scores corresponded to a 10 to 50% reduction in nicotine use. The true directions of causation responsible for these associations cannot be determined by this cross-sectional approach, so we present these effects only as the functional mappings given by the models. Negative affect sum score standard deviations were not significant for alcohol or cannabis in the combined model. Volatility, σ_w , was not significant, though with small p -values for cannabis and nicotine, it is possible that effects would be detectable in a larger sample.

Total R^2 values of each model are given in Table 10. Descriptive sum score statistics were the most predictive for nicotine, explaining 28% of variance in its use. By comparison, the model-based emotion regulation and volatility only explained 10% when used as the sole predictors. Similar proportions of the variance of alcohol and cannabis use were explained by either approach, with 15% for alcohol and 11% for cannabis. The variance explained by all predictors used in tandem was slightly greater than the sum of their separate models, possibly owing to the approximate nature of the the generalized R^2 measure. Subtracting the R^2 of the descriptive statistics model from the R^2 of the combined model reveals that the variance explained by the novel, model-based predictors was independent from the variance explained by descriptive statistics. The descriptors were correlated with model-based indices between 0 and -.2, small enough to arise from sampling variation and insufficient to suggest methodological redundancy.

Table 9.: Multiple Negative Binomial regression of substance use counts on: (a) only descriptive statistics of affect sum scores: mean (μ_{SS}) and standard deviation (σ_{SS}); (b) only model-based predictors: regulation (δ) and volatility (σ_w); (c) both descriptive and model-based statistics. β_0 is the intercept for each model.

	(a) Descriptive			(b) Model-based			(c) Combined		
	Effect	CI	p	Effect	CI	p	Effect	CI	p
Nicotine	β_0	(-5.41, 1.04)	0.18	1.65	(0.77, 2.52)	0.00021	-1.34	(-4.71, 2.02)	0.43
	μ_{SS}	(0.06, 0.27)	*0.0017				0.17	(0.07, 0.27)	*0.0011
	σ_{SS}	(-0.69, -0.06)	*0.019				-0.42	(-0.72, -0.11)	*0.0071
	δ			-2.71	(-4.88, -0.54)	*0.014	-2.85	(-5.02, -0.68)	*0.0099
	σ_w			5.87	(-5.05, 16.79)	0.29	8.86	(-1.46, 19.19)	0.092
Alcohol	β_0	(-6.41, 1.25)	0.19	0.67	(-0.31, 1.65)	0.18	-1.73	(-5.68, 2.22)	0.39
	μ_{SS}	(0, 0.24)	0.05				0.12	(0.01, 0.24)	*0.041
	σ_{SS}	(-0.58, 0.14)	0.24				-0.25	(-0.6, 0.1)	0.16
	δ			-2.59	(-5.14, -0.04)	*0.046	-2.84	(-5.47, -0.2)	*0.035
	σ_w			3.55	(-9.4, 16.49)	0.59	6.98	(-5.43, 19.39)	0.27
Cannabis	β_0	(-5.81, 0.22)	0.069	0.95	(0.19, 1.71)	0.014	-2.42	(-5.6, 0.76)	0.14
	μ_{SS}	(0.02, 0.2)	*0.019				0.12	(0.02, 0.21)	*0.012
	σ_{SS}	(-0.31, 0.23)	0.78				-0.05	(-0.32, 0.21)	0.71
	δ			-2.18	(-4.11, -0.26)	*0.026	-2.16	(-4.14, -0.18)	*0.033
	σ_w			7.48	(-1.95, 16.91)	0.12	8.92	(-0.48, 18.33)	0.063

Table 10.: Generalized R^2 values for models predicting with: (a) only descriptive statistics of affect sum scores (mean and standard deviation); (b) only model-based statistics (regulation and volatility); (c) all four predictors; and (c)-(a), the improvement to R^2 as a result of including the model-based predictors with descriptors.

Model	Predictors	Nicotine	Alcohol	Cannabis
(a) Descriptive Only	μ_{SS}, σ_{SS}	0.28	0.15	0.11
(b) Model-based Only	δ, σ_w	0.10	0.14	0.11
(c) Both	$\mu_{SS}, \sigma_{SS}, \delta, \sigma_w$	0.42	0.31	0.23
(c)-(a) R^2 improvement		0.14	0.16	0.12

4.4 Discussion

The results of our analyses demonstrate that the model-based index of emotion regulation predicted substance use independently of simpler descriptive statistics. The unique associations of each predictor were comparable in magnitude and explained a moderate to large proportion of variance in nicotine use when combined in the linear model. Less variance was explained in alcohol usage, and even further less in cannabis. These effects roughly follow the observed frequencies of each drug in these data, leading us to reserve judgment for larger and more general samples.

Causal interpretations of our results should be considered with caution and skepticism. The most likely scenario is that bidirectional feedback cycles occur between affective state and the decision to use a drug. The association of higher average negative affect with nicotine may reflect a tendency to smoke when coping with unpleasant emotions. Conversely, the association of lower standard deviations of mood with nicotine may be due to the damping effects of nicotine on emotional variability. The regulation and volatility indices were estimated irrespective of how these causal

sequences were ordered, and thus suffer from the same ambiguity. Does substance use produce larger dynamic disturbances, or vice versa? Is substance use undertaken as a surrogate for intrinsic emotion regulation? Elaborated process models can be specified to include the reciprocal causation between emotional states and the choice to use a drug, further distinguishing between the above scenarios. For instance, the following model extends Equation 4.1 to include both direct effects and changes in regulation as a consequence of substance use:

$$\frac{dx_t}{dt} = (\lambda_0 + \lambda_1\psi_t)x_t + \beta\psi_t + w_t, \quad w \sim N(0, \sigma_{w,0} + \sigma_{w,1}\psi_t), \quad (4.8)$$

where ψ_t may be a vector of indicators or quantities of different drugs. λ_1 therefore determines the extent to which the substances impact emotion regulation, $\sigma_{w,1}$ indicates the same for emotional sensitivity, and direct, immediate effects on affect are scaled by β . In the current study, substance use was recorded as a binary variable, requiring it to be mapped to a continuously varying probability of occurrence, or liability. If we take ϕ_t as a dynamical state representing that liability, then that may be in turn modeled as responsive to affect:

$$\frac{d\phi_t}{dt} = \gamma x_t + \zeta\phi_t. \quad (4.9)$$

In this model, γ would determine the direction and rate that the liability changes with affect state, while ζ controls how long the liability lingers regardless of further changes in affect. These parameters could therefore serve as indices for individual liability to addiction based on emotional feedbacks.

For the purposes of this study, we only present these ideas as a motivating vignette. To successfully fit this kind of complex process model with empirical data, the data must meet certain standards of quantity and information content for statistical power and parameter identification. As we have shown, the available data did not

meet a number of those standards. The majority of participants had either zero or few instances of substance use, uninformative response patterns on affect questionnaires, and frequently insufficient within-person sample sizes, leading us to make more conservative choices about model complexity. Our simplified modeling approach and aggregation techniques were chosen to allow comparison across as many individuals from the sample as possible despite that the majority did not report more than a few occasions with a particular drug. Future studies aiming to fit a reciprocal feedback model like Equations 4.8 and 4.9 will require consistent, high-frequency sampling of both affect and substance use. Measured occasions of substance use should be interspersed by occasions without use so that the subsequent patterns specific to affect can be observed. Consequently, a study design should sample at least two or three times the expected frequency of substance use or else include event-contingent sampling strategies. If the parameters of the above model are used as indices in second-level analysis, as we did here, then statistical power will depend on the ratio of parameter standard error to true between-person variation in parameter values. We used simulations, described in the appendix, to compute power for our current, simplified modeling strategy. Further analyses and power calculations for reciprocal feedback models are beyond the scope of our current aims and are left for a subsequent study.

EMA studies involve many complex psychometric assumptions and analytic challenges. We attempted to address as many of the most common problems as possible, though solutions are necessarily subject to discretion. One of the primary goals of our study was therefore to demonstrate several effective methods of handling problems with EMA affect data, including irregular response intervals, uninformative response patterns, and questionnaire aggregation. With these strategies come basic limitations.

First, as our power calculations showed, the resulting analysis only had approximately a 56% chance of detecting a moderate effect of emotion regulation on sub-

stance use. The primary concern with low power is the inability to detect other important effects. For all three substances, emotional volatility consistently had small, near-significant effects that may be observable in a larger sample. The same power-calculation simulations showed that 80% power at $\alpha = .05$ for the current analysis could be achieved with at least 250 participants with 30 timepoints each or 130 participants with at least 115 time points each.

One possible criticism may be aimed at our use of entropy for quality control. We used the power analysis and analytic reasoning to present a general estimate of how our results would change, but ultimately the chosen threshold for entropy is neither strict nor final. Exact calculations that account for the information content of each series would allow calibration of the minimum entropy based on the false positive rate. Because our power calculations do not account for uninformative response patterns, we consider the resulting estimate as a best case scenario.

It also is not certain whether the outcome of our quality control criteria was entirely random. Because the study participants were underage adolescents, it is possible that many individuals who used substances during the study period did not report their usage or other psychological information to avoid possible social and legal consequences. The under-reporting quantified by our methods, either as missing data or uninformative data, may have been even more likely for the most severe cases of substance use. Indeed, the majority of participants did not produce sufficiently informative data, so we must therefore condition our conclusions on an above-average willingness to cooperate with the study and a certain perceived security in doing so.

Another possible criticism regards the use of “safe” as an affect indicator. The question was worded as “How safe are you right now?” leaving some ambiguity in whether responses indicated feelings of safety or rational assessments of the current environment. In the latter case, it may not be appropriate to include among the other

affect indicators. Table 8 shows that it was strongly correlated with the other indicators. Under a latent variable measurement model, we assume that it is correlated with the other indicators because each observed variable represents the underlying phenomenon, namely negative affect. From the alternative perspective of such indicators as a directional network, it may indeed be a rational assessment of the environment from which the other reported subjective experiences follow as a consequence. It is difficult to compare the validity of network and latent variable methods in a general way, and alternative approaches to multivariate affect may yield unique and important insights. We relied on a latent variable or dimension-reduction approach and the assumption that “safety” corresponded to a subjective experience because altogether, the combined information of the ordinal indicators produced a smooth series with a nearly continuous sample space that is more amenable to state-space modeling. The entropy of the safety measure in particular was greater on average than the other indicators, which suggests that it was easier for the participants to interpret and evaluate in a detailed way. Under either interpretation, as a subjective feeling or an evaluation of the situation, safety likely increased the association with substance use because the data were collected in adolescents below the legal age for the consumption of alcohol or nicotine. Acquiring and using drugs likely required engaging in other unsafe situations.

4.4.1 Conclusions

The current study examined the utility of a theoretically conceived measure of emotional variability that describes individual tendencies toward homeostasis, i.e., emotion regulation. Our results showed that emotion regulation was uniquely and independently associated with substance use in high-risk adolescents. Using model-based indices lends to the development of more specific theoretical hypotheses as

compared to generic descriptive indices. Combined use of theoretical and descriptive indices appears to provide the greatest predictive utility. Further work is warranted to determine the nature of the observed associations between emotion regulation and substance use.

4.5 Appendix: Power Analysis

Simulations were used to obtain approximate estimates of the statistical power of the two-step analysis. The following steps were taken to create a model of power given number of people in the sample (N) and average timepoints per person (T). First, a random, Gaussian distribution of N autoregressive coefficients (β) was generated. N random values representing substance use counts were then generated from a negative binomial distribution with parameters dispersion of .2 and mean of 3β . Negative binomial parameter values were chosen such that the descriptive statistics and visual inspection approximated the joint distributions of estimated β_i and substance use counts from the data. Autoregressive time series of length T were generated by convolving (`convolve()` with argument `type='open'`) the cumulative sum of a white noise variable of length T with the transfer function $e^{ln(\beta_i)t}$ values out to length 150, and trimming 150 points from the beginning and end of the resulting convolution. R functions `ar()` and `glm.nb()` from package `MASS` [124] were used to estimate β from the data and regress substance use counts upon the estimated β , respectively. The simulation-estimation routine was carried out for 500 trials per condition, with conditions defined as

$$N = 2^k, k \in [5, 5.5, 6, 6.5, \dots, 8],$$

and

$$T = 2^{5k}, k \in [2, 2.5, 3, 3.5, \dots, 8].$$

For each condition, a true positive rate was calculated as the total percentage of results meeting statistical significance at $p < .05$. The percentage was then regressed upon each corresponding N^j and T^j with $j \in [1, 2, 3, 4]$, producing a quartic linear model of statistical power. The model was used in the study to calculate approximate power for the two-step analysis from inputs N and T .

CHAPTER 5

STUDY III: CONSIDERATIONS FOR EXPERIENCE SAMPLING OF TWIN PAIRS

5.1 Introduction

New study designs in Behavioral Genetics present new opportunities and challenges to classical modeling techniques. An increasing number of study designs utilize time-series measures of behavior and cognition taken in the typical settings of daily life, known as Ecological Momentary Assessment (EMA) [22] or Experience Sampling [88]. It is necessary to adopt efficient modeling strategies for sometimes large volumes of within-person repeated measures data that result from these studies. An increasingly popular approach involves individual-level modeling to estimate stationary properties of the series, or dynamics, that represent trait-like phenotypes [25].

To estimate genetic and environmental influences on individual variation in dynamics, it is assumed that the estimated dynamics are unique to each individual. However, when related individuals are simultaneously sampled in their daily environments, the momentary states from which their dynamics are estimated are not likely to be independent. Accounting for cohabitation and social interaction generally between study participants requires a multivariate modeling approach in which the unique dynamics of each twin can be distinguished from mutual effects upon one another. In this study, we considered technical challenges in obtaining twin-specific dynamical phenotypes from time series data in cohabiting twin pairs who potentially shared experiences and influenced one another throughout the study period. In the process of explicitly modeling such effects, we were able to quantify and test assump-

tions of the twin model that are typically only noted in cross-sectional studies. In the first section, we outline multivariate time series modeling strategies and considerations with respect to biometrical genetic modeling. Second, we use simulations to validate a two-step procedure for estimating the heritability of time-invariant dynamics. Third, we apply our procedure to affect data to estimate both the heritability of emotion regulation dynamics and potentially confounding cross-twin effects.

Classic twin modeling techniques estimate the proportions of variance attributable to additive genetic, common environmental, and unique environmental variation by comparing the phenotypic cotwin correlations for monozygotic (MZ) twins to those of dizygotic (DZ) twins [13, 125]. In these models, heritability (a^2) represents the proportion of phenotypic variation in a population due to additive genetic variation. With twin models, the genomic variation is not measured explicitly but assumed *a priori* given that the genomes of MZ twins are completely correlated while those of DZ twins are on average correlated one-half. In the simplest manifestation of the twin model, any statistical differences between MZ and DZ phenotypic correlations are thought to be attributable to additive genetic factors. If genetic variation is additive, an estimate is given by $a^2 = 2(\rho_{MZ} - \rho_{DZ})$. Conversely, common environmental variance is represented by the portion of the MZ twin correlation that exceeds the additive genetic variation, $c^2 = \rho_{MZ} - a^2$.

To estimate the heritability, it is assumed that the environment contributes to phenotypic similarity in MZ and DZ twins to an equal degree. If environmental influences are present that increase the similarity of MZ twins but not DZ twins, then the heritability will be upwardly biased. In EMA studies of cohabiting twins, environmental effects include social influence from one's cotwin. If aspects of the social relationships between MZ twins systematically differ from DZ twins, then socially relevant phenotypes in the MZ twins may be more or less similar than DZ twins as a

consequence.

Previous discussion of the equal environments assumption (EEA) has been too extensive and varied to cover comprehensively here, but many examples from the literature are illustrative. Studies that focused on parental perceptions of twin similarity generally have not found prominent EEA violations. Two such studies found no violations of EEA across a range of psychiatric disorders [126, 127]. Plomin et al. [128] considered similarity of appearance by personality rating and showed that MZs may actually be treated by parents as more different as a result of visual similarity. Hettema et al. [129] had physical similarity rated by photographs and examined several psychiatric conditions but only found evidence for EEA violations in one, namely bulimia nervosa. However, the EEA for eating attitudes and behaviors was examined with the same methods in a later study by Klump et al. [130], and the significant result by Hettema et al. [129] did not replicate. Other studies examined similarity of twin experiences and physical environments. Negative environmental exposures involving trauma and abuse revealed several significant violations of EEA in models of schizophrenia [131]. Littvay [132] examined the effect of shared physical environments on political attitudes and found negligible effects. Felson [133] conducted a broad review of studies regarding the EEA for a wide range of phenotypes. They conclude that while the EEA is not strictly and universally valid, only small biases to heritability seem to result. Finally, Eaves [134] warned that many rejections of the EEA do not take into account the role of genetic similarity in selection of environments, also known as gene-environment correlation. Such sources of twin similarity may be regarded as nonetheless arising from genetic factors by indirect means.

For this study, we did not specifically aim to address the equal environments assumption on its past terms. The problem of modeling intensive time series data in psychology is relatively new, and the role of the EEA differs in a number of technical

respects. Most twin studies to date have used cross-sectional data with trait measures that are treated as relatively invariant over time. For any study in which state-based measures are available, time-invariant properties of the series may serve as phenotypes in the classical, cross-sectional sense. The central distinction we aim to make is that confounding cross-twin effects may be observable and highly consequential in patterns of state-based twin covariation over time. For instance, a time-lagged association between twins may imply a causal relationship between them, such as a social influence. If the measurement interval of the series is short enough, a simultaneous twin covariance in time may imply some degree of shared experience, be it parental treatment or physical environments. It may therefore be necessary to disentangle these sources of dynamic similarity to estimate dynamics that are unique to each twin. The remaining correlation of time-invariant dynamics can be assumed to arise from the time-invariant sources of genetic and common environmental variation that are conventionally estimated.

We aimed to extract twin-specific parameters of emotion regulation from time series EMA data of positive and negative affect collected in twin pairs over 45 days. In the process, we describe how components of the extraction model represent shared and unique twin experiences and cotwin social influences. We hypothesized that emotion regulation effect sizes and twin correlations would differ when cross-twin effects were not included in the model. Last, we aimed to determine whether the magnitudes of cross-twin regressions and innovation correlations were greater in MZ twins than DZ twins, suggesting a kind of violation of the EEA.

5.2 Models

A dynamical systems model of twin covariation over time can be specified using a vector-autoregressive (VAR) state-space model (SSM) [36, 32]. State-space algebra

is a highly general approach to time series data, combining common elements from structural equation modeling such as latent variables [38] with iterative algorithms to condition each estimate of the latent state on its previous states. The latent variables may therefore be Markov processes in continuous or discrete time. Continuous time processes take the form of differential equations with parameters that are invariant to the potentially random measurement intervals. Discrete time processes assume a constant interval between measurements and are formulated in terms of time lags. Linear systems may be formulated equivalently in terms of either. A linear SSM in discrete time is defined as follows:

$$\mathbf{x}_t = \mathbf{A}\mathbf{x}_{t-1} + \mathbf{B}\mathbf{u}_t + \mathbf{w}_t, \quad (5.1)$$

$$\mathbf{y}_t = \mathbf{C}\mathbf{x}_t + \mathbf{D}\mathbf{u}_t + \mathbf{v}_t, \quad (5.2)$$

$$\mathbf{w} \sim N(0, \mathbf{Q}), \quad \mathbf{v} \sim N(0, \mathbf{R}), \quad t \geq 0, \quad (5.3)$$

where \mathbf{x}_t is the vector of latent states and \mathbf{y}_t is the vector of observed measures. In the state equation (5.1), \mathbf{A} contains the transfer function parameters describing the relation of the state to both its own prior states and those of other latent variables. \mathbf{B} contains regression coefficients of the state onto exogenous inputs (i.e., time-varying covariates) \mathbf{u}_t . \mathbf{Q} is the covariance matrix of innovations \mathbf{w}_t (also known as disturbances or process noise). When \mathbf{x}_t contains the state of affect or other psychological variables, we might regard innovations as the effects of new experiences on the individual.

The measurement equation maps the latent state \mathbf{x}_t to the indicators \mathbf{y}_t with factor loading matrix \mathbf{C} . \mathbf{D} contains the regression coefficients of the indicators onto any exogenous variables. \mathbf{R} is the diagonal covariance matrix of the model residuals \mathbf{v}_t , that is, i.i.d. random variation that does not affect the latent state, such as

measurement error.

When \mathbf{u} includes a column of ones, \mathbf{B} may contain parameters representing factor means or \mathbf{D} can include indicator means. When \mathbf{A} is matrix of zeros, the model reduces to a factor analysis, where \mathbf{Q} is the covariance matrix of the factors.

A state-space model specifying a lag-1 vector autoregression of latent states loading onto p indicators per twin may be specified as follows:

$$\begin{bmatrix} T_{1,t} \\ T_{2,t} \end{bmatrix} = \begin{bmatrix} \beta_1 & \gamma_{1,2} \\ \gamma_{2,1} & \beta_2 \end{bmatrix} \begin{bmatrix} T_{1,t-1} \\ T_{2,t-1} \end{bmatrix} + \begin{bmatrix} w_{1,t} \\ w_{2,t} \end{bmatrix}, \quad w \sim N \left(\begin{bmatrix} 0 \\ 0 \end{bmatrix}, \begin{bmatrix} 1 & \rho \\ \rho & 1 \end{bmatrix} \right) \quad (5.4)$$

$$\begin{bmatrix} y_{1,1,t} \\ \vdots \\ y_{1,p,t} \\ y_{2,1,t} \\ \vdots \\ y_{2,p,t} \end{bmatrix} = \begin{bmatrix} \vec{\lambda} & 0 \\ 0 & \vec{\lambda} \end{bmatrix} \begin{bmatrix} T_{1,t} \\ T_{2,t} \end{bmatrix} + \begin{bmatrix} \mu_{1,1} \\ \vdots \\ \mu_{1,p} \\ \mu_{2,1} \\ \vdots \\ \mu_{2,p} \end{bmatrix} + \begin{bmatrix} v_{1,1,t} \\ \vdots \\ v_{1,p,t} \\ v_{2,1,t} \\ \vdots \\ v_{2,p,t} \end{bmatrix}. \quad (5.5)$$

In measurement model, Equation 5.5, $\vec{\lambda}$ is a vector of p factor loadings relating each indicator $y_{i,j,t}$ to latent states $T_{i,t}$. $\mathbf{D}\mathbf{u}_t$ reduces to a simple vector of indicator means, $\mu_{i,j}$. The complete model can be seen in a form of path diagram in Figure 9. The path diagram resembles a cross-lagged panel model, except that there need not be a defined or small number of occasions. Only the matrices stated in Equations 5.1 and 5.2 are used in a recursive way to compute the model likelihood at each occasion.

Alternative state equations may be substituted for Equation 5.4. For example, the lag-1 vector autoregression may be specified in terms of a first-order differential equation. Differential equations allow continuous-time modeling with parameters that

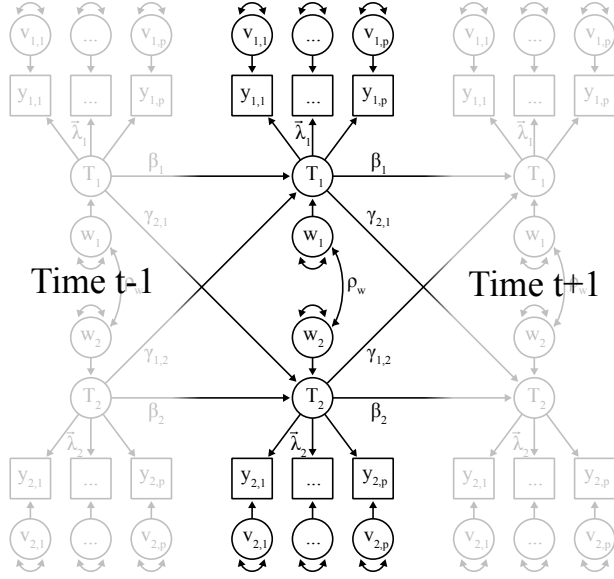


Fig. 9.: Path diagram of state-space twin model

are invariant to irregularities in the observation interval. The expectation of the state at each time is instead a function of its derivatives, $x(t)$, $\dot{x}(t)$, etc.

$$\begin{bmatrix} \dot{T}_1(t) \\ \dot{T}_2(t) \end{bmatrix} = \begin{bmatrix} \lambda_1 & \gamma_{1,2} \\ \gamma_{2,1} & \lambda_2 \end{bmatrix} \begin{bmatrix} T_1(t) \\ T_2(t) \end{bmatrix} + \begin{bmatrix} w_1(t) \\ w_2(t) \end{bmatrix}, \quad w \sim N \left(\begin{bmatrix} 0 \\ 0 \end{bmatrix}, \begin{bmatrix} \sigma_1 & \rho \\ \rho & \sigma_2 \end{bmatrix} \right) \quad (5.6)$$

A popular continuous-time model is the damped linear oscillator (DLO) and its coupled version. These models have been popularized by their use in the Latent Differential Equation approach [LDE, 43], but may also be specified as state-space models for processes that include continuous random noise in the latent state:

$$\begin{bmatrix} \dot{T}_1(t) \\ \ddot{T}_1(t) \\ \dot{T}_2(t) \\ \ddot{T}_2(t) \end{bmatrix} = \begin{bmatrix} 0 & 1 & 0 & 0 \\ \eta_1 & \zeta_1 & \gamma_{2,1} & \gamma_{2,1} \\ 0 & 0 & 0 & 1 \\ \gamma_{1,2} & \gamma_{1,2} & \eta_2 & \zeta_2 \end{bmatrix} \begin{bmatrix} T_1(t) \\ \dot{T}_1(t) \\ T_2(t) \\ \dot{T}_2(t) \end{bmatrix} + \begin{bmatrix} 0 \\ w_1(t) \\ 0 \\ w_2(t) \end{bmatrix}, \quad w \sim N \left(\begin{bmatrix} 0 \\ 0 \\ 0 \\ 0 \end{bmatrix}, \begin{bmatrix} 0 & 0 & 0 & 0 \\ 0 & \sigma_1 & 0 & \rho \\ 0 & 0 & 0 & 0 \\ 0 & \rho & 0 & \sigma_2 \end{bmatrix} \right), \quad (5.7)$$

Iterative algorithms compute the likelihood of each observed occasion conditional on prior observed and estimated values. Specifically, we used the Kalman filter, a method of obtaining minimum-variance unbiased estimates of the latent state at each occasion [46]. In brief, the Kalman filter recursively predicts the latent state at time t from its optimal estimate at $t - 1$, then uses the observed data at t to make an optimal correction to its prediction. The next occasion is then predicted from that corrected estimate. The Kalman filter can be used with Full Information Maximum Likelihood (FIML) as with other SEM,

$$-2 \ln(\mathcal{L}(\hat{\theta}|\mathbf{Y})) = \sum_{t=1}^T [\ln(2\pi|\hat{\Sigma}|) + (y_t - \hat{y}_t)^T \hat{\Sigma}^{-1} (y_t - \hat{y}_t)] \quad (5.8)$$

with the important difference that in place of individual i we have time t , and in place of the between-persons mean μ we have \hat{y}_t , a vector of predicted indicator values at time t conditional on a filtered state prediction from $t - 1$. This likelihood function for state-space models can therefore be optimized to find parameters that minimize the prediction error. Unlike SEM panel process models, an increase in the number of measurement occasions does not increase the size of the model matrices or the complexity of the likelihood function, making it suitable for intensive time series data. Independently modeled individuals, twin pairs, or other kinds of groups may be combined in a multi-group model by summing separate likelihood functions con-

ditional on shared parameters. For a more complete description of the Kalman filter algebra, see for example [36] or [46]. For a guide to specifying SSMs for estimation with OpenMx, see [135].

After estimates of a model phenotype are obtained for each twin, the next step is to estimate their heritability. This can potentially be done in a two-step process by treating a matrix of estimates as observed data and applying conventional twin-modeling strategies. A more statistically rigorous analysis must integrate the precision of its estimates across all levels in a hierarchical manner. For this study, we chose to use a two-step process and leave consideration of hierarchical modeling techniques for future study. Regardless of the strategy used to estimate the heritability of a parameter, it is necessary to consider systematic sampling covariance of the parameters given the model. In small samples, the sampling covariance of the parameters will confound the substantive twin correlations that are due to genetic and environmental factors, leading to biased heritability estimates. The sampling covariance of the parameters of a fully parameterized VAR is given as

$$\hat{\Sigma}(\text{Vec}(\hat{\theta})) = (Z^T Z)^{-1} \otimes \hat{\mathbf{Q}}, \quad (5.9)$$

where Z is the $t \times q$ matrix of estimated latent states. As the covariance of the twin-specific parameters is a function of their innovation covariance, simply accounting for additional sources of phenotypic dependence is not enough to avoid bias. To adjust for the bias, an estimate of the sampling covariance must be obtained and subtracted from the empirical covariance of the parameters. In cases of structural model fitting with constraints on parameter values and fixed parameters, the above algebra may not lead to an accurate result. Alternatively, the Hessian, i.e., the matrix of second partial derivatives of the $-2 \ln(\hat{\mathcal{L}})$ with respect to the parameters, is a more general

way to estimate the sampling covariance,

$$\hat{\Sigma}(\text{Vec}(\hat{\theta})) \approx \left(\frac{1}{2}\mathbf{H}\right)^{-1}. \quad (5.10)$$

Typically, the Hessian is used with maximum likelihood to compute confidence intervals for parameter estimates. The off-diagonal elements are not generally of interest. For any structural decomposition of the parameter covariance matrix however, it is necessary to account for systematic sampling covariance to avoid biased estimation.

In the next sections, we first used simulations to verify the presence of systematic sampling covariance when twin innovations are correlated. Second, we demonstrate how estimates of twin parameter covariance and heritability are affected by inclusion of cross-twin parameters in the model and adjustments for systematic sampling covariance.

5.3 Simulations

Software All analyses were computed using R statistical computing environment [74]. State-space models were specified and optimized using OpenMx, a free, open-source modeling package for R [136]. Model optimization used a combined compute plan consisting of a Simulated Annealing step [137] followed by gradient descent.

5.3.1 Simulation I: Sampling Distributions

The first Monte-Carlo simulation used repeated iterations of a single twin-pair model with constant parameter values to compare an observed sampling distribution to an estimate from the Hessian of the model's $-2\ln(\hat{\mathcal{L}})$. A single VAR SSM was specified as shown in Equation 5.4 with 2 latent states and 3 observed indicators per state. Data-generating parameter values were chosen to be unique and to result in stable, stationary dynamics. Each indicator loaded equally ($\lambda_{i,j} = .5$) with zero

means and residual variances of $\sigma_v^2 = .01$. VAR parameters were given the values $\beta_1 = .6$, $\beta_2 = .65$, $\gamma_{2,1} = .3$, $\gamma_{1,2} = .2$. Innovations were correlated $\rho = .5$. Once the model was specified using package `OpenMx`, the command `mxGenerateData()` was used to generate multivariate series according to the parameter values.

The simulation was run for 500 unique iterations, each with 45 occasions per series. Each iteration produced a set of parameter estimates and a Hessian-based sampling covariance matrix. The average Hessian-based sampling covariance matrix was computed across all iterations of simulation and compared to the distribution of point estimates. Table 11 shows the sampling covariance of the point estimates. Table 12 shows the average Hessian for comparison. In both, the bolded upper triangle gives the Pearson correlation coefficients.

Table 11.: Sampling covariance of VAR parameters from simulation. Correlations are given in bold in the upper triangle.

	β_1	$\gamma_{2,1}$	$\gamma_{1,2}$	β_2
β_1	0.0280	0.50	-0.74	-0.34
$\gamma_{2,1}$	0.0138	0.0276	-0.34	-0.71
$\gamma_{1,2}$	-0.0186	-0.0084	0.0228	0.47
β_2	-0.0079	-0.0162	0.0099	0.0192

The similarity of estimates in Tables 11 and 12 shows that even with the relatively short series length used in this model, the Hessian-based covariance matrix is accurate. Importantly, the twin-specific parameter estimates $\hat{\beta}$ have a moderate, negative correlation. If the model represents MZ twins, then the sampling covariance will bias the heritability estimate downward. If the model represents the DZ twins, then this sampling covariance would potentially bias the heritability upward.

Table 12.: Estimated Hessian-based sampling covariance $\mathbb{E}[(\frac{1}{2}\mathbf{H})^{-1}]$. Correlations are given in bold in the upper triangle.

	β_1	$\gamma_{2,1}$	$\gamma_{1,2}$	β_2
β_1	0.0258	0.50	-0.78	-0.40
$\gamma_{2,1}$	0.0131	0.0259	-0.40	-0.78
$\gamma_{1,2}$	-0.0173	-0.0089	0.0192	0.50
β_2	-0.0089	-0.0174	0.0097	0.0193

5.3.2 Simulation II: Heritability

The second Monte Carlo simulation was used to determine: 1) the effect of excluding cross-twin effects from the model; and 2) whether a bias adjustment using the Hessian-based estimate of the sampling covariance was adequate to recover the true additive genetic and common environmental variance of the parameters. Two models were tested: One as specified in the previous simulation with cross-twin regressions and correlated innovations, and one with those parameters fixed to zero, representing independence of momentary states between twins.

The bias-adjusted twin covariances of $\hat{\beta}$ were computed by taking the average bias-adjusted correlation matrix. That is, each twin-pair model produced a Hessian-based estimate of the sampling covariance of the $\hat{\beta}$ estimates. The total, empirical covariance of $\hat{\beta}$ across all pairs was computed. The Hessian-based covariance from each pair was then subtracted from the empirical, between-pairs covariance matrix,

$$\bar{\Sigma}(\theta)_i = \hat{\Sigma}(\theta) - \left(\frac{1}{2}\mathbf{H}_i\right)^{-1}, \quad i \in 1 \dots N. \quad (5.11)$$

Each adjusted covariance matrix was converted to a correlation matrix, then the mean

of the correlation matrices was taken as the final bias-adjusted correlation matrix:

$$\mathbf{D}_i = \sqrt{\text{diag}(\bar{\Sigma}_i)}. \quad (5.12)$$

$$\text{Adj. Corr.}(\theta) = \frac{1}{N} \sum_i^N \mathbf{D}_i^{-1} \bar{\Sigma}_i \mathbf{D}_i^{-1}. \quad (5.13)$$

Additive genetic and common environmental variances were specified as $a^2 = .6$ and $c^2 = .3$. Common environmental effects are often small in real applications, and often shrink with age. We chose non-zero c^2 to both test the maximally complex scenario, and because our data were collected in younger, adolescent twins for which c^2 effects may be more prominent. By focusing on recovery of twin correlations, our results should generalize to models with only a^2 and e^2 as well. R package MASS was used to generate a multivariate distribution of β values for 100 MZ and 100 DZ twin pairs. Constrained random generation (with argument `empirical=TRUE`) was used to simplify our tests by ensuring that the empirical, data-generating parameter correlations had exactly the specified values without sampling variation.

A covariance matrix of β was specified according to expected genetic and environmental twin correlations as

$$\Sigma(\beta) = \sigma_\beta \begin{bmatrix} a^2 + c^2 + e^2 & a^2 + c^2 & 0 & 0 \\ a^2 + c^2 & a^2 + c^2 + e^2 & 0 & 0 \\ 0 & 0 & a^2 + c^2 + e^2 & .5a^2 + c^2 \\ 0 & 0 & .5a^2 + c^2 & a^2 + c^2 + e^2 \end{bmatrix} = .1 \begin{bmatrix} 1 & .9 & 0 & 0 \\ .9 & 1 & 0 & 0 \\ 0 & 0 & 1 & .6 \\ 0 & 0 & .6 & 1 \end{bmatrix}, \quad (5.14)$$

with $e^2 = 1 - a^2 - c^2 = .1$.

To include bias due to MZ cross-twin effects in the simulation, MZ twins had larger cross-regressions and innovation correlations ($\gamma \sim N(0, .3)$, $\rho = .5$) than DZ

twins ($\gamma \sim N(0, .1)$, $\rho = .2$). Other parameters, including the indicator means, residual variances, and factor loadings, were given the same values as the first simulation.

100 iterations of simulation were run with 750 observations per series. At each iteration, a bias-adjusted correlation matrix was computed as shown in Equations 5.11-5.13.

Table 13 shows the twin correlations for both models, each with and without the additional bias adjustment. The results demonstrate that the twin correlations are most accurately recovered when the expected cross-twin effects are estimated in the model and adjustments are made to correct for the bias due to sampling covariances. The heritability when cross-twin effects were not included in the model was approximately zero, with bias adjustment slightly boosting both MZ and DZ twin correlations. This result is unexpected under the conventional intuition that cross-twin effects linearly contribute to the covariance of a phenotype in typical cross-sectional studies. The cross-twin effects in the SSM serve to explain part of the autocovariance of the series. When excluded, the unexplained autocovariance biases estimates of the autoregressive parameters, diminishing their twin correlations rather than inflating them. In this simulation, the greater cross-twin effects in MZ twins than DZ twins resulted in a lower twin correlation and obfuscation of the heritability of β .

5.4 Application: Affect data

Data were supplied by the Michigan State University Twin Registry [138, 139, 140, 141] and included 314 twin pairs ($N_{MZ} = 171$, $N_{DZ} = 143$) between ages 15 and 25. All participants were adolescent females who met the following inclusion / exclusion criteria for the original aims, including 1) menstruation every 22-32 days for the past 6 months; 2) no hormonal contraceptive use within the past 3 months; 3) no psy-

Table 13.: Estimated twin correlations True values were $r_{\text{MZ}} = .9$, $r_{\text{DZ}} = .6$

Model	Bias	\hat{r}_{MZ}	\hat{r}_{DZ}
$\gamma, \rho \neq 0$,	Unadjusted	0.76 (0.68, 0.836)	0.53 (0.47, 0.597)
$\gamma, \rho \neq 0$,	Adjusted	0.87 (0.79, 0.956)	0.59 (0.52, 0.665)
$\gamma, \rho = 0$,	Unadjusted	0.58 (0.45, 0.711)	0.56 (0.49, 0.639)
$\gamma, \rho = 0$,	Adjusted	0.61 (0.47, 0.736)	0.62 (0.53, 0.697)

chotropic or steroid medications within the past 4 weeks; 4) no pregnancy or lactation within the past 6 months; and 5) no history of genetic or medical conditions known to influence hormone functioning or appetite/weight. Zygosity was determined by a 5-item physical similarity questionnaire and buccal swab DNA testing. The Positive and Negative Affect Schedule (PANAS) [4] was used to assess affect in every participant once per day for 45 days in total. Participants were asked every evening to give a general rating of affect for the course of that day. The PANAS instrument includes twenty affect adjectives including “Enthusiastic”, “Alert”, “Distressed”, “Upset”, and “Anxious”, with 5-point agreement rating scales for each. The instrument was designed to reflect a two-factor affect structure resulting from an Exploratory Factor Analysis (EFA) with “varimax” rotation of the affect indicators.

Quality Control For each twin pair, rows of affect data were aligned by their date of assessment. Requirements for a minimum amount of complete data were necessary to avoid an excess of parameter estimates with extreme error that would add noise to the second-stage biometrical genetic analysis. If either twin had fewer than 15 rows of complete affect data, the whole pair was excluded from the analysis. If a twin pair as a whole had fewer than 15 rows of complete data, that is, had fewer than 15 days containing complete affect records in both twins, then that twin pair was

excluded. These requirements ensured that twins individually had sufficient rows of data for analysis while also sharing a sufficient number of simultaneous measurement occasions. Out of 314 available twin pairs, 276 ($N_{MZ} = 153, N_{DZ} = 123$) met these criteria for quality. The median number of complete rows per twin pair was 34, and 54 pairs had 15 to 25 complete rows of data. No associations were found linking the outcome of our exclusion criteria to age, race, or body mass index (BMI).

Some participants did not respond with more than one rating on one or more items of PANAS. Zero-variance data columns could not be modeled and had to be excluded on a case-by-case basis, though no twin pair had enough of such columns to be excluded as a whole. Table 14 gives the number of individuals per number of unique responses for each item of the PANAS questionnaire. Where an individual only had one unique response on an item, that item was excluded from their model. For instance, “Hostile” was excluded for 102 participants. Across all items, individuals most frequently used 4 response categories. Fewer categories were used for negative affect than positive affect items on average.

5.4.1 Model

Because each twin pair had no more than 45 complete rows of data and only one assessment per day, we chose the simplest parameterization possible and modeled only a lag-1 autoregression in discrete time, giving the following state equation:

Table 14.: Number of individuals per number of unique responses on each item of the PANAS.

# unique responses:	1	2	3	4	5
Interested	1	33	149	235	134
Excited	1	8	69	198	276
Strong	15	70	182	190	95
Enthusiastic	4	30	121	198	199
Proud	7	49	124	194	178
Alert	12	55	160	213	112
Inspired	20	70	143	211	108
Determined	5	31	124	211	181
Attentive	19	54	160	180	139
Active	4	24	81	206	237
Total % (PA)	0.02	0.08	0.24	0.37	0.30
Distressed	9	81	162	167	133
Upset	5	52	127	186	182
Guilty	62	186	149	105	50
Scared	38	145	172	131	66
Hostile	102	167	136	101	46
Irritable	13	71	164	193	111
Ashamed	82	189	153	83	45
Nervous	9	63	159	184	137
Jittery	70	162	148	101	71
Afraid	54	162	162	109	65
Total % (NA)	0.08	0.23	0.28	0.25	0.16

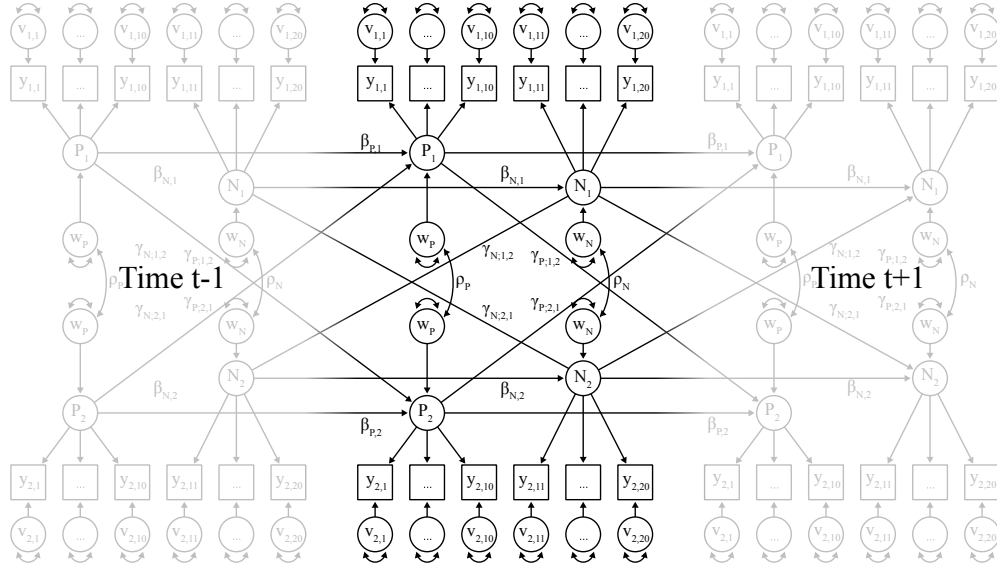


Fig. 10.: Path model representation of the positive and negative affect twin state-space model with cross-twin effects.

$$\begin{bmatrix} P_{1,t} \\ N_{1,t} \\ P_{2,t} \\ N_{2,t} \end{bmatrix} = \begin{bmatrix} \beta_{P;1} & 0 & \gamma_{P;1,2} & 0 \\ 0 & \beta_{N;1} & 0 & \gamma_{N;1,2} \\ \gamma_{P;2,1} & 0 & \beta_{P;2} & 0 \\ 0 & \gamma_{N;2,1} & 0 & \beta_{N;2} \end{bmatrix} \begin{bmatrix} P_{1,t-1} \\ N_{1,t-1} \\ P_{2,t-1} \\ N_{2,t-1} \end{bmatrix} + \begin{bmatrix} w_{P;1,t} \\ w_{N;1,t} \\ w_{P;2,t} \\ w_{N;2,t} \end{bmatrix}, \quad (5.15)$$

$$w \sim N \left(\begin{bmatrix} 0 \\ 0 \\ 0 \\ 0 \end{bmatrix}, \begin{bmatrix} 1 & 0 & \rho_P & 0 \\ 0 & 1 & 0 & \rho_N \\ \rho_P & 0 & 1 & 0 \\ 0 & \rho_N & 0 & 1 \end{bmatrix} \right), \quad (5.16)$$

The \mathbf{A} matrix above contains parameters (β) describing the autoregressive tendency of positive (P) and negative (N) affect in each twin. The off-diagonal elements include parameters γ that regress Twin 1 P_1 onto Twin 2 P_2 and vice versa. The same

is specified for negative affect. The covariance matrix specifies P and N as orthogonal within-twin, but potentially sharing innovations between-twin. While it is possible to expand the number of parameters to include cross-valence within and between-twin correlations, we chose a simple specification to ensure model identification and statistical power.

The measurement equations relating the PANAS indicators to their latent states were specified as follows:

$$\begin{bmatrix} y_{1,1,t} \\ \vdots \\ y_{1,20,t} \\ y_{2,1,t} \\ \vdots \\ y_{2,20,t} \end{bmatrix} = \begin{bmatrix} \vec{\lambda}_P & 0 & 0 & 0 \\ 0 & \vec{\lambda}_N & 0 & 0 \\ 0 & 0 & \vec{\lambda}_P & 0 \\ 0 & 0 & 0 & \vec{\lambda}_N \end{bmatrix} \begin{bmatrix} P_{1,t} \\ N_{1,t} \\ P_{2,t} \\ N_{2,t} \end{bmatrix} + \begin{bmatrix} \mu_{1,1} \\ \vdots \\ \mu_{1,20} \\ \mu_{2,1} \\ \vdots \\ \mu_{2,20} \end{bmatrix} + \begin{bmatrix} v_{1,1,t} \\ \vdots \\ v_{1,20,t} \\ v_{2,1,t} \\ \vdots \\ v_{2,20,t} \end{bmatrix}, \quad (5.17)$$

\mathbf{y}_t was arranged according to the intended dimensions of the PANAS, positive indicators first, and with positive and negative indicators loading onto separate factors. No cross-loadings within or between twin were permitted. The \mathbf{C} matrix is consequently a block-diagonal 40×4 matrix where each $\vec{\lambda}$ is a 10-element vector containing factor loadings. For this model, \mathbf{u}_t was only a vector of ones, resulting in $\mathbf{D}\mathbf{u}_t$ equaling the vector of indicator means.

5.4.2 Analyses

Affect variables were first standardized per individual. The Twin SSM was fit to all twin pairs, resulting in sets of twin-pair specific parameter estimates and model likelihoods. Constrained models with all γ and ρ parameters fixed to zero in the \mathbf{A} and \mathbf{Q} matrices were also fit to each pair. Under certain regularity conditions,

the difference between the $-2\ln(\hat{\mathcal{L}})$ of the saturated and constrained model, or the Likelihood Ratio (LR), is distributed as a non-central χ^2 on 6 degrees of freedom, as we constrained 6 parameters in total [142]. Higher LRs indicate greater degradation of model fit as a result of the parameter constraints. The Likelihood Ratio Test (LRT) of statistical significance consists of determining if the LR is greater than a critical value on the χ^2 distribution computed for some false positive rate α . We used $\alpha = .05$, making $\chi^2_{df=6}$ critical value approximately 12.59.

First, the LRs were regressed onto zygosity, coded as the average genetic correlation ($rG_{DZ} = 0.5, rG_{MZ} = 1.0$). The number of complete rows of data was included in the model to account for LR differences due to sample size. Cohabitation as a binary indicator was also included in the model, though only 17 twin pairs reportedly did not cohabit.

Second, overall cotwin influence effect sizes were computed as $\hat{\gamma}_P = \hat{\gamma}_{P;1,2}^2 + \hat{\gamma}_{P;2,1}^2$, and $\hat{\gamma}_N = \hat{\gamma}_{N;1,2}^2 + \hat{\gamma}_{N;2,1}^2$. These, along with shared experiences $\hat{\rho}_P$ and $\hat{\rho}_N$ were regressed on zygosity.

5.5 Results

Results of model fitting were first examined for errors and problematic outliers. MZ twins had a mean LR of 24.37, a median of 14.52, and a standard deviation of 44.38. DZ twins had a mean LR of 11.22, a median of 7.97, and a standard deviation of 8.63. Three MZ twin pairs had LRs with extreme values of 203.12, 196.01, and 444.12. One MZ pair had an anomalous, negative LR of -3.14 that remained even after alternative optimization strategies were attempted¹. Figure 11 shows series of estimated latent states from the saturated model of the anomalous twin pair.

¹Reruns with simulated annealing followed by gradient descent, also gradient descent with start values set to the estimates of the constrained model.

While positive affect demonstrates typical variability, negative affect had practically no variability other than two extreme values. The twins were highly correlated for positive affect and almost perfectly correlated for negative affect. The twin pairs with the three extreme LRs and the negative LR were excluded from further steps of the analysis.

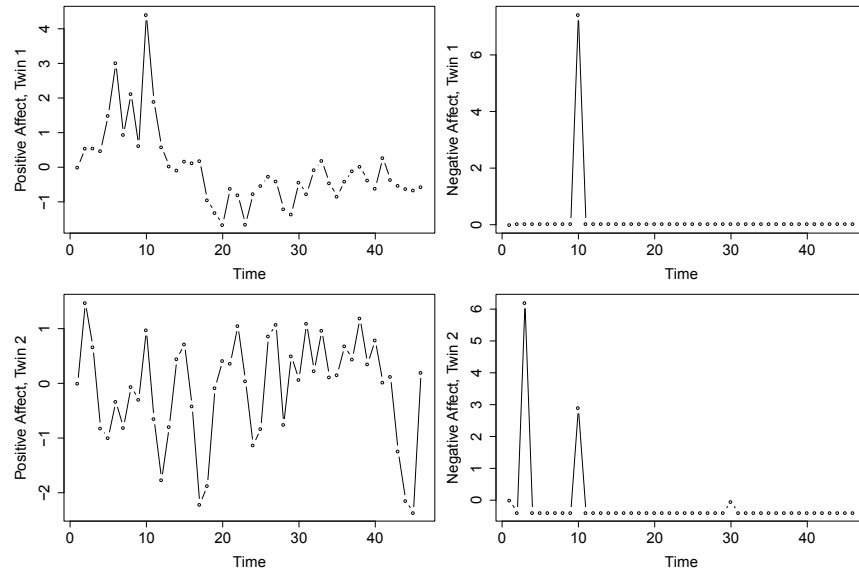


Fig. 11.: Series of estimated latent states in one twin pair that showed statistical anomalies, likely due to a problematic lack of variation.

Initial examination of effects showed extreme correlations driven by outliers in the saturated model (Figure 12). The outlier effects tended to result from problematic data such as shown in Figure 11. Values of β less than -1 and greater than 1 represented unstable systems with rapidly growing variance, and were therefore also violations of the theoretical expectations for those parameters. Furthermore, they were statistical outliers, falling outside of the 95% probability region of the distribution of the remaining estimates. Values of $\hat{\beta} > 1$ fell into the upper tail with probability of 1.18%, and $\beta < -1$ fell into the lower tail, having probability of .002%.

The means of each γ estimate were 0 and standard deviations were all .29, mapping values below -1 and above 1 to a probability of .03%, or about 3.45 standard deviations from the mean. While the stability of the system does not strictly depend on γ falling within $[-1, 1]$, extreme values of γ tended to indicate problems with the fit of the model and are not easily interpreted. Altogether, 47 of the 276 twin were esti-

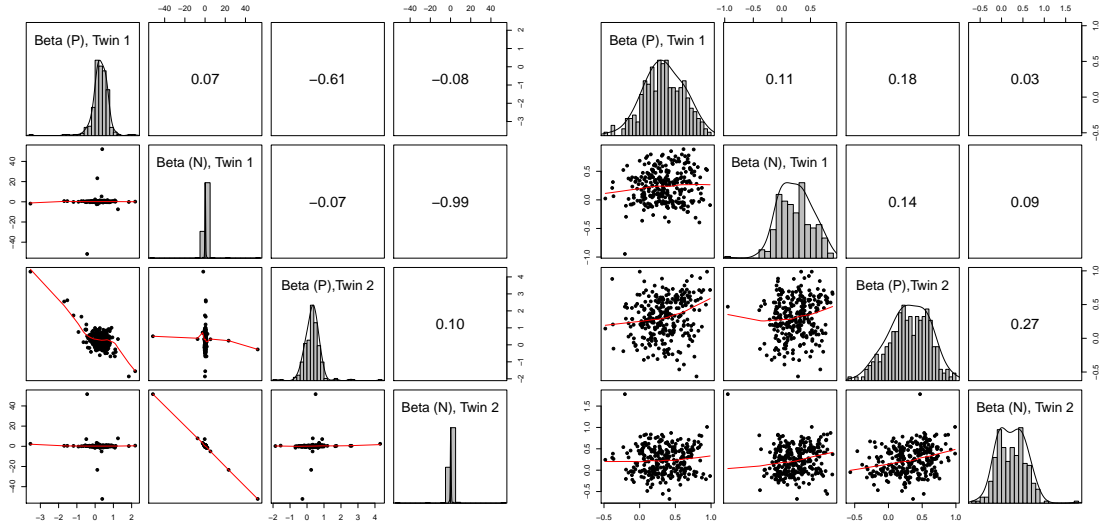


Fig. 12.: Bivariate distributions of estimated effects $\hat{\beta}$. The saturated model (Left) shows extreme correlation driven by outliers. The constrained model (Right) had fewer outliers. Pearson correlations are shown in the upper right triangles.

imated to be unstable or theoretically unlikely systems constituting outliers given the above percentiles. We excluded these twin pairs from the analysis to avoid biased or nonsensical results (such as the correlation of -0.99 shown in Figure 12) and focus only on theoretically feasible values within the $[-1, 1]$ interval. The remaining estimates formed a reasonably Gaussian distribution with much smaller remaining correlations (Figure 13).

LRTs on 6 degrees of freedom resulted in varying statistical significance of cross-twin effects across twin pairs. Table 15 shows the frequencies of LRTs greater than

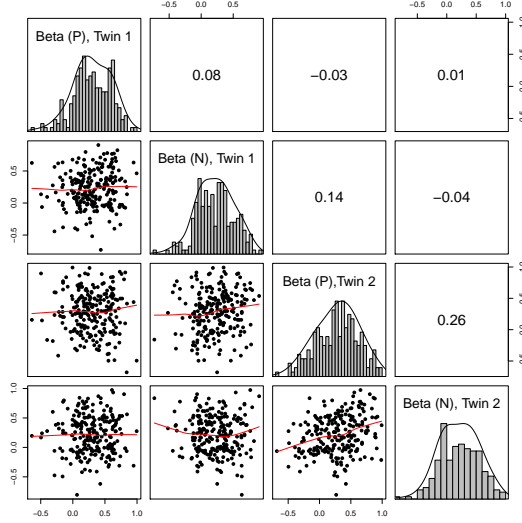


Fig. 13.: Bivariate distributions of estimated effects $\hat{\beta}$ from the saturated model after exclusion of outliers. The extreme correlations disappear and a relatively Gaussian distribution remains. Pearson correlations are shown in the upper right triangle.

the $\chi^2_{df=6}, \alpha = .05$ critical value (12.59) by zygosity. The $\chi^2_{df=1}$ test of association between zygosity and cross-twin effect significance was itself robustly significant with $p < .001$, showing that cross-twin effects were statistically significant for more MZ than DZ twin pairs.

Table 15.: Contingency table of significant Likelihood Ratio Tests (LRT) by zygosity. A significant LRT indicates that the twin pair model fits significantly worse when cross-twin effects are constrained to zero.

LRT:	$p > .05$	$p < .05$	Total
DZ	78	23	101
MZ	63	63	126
Total	141	86	227

$\chi^2_{df=1} = 14.482, p = .0001415$

Cohabitation was checked as a possible source of increased cross-twin influence. MZ and DZ twins were both found to cohabit at the same rate. 7 out of 116 DZs did not cohabit and 10 out of 143 MZs did not cohabit, or about 6 and 7% of the sample, respectively, showing no association with zygosity. After removal of outlier twin pairs, these numbers changed to 7 out of 94 DZs and 8 out of 118 MZs, roughly the same proportion and still with no statistical association with zygosity.

LRs were regressed onto zygosity (coded as rG , average genetic correlation, $DZ = 0.5, MZ = 1.0$), cohabitation, and data completeness (as total number of complete rows of data). Results of the multiple regression are shown in Table 16. On average, the .5 increase in genetic correlation from DZ to MZ was associated with an increase in the LR on average from 3.6 to 11.9, significant at $p < .001$. Data completeness and cohabitation were not significant.

Table 16.: Results of multiple regression of twin-pair LRs onto zygosity, data completeness, and cohabitation. LRs were computed from the difference of the $-2\ln(\hat{\mathcal{L}})$ of models in which twin effect parameters were freely estimated versus models in which they were constrained to zero. Zygosity (rG) was coded as $DZ = 0.5$ and $MZ = 1.0$.

	Estimate	CI-	CI+	p
Intercept	-8.143	-22.721	6.436	2.748E-01
rG	15.537	7.207	23.867	*3.202E-04
Data completeness	0.253	-0.050	0.556	1.035E-01
Cohabitation	3.764	-5.877	13.404	4.450E-01

Descriptive statistics for the estimated $\hat{\beta}$ parameters are shown in Table 17 under both the saturated (cross-twin effects, abbreviated CTFX $\neq 0$) and constrained

(CTFX= 0) model. On average, effect sizes described a tendency to decay toward equilibrium at a rate of approximately a 70% reduction per day from prior positive affect and a 80% reduction per day from prior negative affect. Effects were slightly larger when cross-twin effects were excluded from the model. γ s of PA and NA both had means of zero. Differences in average effect sizes are apparent between zygosity. MZ twins show larger standard deviations of γ , meaning larger positive and negative cross-twin effects on average. MZ innovations were also more than twice as correlated as DZ innovations.

Table 17.: Descriptive statistics for the twin-specific phenotypic parameter estimates $\hat{\beta}$ and cross-twin effects γ and ρ . Excluding twin effects (CTFX) from the model slightly inflated effect sizes, as cross-twin regressions accounted for part of the time dependence.

Model	Parameter	MZ			DZ		
		$\hat{\mu}$	$\hat{\sigma}$	Median	$\hat{\mu}$	$\hat{\sigma}$	Median
CTFX \neq 0	β_P	0.300	0.319	0.313	0.283	0.306	0.278
	β_N	0.211	0.304	0.206	0.227	0.310	0.234
	γ_P	-0.032	0.320	-0.066	0.007	0.259	-0.001
	γ_N	0.013	0.308	-0.040	0.035	0.245	-0.011
	ρ_P	0.263	0.393	0.268	0.122	0.324	0.104
	ρ_N	0.205	0.375	0.196	0.081	0.310	0.047
CTFX= 0	β_P	0.312	0.276	0.315	0.306	0.278	0.309
	β_N	0.223	0.279	0.238	0.236	0.302	0.217

Table 18 shows the results of the multiple regression of twin cross-regressive effects (γ) and innovation covariance (ρ) effect sizes onto cohabitation and zygosity,

which was coded as the expected genetic correlation (rG). All cotwin influence and shared experiences parameters were significantly greater in MZ twins at $p < .05$. Cohabitation was only significant for positive shared experiences ρ_P .

Table 18.: Coefficients from multiple regression of cross-twin effect sizes (γ^2 and ρ) onto zygosity (rG) and cohabitation status. All cross-twin effects were significantly associated with zygosity at $p < .05$.

Effect $\sim rG$	Estimate	CI-	CI+	p
Cotwin Influence (γ_P)	0.122	0.031	0.212	*8.972E-03
Cotwin Influence (γ_N)	0.142	0.029	0.255	*1.446E-02
Shared Experience (ρ_P)	0.280	0.091	0.468	*3.970E-03
Shared Experience (ρ_N)	0.248	0.066	0.431	*8.104E-03
Effect \sim Cohabitation	Estimate	CI-	CI+	p
Cotwin Influence (γ_P)	-0.024	-0.115	0.066	6.027E-01
Cotwin Influence (γ_N)	0.080	-0.033	0.193	1.663E-01
Shared Experience (ρ_P)	0.237	0.048	0.425	*1.462E-02
Shared Experience (ρ_N)	0.048	-0.134	0.230	6.069E-01

Using the procedures outlined in Simulation II, twin correlations for $\hat{\beta}$ were estimated and adjusted for bias due to sampling covariance. Table 19 shows the resulting correlations. The correlations were generally small enough to fall within error variation around zero. It can be seen that in the saturated model that included the cross-twin effects, the sizes of the correlations variously increased or decreased depending on the degree of sampling covariance subtracted out. For the constrained model, the bias adjustment increased the correlations, as the only elements of the sampling covariance that were not close to zero were the diagonals (i.e., sampling

variances).

Table 19.: Twin correlations for autoregressive effects $\hat{\beta}$ with and without bias adjustment.

Model	Bias	$r_{MZ}(\beta_P)$	$r_{MZ}(\beta_N)$	$r_{DZ}(\beta_P)$	$r_{DZ}(\beta_N)$
$\gamma, \rho \neq 0$,	Unadjusted	-0.162	-0.164	0.149	0.113
$\gamma, \rho \neq 0$,	Adjusted	-0.093	-0.081	0.384	0.257
$\gamma, \rho = 0$,	Unadjusted	0.159	0.195	0.327	0.159
$\gamma, \rho = 0$,	Adjusted	0.284	0.356	0.596	0.261

5.6 Discussion

Behavioral genetic studies of phenotypes derived from experience-sampling present a compounding number of statistical challenges over cross-sectional designs. State-based measures of cohabiting twins are likely to reflect many sources of environmental similarity, reflected in their contemporaneous and lagged correlations. In this study, we have demonstrated and applied one strategy for extracting independent features of behavior despite cohabitation and close interaction between twins. In the process, we quantified those interactions and discovered important differences in emotional dynamics dependent on zygosity. Different technical aspects of the twin-pair dynamical system were ascribed substantive interpretations. The correlation of random innovations served as a direct indicator of environmental similarity by way of shared, momentary, affective experiences. Cross-lagged regressions served as an indicator of the average influence of one twin upon the other. The autoregressive parameters unique to each twin modeled individual tendency to regulate emotions unrelated to the two aforementioned environmental tendencies.

We initially used simulations to test a two-step procedure for obtaining individual estimates of the emotion regulation phenotype and its estimated heritability while accounting for unbalanced cross-twin effects. Our first simulation verified that the Hessian-based sampling covariance of the phenotypic parameters is accurate. The results verified that non-negligible sampling covariance should be expected as a function of the twin innovation correlation. Our second simulation demonstrated accurate estimation of the data-generating twin correlations of the phenotype using a correction for its sampling covariance. We simulated MZ twins to have stronger psychological effects on each other and experience more of the same events than DZ twins. Their emotion regulation parameters were generated to covary according to additive genetic and common environmental sources, which were recoverable only when the model accounted for the confounding cross-twin effects.

Our application of the methods to affect data provides evidence that violations of the EEA were present and quantifiable in a few forms. Mean differences in the LRs by zygosity showed that on average, cross-twin effects were significantly more critical to modeling MZ than DZ twins. Effect sizes for cotwin influence and shared experiences were all significantly, positively associated with genetic similarity, even after accounting for cohabitation status. Cohabitation did not appear to play a large role in the model comparisons or cross-twin effects. It was significantly associated with shared positive experiences, but none others. The results suggest that on average, MZ twins participate in each others' lives more completely than DZ twins, experiencing the same events and having larger or more enduring reactions to each others' daily fluctuations. The observed differences of twin state correlation by zygosity may be due to the interplay of genetic factors with environmental selection. Other authors have examined the role of gene-environment correlation in the non-stationary heritability of phenotypic states indexed, for instance, by time [134, 143] or by hormone levels [144].

In the current study, we did not examine the heritability of momentary affect state itself, which was considered transient. We leave the concept of momentary genetic states and their influence on momentary affect to future discussion, as the current study only aimed to account for more obvious, circumstantial sources of within-pair twin covariation.

The model phenotype, emotion regulation, did not appear to be heritable or even strongly a product of common environmental variation in the classical sense. However, the study was severely underpowered to test for that, having only 227 twin pairs in the final analysis. The twin correlations likely varied as a function of sampling error, given that they were close to zero and showed no consistent pattern of positive or negative sign, and the MZ correlation was not positive and greater than the DZ correlation. Despite the lack of statistical power, we nonetheless included the results for the purpose of completeness. Future studies will require many more of both twin pairs and occasions of measurement per twin to obtain reliable heritability estimates of twin-specific parameters. Further simulations to calculate adequate statistical power were beyond the scope of the current study, though they are needed to provide critical guidance for future data collection.

There are many reasons other than statistical power for why emotion regulation as defined here may not be heritable. For one, it may not be as time-invariant as the model assumes. It is likely that the recovery rate of emotional perturbations will change over the lifespan, if not over the course of days, as biological and environmental circumstances change. Our conception would therefore be regarded only as an average value that, though estimable, may not accurately represent any single instance.

Second, the dynamics we specified may not accurately describe the true mechanisms of regulation, whereas alternatives may be more suitable. For instance, one or more second order differential equations may be specified that describe compound

damped oscillations around equilibrium, and such patterns have been previously observed in affect data [44]. Alternatively, models might describe a finite impulse response function unique to a certain kind of perturbation, i.e. a moving average (MA) model. There are numerous ways to characterize the dynamic properties of time series, including autoregressive moving average (ARMA) models, stochastic differential equations, Fourier-transform-based spectra, wavelet analyses, and simple descriptive statistics like the series mean and variance [36].

Third, the observation interval may be too large to detect the short-term dynamics of the given affect states. The PANAS questions elicit day-long retrospective ratings for relatively fleeting emotional experiences, and it is not clear how each respondent arrives at their summary response of each day's emotions. Shorter intervals might capture more momentary assessments and rapid fluctuations that are otherwise forgotten or discounted by the respondent by the end of the day.

Fourth, if we take our result at face value, we might conclude that regulation is largely an idiosyncratic product of learning and experience unique to each individual. This possibility is not exclusive from the previous three, and the current construct of emotion regulation may be a useful indicator in studies of mental health. While it is certainly possible to conceptualize complex traits that are useful and informative without a strong genetic basis, some non-zero heritability is typically expected due to the unavoidable and innumerable genetic covariates involved in the execution of any given human behavior. The complete lack of a genetic signal here most strongly suggests problems of model specification or statistical power.

Other limitations of the data made extraction of a meaningful emotion regulation phenotype difficult. The PANAS has known psychometric problems, namely a lack of clear meaning for zero or neutral values. Russell [145] points out, among other critiques, that dividing a bipolar scale into two unipolar scales in the manner of the

PANAS results in an L-shaped distribution that may be arbitrarily correlated. Studies have variously allowed factors to correlate, but the practical significance of doing so is not clear, particularly when the correlation may be due to problems with measurement itself. To avoid introducing several additional parameters and associated problems with model solvability, we did not include cross-valence factor correlations. For the same reasons, we also treated the 5-point PANAS items as continuous and did not use Item Response Theory (IRT) models [146] or other methods of handling ordinal data. To date, the latter options are not yet available in the OpenMx state-space modeling user interface. As a consequence of this exclusion, we expect that the standard errors of our parameter estimates may be slightly inaccurate and associations with the indicators may be underestimated. Treating the ordinal variables as interval only caused computational problems when the variability of many items was extremely low. It could be seen in Table 14 and Figure 11 that negative affect scores from many participants were grossly invariant. While most of the problematic variables were omitted from the analyses beforehand, those that ended up being modeled produced a variety of anomalous parameter estimates and fit statistics that were ultimately discarded from the analysis.

Obtaining novel and heritable endophenotypes is a popular goal of behavioral genetics, and our list of limitations toward that goal is admittedly quite long. There are currently few data sets like the one used here, with both a large number of intensive repeated affect measures and genetic information, whether by way of twin pairs or genotypes. The most important goal of this study is therefore not to validate a novel phenotype, but to further illuminate the methodological path towards doing so and our current place along it. Our simulations and results should be considered when investigating the dynamics of emotions and the extraction of theoretical phenotypes from twin pair time series in general. Following conventions for the validation of

latent variables, biometrical genetic signals such as heritability and common environment may be considered possible criteria by which to validate candidate phenotypes. It may be informative to compare biometrical genetic analyses of parameters from competing dynamical models to compare their biological proximity, or conversely, statistical artifice. As mentioned above, even moderate degrees of heritability offer some indication that the specified dynamics are stable and statistically reliable.

Summary We proposed a vector-autoregressive state-space model of twin behavior in experience-sampling designs. The model accounts for cross-twin effects to extract unique, twin-specific indices on a model phenotype. Our analyses showed that cross-twin effects were statistically present in affect data in two forms: cotwin social influence and shared experiences. Accounting for cotwin influence and shared experiences in the model had a substantial effect on both estimates of the model phenotype and its subsequent twin correlations. Further study is required to establish best practices in data collection, psychometrics, and modeling to improve the reliability of within-person effect sizes and biometrical genetic inferences.

CHAPTER 6

HIERARCHICAL MODELING FOR BIOMETRICAL GENETIC ANALYSIS OF DYNAMICS

6.1 Introduction

In the previous chapter, we used a two-step procedure to estimate the heritability of a stationary dynamic representing emotion regulation. Our analyses used an approximate method to account for the imprecision of the estimated dynamics in computing their twin correlations. We did not provide confidence intervals for the resulting biometrical genetic variance components, nor did we use conventional hypothesis testing to determine their significance. It is a major limitation of two-step analyses that these crucial elements of statistical inference are difficult to accurately assess. In this chapter, we give a brief overview of the most common modeling strategies and study design requirements for a complete analysis of the heritability of dynamical phenotypes.

A maximally rigorous approach to hierarchical analyses should jointly estimate the phenotypic parameters with their biometrical genetic variance components. Simultaneous, single-step approaches, or hierarchical models, allow us to accurately estimate the precision of parameters at the highest levels of the hierarchy that depend strongly on the precision of lower-level parameters. Hypothesis testing by generic methods such Likelihood Ratio Test may also be possible and simple to conduct with the results of a hierarchical model.

Additionally, hierarchical models allow information at one level of analysis to be utilized during estimation of other levels. The manner in which this is done

depends on the statistical approach chosen for the model, which we will discuss in the next section. For example, in Bayesian analyses, biometrical genetic variance components define a prior distribution for the individual dynamics. Conditioning parameter estimates on a prior distribution can have a regularizing effect, drawing them closer to their mean value and counteracting additional variance due to their sampling error. Models fit with maximum likelihood can be specified equivalently by including the multivariate density function of the parameters in the total likelihood to be maximized.

6.2 Power and Bias by Sample Size

Before we examine hierarchical modeling strategies, it is useful to test the sample requirements of a hierarchical two-step analysis. Sample size involves both a number of individuals or twin pairs, N , and the number of occasions comprising each individual's series, T . We need to determine the power, bias, and variance of a 2-step process under various combinations of N and T .

We can set realistic expectations by examining model limitations under the best-case scenario: a simple model, no measurement error, and a high heritability of the parameters. For several values of the number of twin pairs, N , and occasions per pair, T , N pairs of univariate, lag-1 autoregressive processes without measurement error were simulated with T occasions for both MZs and DZs. AR(1) parameters unique to each twin were distributed according to a large heritability ($\sigma_A^2 = .8$). Denoting time as t , family index as i , twin index as j , and zygosity as z , we have:

$$y_{i,j,t} = \alpha_{i,j}y_{i,j,t-1} + \epsilon_t, \quad \epsilon \sim N(0, \sigma_\epsilon), \quad i \in \{1 \dots N\}, \quad j \in \{1, 2\} \quad (6.1)$$

$$\alpha \sim MVN(.5, \Sigma), \quad (6.2)$$

$$\Sigma = \sigma_\alpha \begin{bmatrix} \sigma_A^2 + \sigma_C^2 + \sigma_E^2 & z_j \sigma_A^2 + \sigma_C^2 \\ z_j \sigma_A^2 + \sigma_C^2 & \sigma_A^2 + \sigma_C^2 + \sigma_E^2 \end{bmatrix}, \quad z \in \{0.5, 1\}. \quad (6.3)$$

We defined power as the probability of rejecting a null hypothesis that $\sigma_A^2 = 0$ when the true $\sigma_A^2 = .8$. Figure 14 and Table 20 show empirical, simulation-based estimates of the power, effect size, and standard error derived from 500 iterations of simulation per combination of sample sizes N and T .

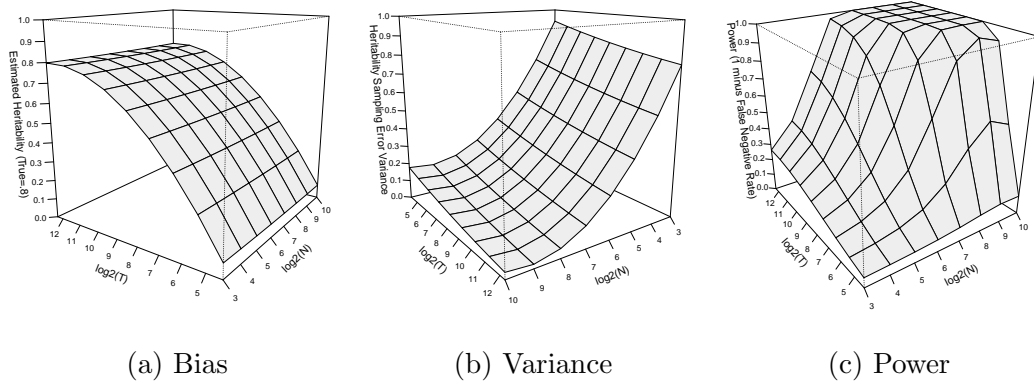


Fig. 14.: Bias, variance, and statistical power for $\sigma_{A,\alpha}^2 = .8$ given within (T) and between (N) person sample sizes.

Generally, smaller T leads to a larger sampling variance of α , diluting its covariance and leading to downward bias of σ_A^2 . This is only strictly the case when twins' parameters $\alpha_{i,1}$ and $\alpha_{i,2}$ are not additionally dependent due to shared disturbances or unmodeled, cross-regressive effects, as discussed in the Chapter 5. Smaller values of N primarily lead to a larger variances of σ_A^2 , as is expected in the case of a simple, non-hierarchical correlation. As $T \rightarrow \infty$, the power conditional on N should approach

Table 20.: Statistical power for a $\sigma_{A,\alpha}^2 = .8$ given within (T) and between (N) person sample sizes.

		Measurement occasions (T)								
		20	40	80	160	320	640	1280	2560	5120
Twin pairs (N)	8	0.06	0.09	0.12	0.15	0.19	0.22	0.24	0.26	0.26
	16	0.06	0.10	0.15	0.21	0.27	0.32	0.37	0.40	0.41
	32	0.07	0.13	0.22	0.32	0.43	0.53	0.61	0.66	0.69
	64	0.07	0.18	0.35	0.55	0.72	0.85	0.92	0.96	0.97
	128	0.09	0.28	0.59	0.86	0.98	1.00	1.00	1.00	1.00
	256	0.10	0.43	0.87	1.00	1.00	1.00	1.00	1.00	1.00
	512	0.11	0.55	0.96	1.00	1.00	1.00	1.00	1.00	1.00

that of a non-hierarchical twin model. The estimates in the last column of Table 20 are just slightly lower than the power to reject $H_0 : r_{DZ} = 0$ when $H_A : r_{DZ} = .4$ given the same respective values of N . It is a key aim of hierarchical modeling to reduce or eliminate the downward bias to α due to small values of T . This can be done via the regularizing effect of jointly estimating σ_A^2 with α . In the next section, we will examine a few modeling approaches to doing so.

As a final note on power, these cursory simulations are only intended to demonstrate the dependence of bias, variance, and power on sample size. They are not to be taken as a power calculation table in general, as the precision of a dynamic parameter depends on the specification of the model, the signal-to-noise ratio, dependence of parameters as studied in Chapter 5, and empirical identification in certain nonlinear models such as that presented in Chapter 3. If the above sample sizes appear unattainable for certain study designs, then it may be worthwhile to check

the necessary power for alternative dynamic specifications that might account for a greater proportion of variability in y_t .

6.3 Modeling Strategies

A hierarchical biometrical genetic analysis of dynamics requires two main components: a phenotype model with individual and group level parameters, and a structural genetic model of the unique and shared heritability of those parameters. For the sake of simplicity and generality, we will only examine a univariate twin model of a phenotype drawn from simple Gaussian processes.

The density of data Y conditional on dynamics, θ , and biometrical genetic variance components, ACE , can be determined according to Bayes theorem:

$$f(Y|ACE) = \frac{f(Y|\theta, ACE)f(\theta|ACE)}{f(Y)} \quad (6.4)$$

A maximum likelihood approach to a fixed-effects hierarchical model involves optimizing all of the individual parameters jointly with the between-persons parameters. This approach is described as the hierarchical likelihood, or *h-likelihood*, as detailed by Lee, Nelder, and Pawitan [147]. If we assume that both the prediction errors of the individual dynamical system and the parameters of those systems are multivariate normally distributed, then the joint density function, excluding the denominator, is computed as

$$f_Y(y_{i,t} \in \mathbf{Y} | ACE) = \prod_{i=1}^N \left[\prod_{t=0}^T \left[f(y_{i,t} | \theta_i, ACE) \right] f(\theta_i | ACE) \right] \quad (6.5)$$

$$= \prod_{i=1}^N \left[\prod_{t=0}^T \left[\frac{\exp \left(-0.5 (\mathbf{r}_{i,t} - \hat{\mathbf{x}}_{i,t}) \hat{\Sigma}_{i,t}^{-1} (\mathbf{r}_{i,t} - \hat{\mathbf{x}}_{i,t})^\top \right)}{\sqrt{(2\pi)^k |\hat{\Sigma}_{i,t}|}} \right] \right. \\ \left. \times \frac{\exp \left(-0.5 (\theta_i - \bar{\theta}) \hat{\Theta}^{-1} (\theta_i - \bar{\theta})^\top \right)}{\sqrt{(2\pi)^k |\hat{\Theta}_i|}} \right] \quad (6.6)$$

By taking minus two times the log of this function, we obtain the deviance function to minimize:

$$-2 \ln \hat{\mathcal{L}}(\theta, ACE | \mathbf{Y}) = \sum_{i=1}^N \left[\sum_{t=0}^T \left[\ln |\hat{\Sigma}_{i,t}| + (\mathbf{r}_{i,t} - \hat{\mathbf{x}}_{i,t}) \hat{\Sigma}_{i,t}^{-1} (\mathbf{r}_{i,t} - \hat{\mathbf{x}}_{i,t})^\top \right] \right] \quad (6.7)$$

$$+ \ln |\hat{\Theta}| + (\theta_i - \bar{\theta}) \hat{\Theta}^{-1} (\theta_i - \bar{\theta})^\top \quad (6.8)$$

$$+ kN(T + 1) \ln(2\pi) \quad (6.9)$$

This likelihood function can be described as a combination of the twin pair-level state space model likelihood and the biometrical genetic model likelihood. Each total person likelihood is summed and added to the likelihood of each individual parameter θ_i given the ACE model-expected covariance Θ (6.8). The constant terms are aggregated in (6.9). For maximum likelihood estimation, both the solution and its estimated precision depend on derivatives with respect to θ and ACE in which the constant term disappears and is inconsequential.

Maximum likelihood fitting is not advisable for hierarchical models because a hierarchical likelihood like the one above will not have a global maximum. In equation 6.4, the second term, $f(\theta_i | ACE)$ describes a density that approaches infinity as the sum of the hierarchical variance components approaches zero. Because θ are

degrees of freedom that are jointly determined with their variance components, the global maximum is infinity where $\theta_i = \mathbb{E}[\theta]$ and $\sigma_\theta^2 = 0$. If T is large enough, then $f(y_{i,t}|\theta_i, ACE)$ may create local maxima sufficiently far from the mean value to avoid the singularity. However, obtaining a local maximum may require limiting the precision or number of iterations of the optimization procedure and is thus arbitrary and potentially unreliable.

The h-likelihood function may also be difficult to optimize in large samples due to the high dimensionality of the fixed effects. In a typical study of twin pairs or independent individuals, most of the fixed effects will be independent and do not need to be optimized jointly. A highly efficient strategy is to iteratively fit each person or twin-pair model with fixed start values of the latent variance components. After all fixed effects are estimated this way, the latent variance components can be fit to the last, best solutions of the individual or twin pair models. Repeating this procedure results in convergence to a joint solution of the person and hierarchical parameters, as optimization alternates between levels of the hierarchy while conditioning each on the most recent solutions of the others. This and any other optimization procedure should be restricted to avoid the aforementioned global singularity in the hierarchical likelihood. Figure 15 presents the results of a simulation in which the alternating optimization procedure was executed with a very high model convergence tolerance. The results show substantial regularization of estimates toward their true values. The estimates of σ_A^2 are biased slightly upward toward the singularity, as the chosen tolerance was not specifically optimal for this case.

An alternative random-effects method involves marginalizing out θ for Twin 1 and Twin 2 such that no individual fixed effects need to be estimated. Marginalizing out a parameter in this case means integrating over the likelihood of the data given that parameter, and weighting by the likelihood of that parameter given the variance

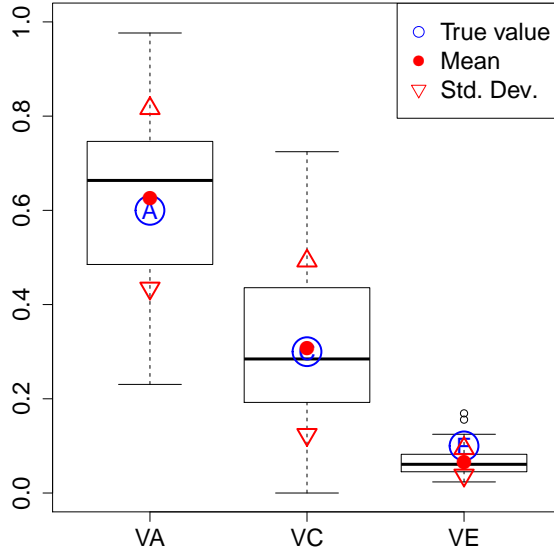


Fig. 15.: Simulation of hierarchical AR(1) processes ($N = 64, T = 1280$) with the autoregressive parameters distributed according to $\sigma_A^2 = .6, \sigma_C^2 = .3, \sigma_E^2 = .1$. 60 iterations were run. Blue letters represent data-generating parameter values. Estimates were obtained using Maximum Likelihood Estimation.

components:

$$f_Y(y_{i,t} \in \mathbf{Y} | ACE) = \prod_{i=1}^N \left[\prod_{t=0}^T \int \int f(y_{i,t} | \theta_1, \theta_2) f(\theta_1, \theta_2 | ACE) d\theta_1, d\theta_2 \right]. \quad (6.10)$$

The integral for this strategy can be computed in a variety of ways. For one, a cubature approximation evaluates the likelihood of the data given a set of combinations of $\theta_{1,g}$ and $\theta_{2,h}$ over a $Q \times Q$ grid, where $g, h \in 1 \dots Q$.

$$f_Y(y_{i,t} \in \mathbf{Y} | ACE) = \prod_{i=1}^N \left[\prod_{t=0}^T \sum_g \sum_h f(y_{i,t} | \theta_{1,g}, \theta_{2,h}) \omega(\theta_{1,g}, \theta_{2,h} | ACE) \right], \quad (6.11)$$

where $\omega_{g,h}$ are weights to be computed as a function of the bivariate normal density of θ parameterized by ACE .

Marginal maximum likelihood with cubature can be used with convex optimization because it involves far fewer parameters than the fixed-effects model. However, its computational feasibility is limited by the need for a large value of Q to accurately approximate the integral and span the space of likely values of $\vec{\theta}$. For large samples, this may become prohibitive without parallel computation. Furthermore, the maximization process will result in the same convergence problems as the fixed-effects h-likelihood, with a singularity at $\Theta = 0$.

The convergence problems and computational demands of hierarchical modeling via maximum likelihood have led many to consider Bayesian methods to be the gold standard. Relevant applications of Bayesian hierarchical modeling to emotion regulation and affect have been demonstrated by Oravecz et al. [148, 117]. The authors briefly cite the problems with marginal likelihood maximization, but do not consider the non-marginalized h-likelihood approach.

In brief, Bayesian modeling algorithms do not rely on optimization of an objective function. Rather, they use Markov Chain Monte Carlo (MCMC) to randomly sample the posterior distribution of each parameter conditional on the data, the model, and prior distributions. As the name suggests, the MCMC algorithm uses Markov chains to randomly explore the parameter space according to step-wise acceptance criteria. Acceptance of a new random step in the chain is probabilistic and a function of the relative posterior densities of the data at the current and previous steps. The result is that the steps of the chain will accumulate to an approximation of the posterior distribution of the parameters. An introduction to Bayesian methods with R and STAN is given by McElreath [149].

The point estimates obtained through maximum likelihood correspond to the mode of an estimated posterior distribution sampled over a uniform prior. When a posterior distribution can be produced through MCMC, there is no particular reason

to favor the mode, or maximum a posteriori (MAP) estimate, and often the mean, median, or other statistics are used instead.

In some ways similar to the h-likelihood method demonstrated in Figure 15, this algorithm also avoids the singularity at $\Theta=0$ by way of its limitations. Theoretically, the singularity would only be expressible by the MCMC given infinitely small step size and an infinitely long chain. Otherwise, the problem is avoided through sufficiently large step sizes and random acceptance rates.

Simulations were used to test the computational, convergence, and regularization properties of the Bayesian approach. Using R package `rstan`, a model was specified according to equations 6.1 through 6.3 and data were simulated identically to the power simulations, with the exception that the data-generating α values were themselves generated to produce empirical variance components of exactly $\sigma_A^2 = .6$, $\sigma_C^2 = .3$, and $\sigma_E^2 = .1$. Empirical correlations were fixed to gauge bias and variance from a single, large-sample simulation while gauging the computation time, rather than averaging over several small iterations.

In the first simulation, 300 twin pairs of each zygosity were generated, with 5000 occasions per twin. These dimensions correspond roughly to those of the postural control data set used in Chapter 3, though that did not involve twin pairs. In the second, 800 twin pairs of each zygosity were generated, with only 150 occasions per twin, representing the conventional requirements for a fully powered twin study and the typical amount of within-person data that can be afforded in a momentary assessment study of self-reported experiences. Only 500 steps of MCMC were performed, and results were computed after discarding the first 150 samples as part of the warmup period and every second sample to reduce autocorrelation in the remaining 175 samples. Results should be considered in light of the fact that this is a smaller posterior sample to use than would be ideal for a complete analysis. With these specifications,

the MCMC took approximately 6 hours to compute the first set and 2 hours to compute the second. Figure 16 shows the posterior distributions of parameter estimates from these simulations.

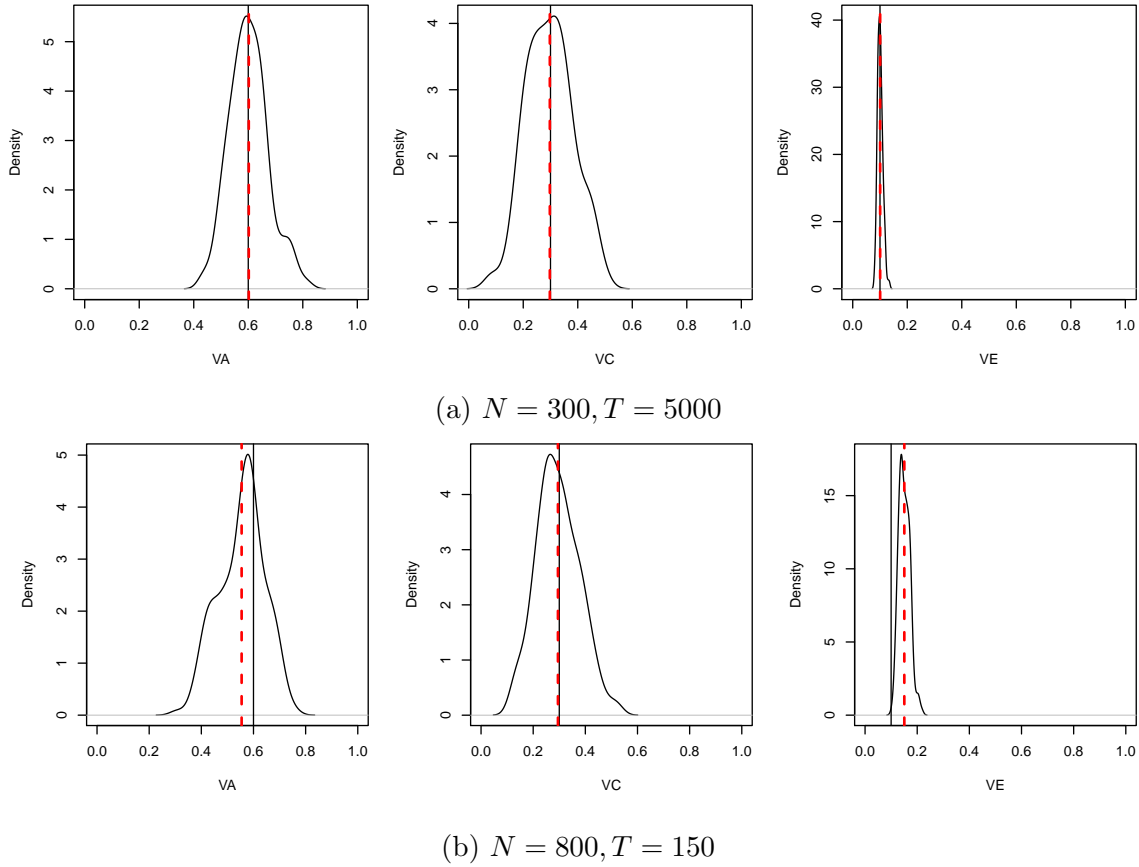


Fig. 16.: Resulting Bayesian posterior parameter distributions from simulated large-sample studies. The dotted red line is the mean of the posterior distribution, and the solid black line is the true data-generating value.

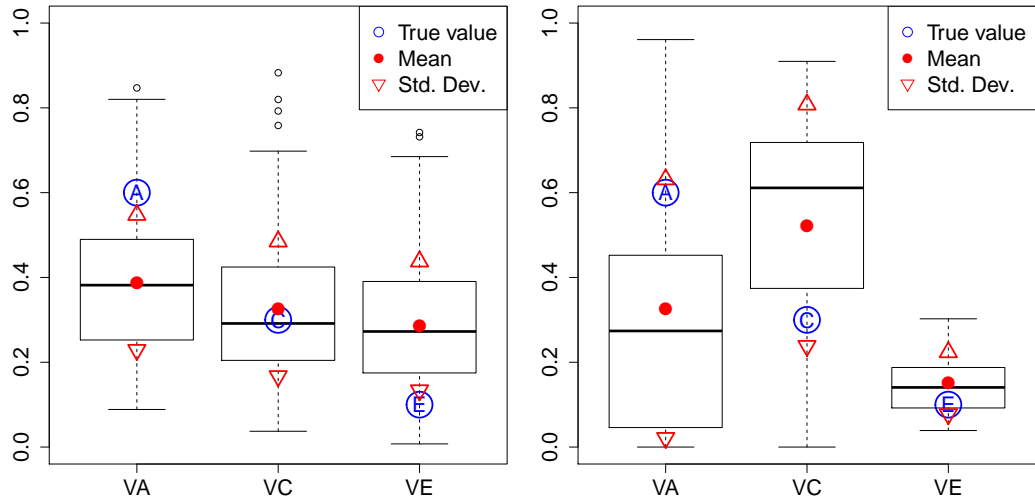
In the first simulation with $N = 300$ MZ and DZ pairs, and $T = 5000$, the posterior means are remarkably close to their true values, at $\sigma_A^2 = .602$, $\sigma_C^2 = .298$, and $\sigma_E^2 = .101$. In the second simulation with $N = 800$ MZ and DZ pairs and $T = 150$, they remained far closer than expected given the biases found in our simulations, with

$\sigma_A^2 = .555$, $\sigma_C^2 = .295$, and $\sigma_E^2 = .151$. Figure 14a shows that in a 2-step analysis, we should expect to estimate to be at most half of its true heritability. Remarkably, it appears that with $N = 800$ twin pairs, the regularizing effect of the between-persons distribution on the estimates was sufficient to nearly eliminate that expected bias.

We conclude this section with a final simulation of the data dimensions from Chapter 5, $N = 150$, $T = 45$, which by our power calculations has too few of both twin pairs and occasions per twin to reliably estimate heritability. For these simulations, the empirical twin correlations were not constrained to exact values, and results were averaged over 30 iterations. 500 steps of MCMC were used per iteration, discarding the first 200 and every second posterior sample.

For comparison, the same simulation was conducted with the alternating-optimization h-likelihood algorithm described earlier. Because the data are relatively few, the procedure is prone to the singularity where $\hat{\Theta} = 0$. After a few preliminary diagnostic tests, it was determined that at $N = 150$, $T = 45$, σ_E^2 and hence the diagonal elements of $\hat{\Theta}$, shrink excessively relative to the off-diagonals after 3 alternations. No tolerance criteria were defined, and instead this maximum number of 3 iterations was used. Such tuning is not necessarily possible without a prior expectation for the effect sizes. If only one iteration is used, the algorithm reduces to a two-step analysis and the results resemble those of our simulations in the previous section. If too many iterations are used, the twin correlations will approach unity, i.e., singular $\hat{\Theta}$.

The results of this brief vignette, shown in Figure 17, further demonstrate the property that in a hierarchical model, bias in between-person statistics that would otherwise result from insufficient within-person precision is greatly mitigated. In this case however, it appears both sample dimensions are insufficient to completely overcome the downward bias to the heritability in the Bayesian model, and with h-likelihood, σ_A^2 and σ_C^2 are variously inflated to unpredictable degrees.



(a) Bayesian model with MCMC, 500 steps. (b) Alternating h-likelihood optimization, 3 iterations.

Fig. 17.: Simulation of hierarchical AR(1) processes ($N = 150, T = 45$) with the autoregressive parameters distributed according to $\sigma_A^2 = .6, \sigma_C^2 = .3, \sigma_E^2 = .1$. 30 iterations were run. Blue letters represent data-generating parameter values.

6.4 Application: Heart Rate

A simple data application was conducted with ECG sensor data collected in 306 MZ twins and 478 DZ twins. The ECG series were collected as part of CO₂ challenge by Roberson-Nay [150]. Only the first four minutes of data were used, representing only baseline variation before CO₂ was administered. Heart rate sampled at 1Hz was computed from the ECG data, which was originally sampled at 1000 Hz. The resulting rate series was modeled as the same hierarchical AR(1) process examined above. An alternative model was fit describing a hierarchical, biometrical genetic analysis of just individual series means μ and standard deviations σ . Models were fit using R package `rstan` as before. Table 21 gives the mean estimates and 95% credible intervals of the standardized variance components for the parameters of the

two models.

Table 21.: Biometrical genetic variance components of model parameters from two models of heart rate measures: independent and identically distributed (i.i.d.) and an AR(1) model. μ is mean heart rate, σ is the standard deviation, and β is the lag-1 autoregression coefficient from the AR(1) model.

	Mean Variance Component (95% Credible Interval)		
	σ_A^2	σ_C^2	σ_E^2
i.i.d model: μ	0.43 (0.35-0.48)	0.08 (0.00-0.17)	0.50 (0.45-0.54)
i.i.d model: σ	0.45 (0.36-0.51)	0.09 (0.01-0.20)	0.47 (0.42-0.51)
AR(1) model: β	0.38 (0.30-0.44)	0.07 (0.01-0.17)	0.55 (0.50-0.60)

All three parameters result in substantively interesting heritabilities, but the model-based AR(1) parameter was not more heritable than the simpler descriptive statistics. We can interpret this as an indication that the parameter of an AR(1) process model does not represent a biological mechanism better than generic indices of variability.

CHAPTER 7

DISCUSSION

7.1 Summary of Findings

The aims of this dissertation were to define and estimate new control-theoretic phenotypes from individual data for health-related research, then consider biometrical genetic analysis of such phenotypes. As a matter orienting to an effective long-term methodology, we studied an ideal case of high-quality data with precise theoretical propositions. That is, we estimated theoretical model-based indices of many physiological functions involved in stable, upright standing from COM data. Then, we defined a simplified control scheme to estimate the regulatory properties of emotion from affect data exhibiting a large number of standard psychometric deficiencies and challenges. In the second half, we turned our attention to several issues prerequisite to the biometrical genetic modeling of such dynamics. We considered the variety of conceptual and statistical complications to our goals that arise from the dependence of affect states in cohabiting twins. Then we briefly compared statistical frameworks for hierarchical genetic models of dynamics. Finally, a Bayesian procedure was demonstrated to obtain correct, unbiased results in simulation and subsequently applied to a sample of heart rate data, yielding moderate heritability estimates for three potentially useful indices.

In our analysis of postural sway, conclusions were not as simple as total acceptance or rejection of the theoretical model. Indices varied in their intraclass reliability, association with previously linked covariates, and replication of previous findings such as those of Tietäväinen et al.[65]. Direct fitting via state-space modeling permitted

a more detailed post-hoc analysis than was possible in the other preceding methods. The theoretical processes appeared to be quite accurate for some individuals with some variation in others. In reality, such processes are not likely a clear choice between Langevin random walk, harmonic oscillation, and the system proposed by Asai et al.[48]. Our results suggest that at different times and in different people, the active mechanisms may vary substantially leading to the intertwined expression of all such patterns. Further progress could be made by using the same methods to to consider the many competing theoretical control schemes from the literature.

The case of postural control represents a desirable level of detail to achieve with models of psychological processes. In both studies of emotion regulation, the data were not sufficiently numerous nor interpretable to test comparably complex theoretical propositions. The simplest possible control scheme had to be chosen as a starting point. This decision was informed partly by the way the simplified alternative posture control models, denoted SDDE and SDE, seemed to produce more reliable parameters with stronger associations to their known covariates. Informally, the complex model allowed the more specific theoretical assertions to be tested but diffused relevant information in the data across many more parameters. Similarly, picking a simple model of emotion regulation allowed us to look for more general and reliable associations with substance use than would have likely been possible with the bivariate regulation-risk model that was subsequently proposed. While conjectures may be as complicated as one desires for the sake of developing a theory, our results demonstrate the costs of model complexity when designing indices for practical use.

Chapter 5 demonstrated that one domain of applications for these methods, namely EMA or Experience Sampling, entails problems of subject dependence that may not be solved by integrated hierarchical modeling alone. It is relatively straight forward to account for twin state dependence using a multivariate model such as

vector autoregression. Accounting for the sampling correlation of dynamics in the higher-order genetic model is more nuanced. The most direct solution would be to collect within-person samples large enough to minimize the sampling error of the estimated dynamics, but that is unlikely to be a fair option for the few available data sets nor potential data sets generated with a limited budget. The method chosen for the two-step analysis was somewhat crude in that it averaged the sampling covariance matrix across all twin pairs. In the MLE hierarchical modeling approach considered in Chapter 6, recalculation of each twin pair Hessian during optimization might allow us to account for each pair exactly in the expected covariance matrix. This is not currently possible with `OpenMx`, as there are no front-end way to reference the Hessian in algebraic operations. It is unclear how to best approach the same problem in the Bayesian framework. Possibly, a prior joint distribution can be analytically derived as a function of the estimated disturbance covariance that counteract the exact amount of expected inflation of the twin covariances, as the latter is known to be $(Z^T Z)^{-1} \otimes \hat{Q}$, where Z is the state estimates and \hat{Q} is the disturbance covariance matrix.

7.2 Limitations

As we have seen, much statistical power is gained through the regularizing properties of hierarchical models, and that can partly mitigate the limitations on model complexity in most EMA study designs. The broader paradigmatic problem with EMA remains an issue of valid measurement strategies for subjective mental content like affect. Most psychological self-report instruments incorporate Likert scales, which use a small range of integers to represent different levels of agreement with a statement of inquiry [151]. Most often, five and seven-point scales are considered to capture a gradation of agreement that is sufficiently fine-grained, with additional response options having diminishing utility. Bipolar scales may designate a middle

value and two or three graded degrees of agreement and disagreement to either side, whereas unipolar scales start with 0 to represent “not at all,” and each additional increment represents an increase in the level of agreement.

What exactly is happening when respondents attempt to quantify their subjective states? A Likert scale for assessing affect requires the respondent to dissociate happiness, sadness, anger, etc. from the context in which each arises and map it to a numerical value. This process takes place entirely in the respondent’s mind, and is inaccessible. Although scales are coded in linear increments, there is no basis to assume that one’s perceived magnitude of subjective intensity across experiences varies in a linear way. E. C. Poulton [152] wrote, “The easiest way to bias a person’s judgements is to ask him to judge stimuli for which he has no familiar units.” Poulton authored several papers on the quantitative estimation of subjective judgments, typically those of real, auditory and spatial stimuli. These comparisons between subjective judgment and objective magnitudes revealed a number of biases in intuitive quantification resulting from, for instance, anchoring [153], limited range of both scale and the available stimulus, and variable subjective discernment. We can consult reviews of these biases [154, 152, 155] for ideas about what likely occurs in the reporting of affect as well:

1. Centering Bias: Responses are centered according to the available range of the stimulus.
2. Stimulus or Response Equalizing: The full scale of responses is used for only the available range of the stimulus. Also the converse, that only the available scale is used for the full range of the stimulus.
3. Stimulus Spacing and Frequency Biases: Equal intervals on the scale are taken to represent equal intervals of estimation of the magnitude or probability of the

stimulus.

4. Contraction: Responses regress to the center; Upper extremes and differences are underestimated and lower extremes and differences are overestimated.
5. Sequential Contraction: Ratings tend to contract toward prior ratings in sequence.
6. Local contraction: At the lower end of a rating scale, subjective incremental increases require greater objective increase, and subjective incremental decreases require lower objective decrease. The reverse is true for the upper end of a scale.
7. Asymmetric Transfer Bias: When a majority portion of the rating scale is fit to an available range of the stimulus as with (2), the remaining portion may be inadequate to represent an increase in the range of the stimulus, causing unevenly proportioned representation.

These biases commonly stem, in part, from the basic problem of quantizing and bounding observations for which there are no obvious boundaries or proportional subdivisions. They apply insofar as we regard the act of reporting any subjective experience, like affect, as an attempt of the respondent to estimate and quantize a true, experiential dimension that happens to have no empirical measure.

Are affect questionnaire items what Kendler [156] called *indexical*, i.e., indicators of a true underlying dimension subject to measurement error, or *constitutive*, in which affect is defined to be their sum, taken at face value? The latter interpretation might be justified by the question, who are we to tell respondents that their subjective reports are erroneous? In the constitutive view, they may be valid expressions and an aggregate dimension is nothing more than their total. The distinction between indexical and constitutive corresponds respectively to the decision to use either factor

scores or sum scores, though the choice is not often made for that reason. Using factor scores means discarding potentially useful sources of variance specific to each indicator. If the psychometric theory supposes an indexical nature, then much work must be done with techniques like Item Response Theory to examine the kind of nonlinear mapping problems raised by Poulton [154] and Measurement Invariance to ensure consistency of the latent construct.

While much work has been done to understand subjective assessment, it does not mean that the most common psychometric instruments in use have taken that work into account. In Chapter 5, affect was measured using the PANAS, which is just one subjective report instrument that has been developed and proliferated via a process of ignoring all criticism. Its authors used low-powered, exploratory analyses of adjective checklists to determine a certain correlation structure of two underlying dimensions, positive and negative affect. They proclaimed the correlation structure to be a “fundamental psychometric principle” of affect[157]. James Russell, whose original work on adjective checklists led to the PANAS [3], subsequently demonstrated how their principle result was an artifact of poor instrument construction [158]. In brief, he showed that splitting a univariate distribution by measuring it with two independent, unipolar items results in arbitrary correlation structure between them because the null responses on one can only be interpreted by knowing their place on the other. Variation in the possible overlap of the low ends of each scale results in arbitrary correlation between them that depends on both how the scale is subjectively understood by the respondent and their resulting response distributions. If the boundaries of the scale are not clearly defined or individually calibrated, there is no strong basis for comparing ratings directly between participants or drawing conclusions about the distributions of affect in general. We should not only expect that poorly constructed and insufficiently validated psychometric instruments to have a large amount of mea-

surement error or bias, as if they were just faulty sensors, but in the ways Russell explains, they may also be prone to producing meaningless and misleading artifactual features.

7.3 Future Directions

In Chapter 6, we produced heritability estimates for both a token candidate phenotype and two descriptive statistics for comparison. We did not proceed to the more complex issue of multivariate genetic analysis when the ontology of multiple dynamics are of interest. Multivariate genetic variance decompositions can take many forms, including atheoretical cholesky decompositions and the independent or common pathway models[159]. The problem of multivariate genetic modeling can be summarized as one of determining the number and overlap of additive genetic sources of the covariance structure relating multiple phenotypes.

Multivariate genetic analysis is usually intended to investigate the genetic etiology of relatively well-established phenotypic constructs, such as DSM psychiatric disorders [160, 161]. It can also be used to obtain a deeper understanding of new phenotypes derived from theoretical models in the ways we have considered here. Suppose that we specify multivariate genetic models that include phenotypic dynamics from multiple, competing models fit to the same time series data. A strong genetic covariance of parameters derived from different models suggests that they may be representing similar biological pathways. If the parameters of one particular model are heritable but do not share additive genetic sources of variation among themselves, that would seem to indicate that the model accesses multiple, distinct biological pathways- a validating result if theoretically expected.

Multivariate analyses of heritability is a particularly interesting tool for theoretical model validation because it enables us to link the ontology of new constructs

together at any level of abstraction, even when the relevant biological paths cannot yet be known. This is potentially important for fields like cognitive science, where theories of mental processes are necessarily posed in terms of emergent computational, statistical, and information-theoretic abstractions. The studies conducted here concerned similarly abstract cognitive phenotypes. Emotion regulation, as have discussed, is likely a broad aggregate of cognitive and situational factors each contributing partial regulatory functions. They are likely too diffuse to relate to particular neural circuits, at least in the complex, *in situ* mode of EMA. Some of the components of posture control have been conceptualized in the cognitive domain as well. The tilt insensitivity radius that we estimated is thought to relate to the resolution of a cognitive model of one's body in space, and thus reliably estimating it would access an otherwise obscure fact of human perception and information processing. With the modeling strategies explored in this dissertation, we can anticipate many new applications in psychophysiology that will bridge the gaps between biology and emergent behaviors.

REFERENCES

- [1] Ethem Alpaydin. *Introduction to machine learning*. eng. 2nd ed.. Adaptive computation and machine learning. Cambridge, Mass.: MIT Press, 2010. ISBN: 9780262012430.
- [2] Lewis R. Goldberg. “The Structure of Phenotypic Personality Traits”. eng. In: *American Psychologist* 48.1 (1993), pp. 26–34. ISSN: 0003-066X.
- [3] James A. Russell. “A circumplex model of affect”. eng. In: *Journal of Personality and Social Psychology* 39.6 (1980), pp. 1161–1178. ISSN: 0022-3514.
- [4] D Watson, L A Clark, and A Tellegen. “Development and validation of brief measures of positive and negative affect: the PANAS scales”. eng. In: *Journal of personality and social psychology* 54.6 (1988), p. 1063. ISSN: 0022-3514.
- [5] Thomas M Achenbach. “The classification of children’s psychiatric symptoms: a factor-analytic study.” In: *Psychological Monographs: general and applied* 80.7 (1966), p. 1.
- [6] M.A Turk and A.P Pentland. “Face recognition using eigenfaces”. eng. In: *Proceedings. 1991 IEEE Computer Society Conference on Computer Vision and Pattern Recognition*. IEEE Comput. Soc. Press, 1991, pp. 586–591. ISBN: 0818621486.
- [7] W Zhao, R Chellappa, and A Krishnaswamy. “Discriminant analysis of principal components for face recognition”. eng. In: *Proceedings Third IEEE International Conference on Automatic Face and Gesture Recognition*. IEEE, 1998, pp. 336–341. ISBN: 0818683449.

- [8] Aapo Hyvärinen and Erkki Oja. “Independent component analysis: algorithms and applications”. eng. In: *Neural Networks* 13.4-5 (2000), pp. 411–430. ISSN: 0893-6080.
- [9] V. D. Calhoun et al. “A method for making group inferences from functional MRI data using independent component analysis”. eng. In: *Human Brain Mapping* 14.3 (2001), pp. 140–151. ISSN: 1065-9471.
- [10] David M Cole, Stephen M Smith, and Christian F Beckmann. “Advances and pitfalls in the analysis and interpretation of resting-state FMRI data”. eng. In: *Frontiers in Systems Neuroscience* 4 (2010). ISSN: 1662-5137. URL: <https://doaj.org/article/705fa59020434b70854240554cd09a1e>.
- [11] Lee J. Cronbach and Paul E. Meehl. “Construct validity in psychological tests”. eng. In: *Psychological Bulletin* 52.4 (1955), pp. 281–302. ISSN: 0033-2909.
- [12] Susan E. Whitely. “Construct validity: Construct representation versus nomothetic span”. eng. In: *Psychological Bulletin* 93.1 (1983), pp. 179–197. ISSN: 0033-2909.
- [13] Kenneth Mather. *Biometrical genetics : the study of continuous variation*. eng. 3rd ed.. London ; New York: Chapman and Hall, 1982. ISBN: 0412228904.
- [14] Jian Yang et al. “GCTA: A Tool for Genome-wide Complex Trait Analysis”. eng. In: *The American Journal of Human Genetics* 88.1 (2011), pp. 76–82. ISSN: 0002-9297.
- [15] H J Eysenck and D B Prell. “The inheritance of neuroticism: an experimental study”. eng. In: *The Journal of mental science* 97.408 (1951), p. 441. ISSN: 0368-315X.

- [16] William S Bush and Jason H Moore. “Chapter 11: Genome-Wide Association Studies”. eng. In: 8.12 (2012), e1002822. ISSN: 1553-734X.
- [17] International Schizophrenia Consortium et al. “Common polygenic variation contributes to risk of schizophrenia and bipolar disorder”. In: *Nature* 460.7256 (2009), p. 748.
- [18] Daniel J Weiner et al. “Polygenic transmission disequilibrium confirms that common and rare variation act additively to create risk for autism spectrum disorders”. In: *Nature Genetics* 49.7 (2017). ISSN: 1061-4036.
- [19] Huwenbo Shi, Gleb Kichaev, and Bogdan Pasaniuc. “Contrasting the Genetic Architecture of 30 Complex Traits from Summary Association Data”. eng. In: *The American Journal of Human Genetics* 99.1 (2016), pp. 139–153. ISSN: 0002-9297.
- [20] Evan A Boyle, Yang I Li, and Jonathan K Pritchard. “An Expanded View of Complex Traits: From Polygenic to Omnigenic”. eng. In: *Cell* 169.7 (2017), pp. 1177–1186. ISSN: 0092-8674.
- [21] Peter M Visscher et al. “Statistical Power to Detect Genetic (Co)Variance of Complex Traits Using SNP Data in Unrelated Samples (Power to Detect Genetic (Co)Variance)”. eng. In: 10.4 (2014), e1004269. ISSN: 1553-7390.
- [22] Saul Shiffman, Arthur A Stone, and Michael R Hufford. “Ecological momentary assessment”. eng. In: *Annual review of clinical psychology* 4 (2008). doi:10.1146/annurev.clinpsy.3.022806.091415, p. 1. ISSN: 1548-5943.
- [23] Paul Langevin. “Sur la théorie du mouvement brownien”. In: *Compt. Rendus* 146 (1908), pp. 530–533.

- [24] Robin R Vallacher, Paul Van Geert, and Andrzej Nowak. “The Intrinsic Dynamics of Psychological Process”. eng. In: *Current Directions in Psychological Science* 24.1 (2015), pp. 58–64. ISSN: 0963-7214.
- [25] Steven M Boker. “Consequences of Continuity: The Hunt for Intrinsic Properties within Parameters of Dynamics in Psychological Processes”. eng. In: *Multivariate Behavioral Research* 37.3 (2002), pp. 405–422. ISSN: 0027-3171. URL: http://www.tandfonline.com/doi/abs/10.1207/S15327906MBR3703_5.
- [26] John R Nesselroade. “Elaborating the Differential in Differential Psychology”. eng. In: *Multivariate Behavioral Research* 37.4 (2002), pp. 543–561. ISSN: 0027-3171. URL: http://www.tandfonline.com/doi/abs/10.1207/S15327906MBR3704_06.
- [27] Robert E Lucas et al. “Econometric policy evaluation: A critique”. In: *Carnegie-Rochester conference series on public policy*. Vol. 1. 1. 1976, pp. 19–46.
- [28] Lawrence Summers, Nils Gottfries, and Birgit Grodal. “The Scientific Illusion in Empirical Macroeconomics; Comments”. eng. In: *The Scandinavian Journal of Economics* 93.2 (1991), p. 129. ISSN: 03470520. URL: <http://search.proquest.com/docview/200635713/>.
- [29] Randy A Sansone et al. “Childhood Trauma, Borderline Personality Symptomatology, and Psychophysiological and Pain Disorders in Adulthood”. eng. In: *Psychosomatics* 47.2 (2006), pp. 158–162. ISSN: 0033-3182.
- [30] Michel J. Dugas et al. “Group Cognitive-Behavioral Therapy for Generalized Anxiety Disorder: Treatment Outcome and Long-Term Follow-Up”. eng. In: *Journal of Consulting and Clinical Psychology* 71.4 (2003), pp. 821–825. ISSN: 0022-006X.

- [31] American Psychiatric Association et al. *Diagnostic and statistical manual of mental disorders (DSM-5®)*. American Psychiatric Pub, 2013.
- [32] Yaakov Bar-Shalom, X.-Rong Li, and Thiagalingam Kirubarajan. *Estimation with Applications to Tracking and Navigation: Theory, Algorithms and Software*. eng. New York, USA: John Wiley & Sons, Inc., 2002. ISBN: 9780471416555.
- [33] Karl Johan Åström and Richard M Murray. *Feedback systems : an introduction for scientists and engineers*. eng. Princeton: Princeton University Press, 2008. ISBN: 9780691135762.
- [34] Kevin L McKee and Michael C Neale. “Direct estimation of the parameters of a delayed, intermittent activation feedback model of postural sway during quiet standing”. In: *PloS one* 14.9 (2019).
- [35] Kevin McKee et al. “Emotion Regulation Dynamics Predict Substance Use in High-Risk Adolescents”. In: *Addictive Behaviors* (2020), p. 106374. ISSN: 0306-4603. DOI: <https://doi.org/10.1016/j.addbeh.2020.106374>. URL: <http://www.sciencedirect.com/science/article/pii/S0306460319312043>.
- [36] William W. S Wei. *Time series analysis : univariate and multivariate methods*. eng. 2nd ed.. doi:10.1093/oxfordhb/9780199934898.013.0022. Boston: Pearson Addison Wesley, 2006. ISBN: 0321322169.
- [37] Nancy Brandon Tuma. *Social dynamics : models and methods*. eng. Quantitative studies in social relations. Orlando: Academic Press, 1984. ISBN: 0127036709.
- [38] Kenneth A Bollen. *Structural equations with latent variables*. eng. Wiley series in probability and mathematical statistics. Applied probability and statistics. doi:10.1002/9781118619179. New York: Wiley, 1989. ISBN: 0471011711.

- [39] J. J. Mcardle and David Epstein. “Latent Growth Curves within Developmental Structural Equation Models”. eng. In: *Child Development* 58.1 (1987), pp. 110–133. ISSN: 00093920.
- [40] James P. Selig and Todd D. Little. “Discriminant analysis of principal components for face recognition”. eng. In: *Handbook of developmental research methods*. The Guilford Press, 2012. ISBN: 978-1-60623-609-3.
- [41] Arden Moscati et al. “Cross-Lagged Analysis of Interplay Between Differential Traits in Sibling Pairs: Validation and Application to Parenting Behavior and ADHD Symptomatology”. eng. In: *Behavior Genetics* 48.1 (2018), pp. 22–33. ISSN: 0001-8244.
- [42] Steven M Boker and John R Nesselroade. “A Method for Modeling the Intrinsic Dynamics of Intraindividual Variability: Recovering the Parameters of Simulated Oscillators in Multi-Wave Panel Data”. eng. In: *Multivariate Behavioral Research* 37.1 (2002), pp. 127–160. ISSN: 0027-3171. URL: http://www.tandfonline.com/doi/abs/10.1207/S15327906MBR3701_06.
- [43] Yueqin Hu et al. “Coupled Latent Differential Equation With Moderators: Simulation and Application”. eng. In: *Psychological Methods* 19.1 (2014), pp. 56–71. ISSN: 1082-989X.
- [44] Kevin L Mckee et al. “Adaptive Equilibrium Regulation: Modeling Individual Dynamics on Multiple Timescales”. eng. In: *Structural Equation Modeling: A Multidisciplinary Journal* 25.6 (2018), pp. 888–905. ISSN: 1070-5511. URL: <http://www.tandfonline.com/doi/abs/10.1080/10705511.2018.1442224>.
- [45] Kevin L Mckee, Michael D Hunter, and Michael C Neale. “A Method of Correcting Estimation Failure in Latent Differential Equations with Comparisons

- to Kalman Filtering”. eng. In: *Multivariate behavioral research* (2019), p. 1. ISSN: 0027-3171.
- [46] Rudolf E Kalman and Richard S Bucy. “New Results in Linear Filtering and Prediction Theory”. In: *Transactions of the ASME, Series D, Journal of Basic Engineering* 83 (Mar. 1961). doi:10.1115/1.3658902, pp. 95–108. DOI: 10.1115/1.3658902.
- [47] Charles K. Chui and Christopher Heil. “An Introduction to Wavelets”. eng. In: *Computers in Physics* 6.6 (1992), pp. 697–697. ISSN: 0894-1866.
- [48] Yoshiyuki Asai et al. “A Model of Postural Control in Quiet Standing: Robust Compensation of Delay-Induced Instability Using Intermittent Activation of Feedback Control (Intermittent Postural Control)”. eng. In: *PLoS ONE* 4.7 (2009). ISSN: 1932-6203.
- [49] John G Milton et al. “Microchaos in human postural balance: Sensory dead zones and sampled time-delayed feedback”. eng. In: *Physical review. E* 98.2-1 (2018). ISSN: 2470-0053.
- [50] Collins and CJ De Luca. “Random walking during quiet standing”. eng. In: *Physical review letters* 73.5 (1994). ISSN: 1079-7114.
- [51] D Lafond, M Duarte, and F Prince. “Comparison of three methods to estimate the center of mass during balance assessment”. eng. In: *Journal of Biomechanics* 37.9 (2004), pp. 1421–1426. ISSN: 0021-9290.
- [52] J. Collins and C. Luca. “Open-loop and closed-loop control of posture: A random-walk analysis of center-of-pressure trajectories”. eng. In: *Experimental Brain Research* 95.2 (1993), pp. 308–318. ISSN: 0014-4819.

- [53] Tomohisa Yamamoto et al. “Universal and individual characteristics of postural sway during quiet standing in healthy young adults”. In: *Physiological Reports* 3.3 (2015), n/a–n/a. ISSN: 2051-817X.
- [54] V M Zatsiorsky and M Duarte. “Rambling and trembling in quiet standing”. eng. In: *Motor control* 4.2 (2000). ISSN: 1087-1640.
- [55] Christoph Maurer and Robert Peterka. “A New Interpretation of Spontaneous Sway Measures Based on a Simple Model of Human Postural Control”. eng. In: *Journal of Neurophysiology* 93.1 (2005), pp. 189–200. ISSN: 0022-3077. URL: <http://search.proquest.com/docview/17532505/>.
- [56] Peter Gawthrop et al. “Intermittent control: a computational theory of human control”. eng. In: *Biological Cybernetics* 104.1 (2011), pp. 31–51. ISSN: 0340-1200.
- [57] John Milton et al. “Control at stability’s edge minimizes energetic costs: expert stick balancing”. eng. In: *Journal of the Royal Society, Interface* 13.119 (2016). ISSN: 1742-5662.
- [58] Kenjiro Michimoto et al. “Reinforcement learning for stabilizing an inverted pendulum naturally leads to intermittent feedback control as in human quiet standing.” eng. In: *Conference proceedings : ... Annual International Conference of the IEEE Engineering in Medicine and Biology Society. IEEE Engineering in Medicine and Biology Society. Annual Conference 2016* (2016), pp. 37–40. ISSN: 1557-170X. URL: <http://search.proquest.com/docview/1875403601/>.
- [59] P. J Gawthrop and L Wang. “Intermittent model predictive control”. eng. In: *Proceedings of the Institution of Mechanical Engineers, Part I: Journal of*

- Systems and Control Engineering* 221.7 (2007), pp. 1007–1018. ISSN: 0959-6518.
- [60] Peter Gawthrop et al. “Intermittent control models of human standing: similarities and differences”. eng. In: *Biological cybernetics* 108.2 (2014). ISSN: 1432-0770.
- [61] Eurich and Milton. “Noise-induced transitions in human postural sway”. eng. In: *Physical review. E, Statistical physics, plasmas, fluids, and related interdisciplinary topics* 54.6 (1996). ISSN: 1063-651X.
- [62] Alessandra Bottaro et al. “Bounded stability of the quiet standing posture: An intermittent control model”. eng. In: *Human Movement Science* 27.3 (2008), pp. 473–495. ISSN: 0167-9457.
- [63] Taishin Nomura et al. “Modeling human postural sway using an intermittent control and hemodynamic perturbations”. eng. In: *Mathematical Biosciences* 245.1 (2013), pp. 86–95. ISSN: 0025-5564.
- [64] Hongqiao Wang and Jinglai Li. “Adaptive Gaussian Process Approximation for Bayesian Inference with Expensive Likelihood Functions”. eng. In: *Neural Computation* 30.11 (2018), pp. 3072–3094. ISSN: 0899-7667.
- [65] A Tietäväinen et al. “Bayesian inference of physiologically meaningful parameters from body sway measurements”. eng. In: *Scientific reports* 7.1 (2017). ISSN: 2045-2322.
- [66] R Zachariah Aandahl et al. “Exact vs. approximate computation: reconciling different estimates of Mycobacterium tuberculosis epidemiological parameters”. eng. In: *Genetics* 196.4 (2014). ISSN: 1943-2631.

- [67] Damiana A. Dos Santos et al. “A data set with kinematic and ground reaction forces of human balance”. eng. In: *PeerJ* 5.7 (2017). ISSN: 2167-8359. URL: <https://doaj.org/article/a4e758f92c694f82a5b88cc46d08f919>.
- [68] R J Peterka. “Sensorimotor integration in human postural control.” eng. In: *Journal of neurophysiology* 88.3 (2002), pp. 1097–1118. ISSN: 0022-3077. URL: <http://search.proquest.com/docview/72053817/>.
- [69] Ian D. Loram and Martin Lakie. “Direct measurement of human ankle stiffness during quiet standing: the intrinsic mechanical stiffness is insufficient for stability”. In: *Journal of Physiology* 545.3 (2002), pp. 1041–1053. ISSN: 0022-3751.
- [70] Maura Casadio, Pietro G. Morasso, and Vittorio Sanguineti. “Direct measurement of ankle stiffness during quiet standing: implications for control modelling and clinical application”. eng. In: *Gait & Posture* 21.4 (2005), pp. 410–424. ISSN: 0966-6362.
- [71] Yao Li, W. S Levine, and G. E Loeb. “A Two-Joint Human Posture Control Model With Realistic Neural Delays”. eng. In: *IEEE Transactions on Neural Systems and Rehabilitation Engineering* 20.5 (2012), pp. 738–748. ISSN: 1534-4320.
- [72] M. Woollacott, C. Hosten, and B. Rö sblad. “Relation between muscle response onset and body segmental movements during postural perturbations in humans”. eng. In: *Experimental Brain Research* 72.3 (1988), pp. 593–604. ISSN: 0014-4819.
- [73] Kenneth V. Price, Rainer M. Storn, and Jouni A. Lampinen. *Differential Evolution - A Practical Approach to Global Optimization*. Natural Computing. ISBN 540209506. Springer-Verlag, Jan. 2006.

- [74] R Core Team. *R: A Language and Environment for Statistical Computing*. R Foundation for Statistical Computing. Vienna, Austria, 2019. URL: <https://www.R-project.org/>.
- [75] Katharine M. Mullen et al. “DEoptim: An R Package for Global Optimization by Differential Evolution”. eng. In: *Journal of Statistical Software* 40.6 (2011). ISSN: 1548-7660. URL: <https://doaj.org/article/0bce016984cf47e2ad98242c36d07294>.
- [76] Dirk Eddelbuettel and James Joseph Balamuta. “Extending extitR with extitC++: A Brief Introduction to extitRcpp”. In: *PeerJ Preprints* 5 (Aug. 2017), e3188v1. ISSN: 2167-9843. DOI: 10.7287/peerj.preprints.3188v1. URL: <https://doi.org/10.7287/peerj.preprints.3188v1>.
- [77] Dirk Eddelbuettel and Conrad Sanderson. “RcppArmadillo: Accelerating R with high-performance C++ linear algebra”. In: *Computational Statistics and Data Analysis* 71 (Mar. 2014), pp. 1054–1063. URL: <http://dx.doi.org/10.1016/j.csda.2013.02.005>.
- [78] H Akaike. “A new look at the statistical model identification”. eng. In: *IEEE Transactions on Automatic Control* 19.6 (1974), pp. 716–723. ISSN: 0018-9286.
- [79] Maciej Bosek, Bronisław Grzegorzewski, and Andrzej Kowalczyk. “Two-dimensional Langevin approach to the human stabilogram”. eng. In: *Human Movement Science* 22.6 (2004), pp. 649–660. ISSN: 0167-9457.
- [80] Maciej Bosek et al. “Degradation of postural control system as a consequence of Parkinson’s disease and ageing”. eng. In: *Neuroscience letters* 376.3 (2005). ISSN: 0304-3940.

- [81] Julia Gottschall et al. “Exploring the dynamics of balance data - movement variability in terms of drift and diffusion”. eng. In: *Physics Letters A* 373.8 (2009), pp. 811–816. ISSN: 0375-9601.
- [82] Michael Lauk et al. “Human Balance out of Equilibrium: Nonequilibrium Statistical Mechanics in Posture Control”. eng. In: *Physical Review Letters* 80.2 (1998), pp. 413–416. ISSN: 0031-9007.
- [83] Taian de Mello Martins Vieira, Liliam Fernandes de Oliveira, and Jurandir Nadal. “An overview of age-related changes in postural control during quiet standing tasks using classical and modern stabilometric descriptors”. eng. In: *Journal of Electromyography and Kinesiology* 19.6 (2009), e513–e519. ISSN: 1050-6411.
- [84] P A Hageman, J M Leibowitz, and D Blanke. “Age and gender effects on postural control measures”. eng. In: *Archives of physical medicine and rehabilitation* 76.10 (1995). ISSN: 0003-9993.
- [85] Dingding Lin et al. “Reliability of COP-based postural sway measures and age-related differences”. eng. In: *Gait & Posture* 28.2 (2008), pp. 337–342. ISSN: 0966-6362.
- [86] J J Collins et al. “Age-related changes in open-loop and closed-loop postural control mechanisms”. eng. In: *Experimental brain research* 104.3 (1995). ISSN: 0014-4819.
- [87] M Cenciarini et al. “Stiffness and Damping in Postural Control Increase With Age”. eng. In: *IEEE Transactions on Biomedical Engineering* 57.2 (2010), pp. 267–275. ISSN: 0018-9294.

- [88] Joel M. Hektner. *Experience sampling method : measuring the quality of everyday life*. eng. doi:10.4135/9781412984201. Thousand Oaks, Calif.: Sage Publications, 2007. ISBN: 1412949238.
- [89] Timothy A. Brown, Bruce F. Chorpita, and David H. Barlow. “Structural Relationships Among Dimensions of the DSM IV Anxiety and Mood Disorders and Dimensions of Negative Affect, Positive Affect, and Autonomic Arousal”. eng. In: *Journal of Abnormal Psychology* 107.2 (May 1998). doi:10.1002/eat.1050, pp. 179–192. ISSN: 0021-843X.
- [90] David Watson, Lee Anna Clark, and Greg Carey. “Positive and Negative Affectivity and Their Relation to Anxiety and Depressive Disorders”. eng. In: *Journal of Abnormal Psychology* 97.3 (1988). doi:10.1037/0021-843X.97.3.346, pp. 346–353. ISSN: 0021-843X.
- [91] David Watson. “Rethinking the Mood and Anxiety Disorders: A Quantitative Hierarchical Model for DSM-V”. eng. In: *Journal of Abnormal Psychology* 114.4 (Nov. 2005). doi:10.1037/0021-843X.114.4.522, pp. 522–536. ISSN: 0021-843X.
- [92] Eric Stice et al. “Subtyping binge eating disordered women along dieting and negative affect dimensions”. eng. In: *International Journal of Eating Disorders* 30.1 (July 2001), pp. 11–27. ISSN: 0276-3478.
- [93] Jon D. Kassel, Laura R. Stroud, and Carol A. Paronis. “Smoking, Stress, and Negative Affect: Correlation, Causation, and Context Across Stages of Smoking”. eng. In: *Psychological Bulletin* 129.2 (Mar. 2003). doi:10.1037/0033-2909.129.2.270, pp. 270–304. ISSN: 0033-2909.
- [94] Kathleen Debevec and William D. Diamond. “Social smokers: Smoking motivations, behavior, vulnerability, and responses to antismoking advertising”.

- In: *Journal of Consumer Behaviour* 11.3 (May 2012). doi:10.1002/cb.1373, pp. 207–216. ISSN: 1472-0817.
- [95] Thomas H Brandon. “Negative Affect as Motivation to Smoke”. In: *Current Directions in Psychological Science* 3.2 (Apr. 1994). doi:10.1111/1467-8721.ep10769919, pp. 33–37. ISSN: 0963-7214.
- [96] Ulrich W. Ebner-Priemer et al. “Unraveling Affective Dysregulation in Borderline Personality Disorder: A Theoretical Model and Empirical Evidence”. eng. In: *Journal of Abnormal Psychology* 124.1 (Feb. 2015). doi:10.1037/abn0000021, pp. 186–198. ISSN: 0021-843X.
- [97] Michael Eid and Ed Diener. “Intraindividual Variability in Affect: Reliability, Validity, and Personality Correlates”. eng. In: *Journal of Personality and Social Psychology* 76.4 (1999). doi:10.1037/0022-3514.76.4.662, pp. 662–676. ISSN: 0022-3514.
- [98] Peter Kuppens et al. “Individual Differences in Core Affect Variability and Their Relationship to Personality and Psychological Adjustment”. eng. In: *Emotion* 7.2 (2007). doi:10.1037/1528-3542.7.2.262, pp. 262–274. ISSN: 1528-3542.
- [99] W. Stewart Agras and Christy F. Telch. “The effects of caloric deprivation and negative affect on binge eating in obese binge-eating disordered women”. eng. In: *Behavior Therapy* 29.3 (1998). doi:10.1016/S0005-7894(98)80045-2, pp. 491–503. ISSN: 0005-7894.
- [100] E Stice et al. “Negative affect moderates the relation between dieting and binge eating”. eng. In: *The International journal of eating disorders* 27.2 (Mar. 2000). ISSN: 0276-3478.

- [101] Eric Stice, Katherine Presnell, and Diane Spangler. “Risk Factors for Binge Eating Onset in Adolescent Girls: A 2-Year Prospective Investigation”. eng. In: *Health Psychology* 21.2 (Mar. 2002), pp. 131–138. ISSN: 0278-6133.
- [102] N L Cooney et al. “Alcohol cue reactivity, negative-mood reactivity, and relapse in treated alcoholic men”. eng. In: *Journal of abnormal psychology* 106.2 (May 1997). doi:10.1037/0021-843X.106.2.243. ISSN: 0021-843X.
- [103] Katie Witkiewitz and G. Alan Marlatt. “Relapse Prevention for Alcohol and Drug Problems”. eng. In: *American Psychologist* 59.4 (May 2004), pp. 224–235. ISSN: 0003-066X.
- [104] Nisha C Gottfredson and Andrea M Hussong. “Drinking to dampen affect variability: findings from a college student sample”. eng. In: *Journal of studies on alcohol and drugs* 74.4 (2013). doi:10.15288/jsad.2013.74.576, p. 576. ISSN: 19371888.
- [105] Saul Shiffman and Andrew J. Waters. “Negative Affect and Smoking Lapses: A Prospective Analysis”. eng. In: *Journal of Consulting and Clinical Psychology* 72.2 (Apr. 2004). doi:10.1037/0022-006X.72.2.192, pp. 192–201. ISSN: 0022-006X.
- [106] Kathleen A. O’Connell and Saul Shiffman. “Negative affect smoking and smoking relapse”. In: *Journal of Substance Abuse* 1.1 (1988). doi:10.1016/S0899-3289(88)80005-1, pp. 25–33. ISSN: 0899-3289. DOI: [https://doi.org/10.1016/S0899-3289\(88\)80005-1](https://doi.org/10.1016/S0899-3289(88)80005-1). URL: <http://www.sciencedirect.com/science/article/pii/S0899328988800051>.
- [107] M Wichers et al. “Unveiling patterns of affective responses in daily life may improve outcome prediction in depression: A momentary assessment study”.

- eng. In: *Journal of Affective Disorders* 124.1 (2010), pp. 191–195. ISSN: 0165-0327.
- [108] Frenk Peeters et al. “Diurnal Mood Variation in Major Depressive Disorder”. eng. In: *Emotion* 6.3 (Aug. 2006), pp. 383–391. ISSN: 1528-3542.
- [109] J Palmier-Claus et al. “Affective variability predicts suicidal ideation in individuals at ultra-high risk of developing psychosis: An experience sampling study”. eng. In: *British Journal of Clinical Psychology* 51.1 (Mar. 2012), pp. 72–83. ISSN: 0144-6657. DOI: 10.1111/j.2044-8260.2011.02013.x. URL: <http://search.proquest.com/docview/1285088898/>.
- [110] Tom Hollenstein et al. “Sympathetic and parasympathetic responses to social stress across adolescence”. eng. In: *Developmental psychobiology* 54.2 (2012), p. 207. ISSN: 0012-1630.
- [111] Sander L Koole. “The psychology of emotion regulation: An integrative review”. eng. In: *Cognition and Emotion* 23.1 (2009), pp. 4–41. ISSN: 0269-9931. URL: <http://www.tandfonline.com/doi/abs/10.1080/02699930802619031>.
- [112] Bradley M Appelhans and Linda J Luecken. “Heart rate variability as an index of regulated emotional responding”. In: *Review of general psychology* 10.3 (2006), pp. 229–240.
- [113] June Gruber et al. “Risk for mania and positive emotional responding: too much of a good thing?” In: *Emotion* 8.1 (2008), p. 23.
- [114] Jamil Zaki and W Craig Williams. “Interpersonal emotion regulation.” In: *Emotion* 13.5 (2013), p. 803.

- [115] Brett Marroquén. “Interpersonal emotion regulation as a mechanism of social support in depression”. In: *Clinical psychology review* 31.8 (2011), pp. 1276–1290.
- [116] James J Gross. “The emerging field of emotion regulation: An integrative review”. In: *Review of general psychology* 2.3 (1998), pp. 271–299.
- [117] Zita Oravecz, Francis Tuerlinckx, and Joachim Vandekerckhove. “A Hierarchical Latent Stochastic Differential Equation Model for Affective Dynamics”. eng. In: *Psychological Methods* 16.4 (2011). doi:10.1037/a0024375, pp. 468–490. ISSN: 1082-989X.
- [118] Pascal R. Deboeck and C. S. Bergeman. “The Reservoir Model: A Differential Equation Model of Psychological Regulation”. eng. In: *Psychological Methods* 18.2 (2013). doi:10.1037/a0031603, pp. 237–256. ISSN: 1082-989X.
- [119] Timothy P Carmody. “Affect regulation, nicotine addiction, and smoking cessation”. In: *Journal of Psychoactive Drugs* 24.2 (1992), pp. 111–122.
- [120] Michael J Mason et al. “Neighborhood disorder, peer network health, and substance use among young urban adolescents”. eng. In: *Drug and Alcohol Dependence* 178 (2017). doi:10.1016/j.drugalcdep.2017.05.005, pp. 208–214. ISSN: 0376-8716.
- [121] J. A. Nelder and R. Mead. “A Simplex Method for Function Minimization”. eng. In: *The Computer Journal* 7.4 (1965). doi:10.1093/comjnl/7.4.308, pp. 308–313. ISSN: 0010-4620.
- [122] N. J. D. Nagelkerke. “A Note on a General Definition of the Coefficient of Determination”. eng. In: *Biometrika* 78.3 (1991), pp. 691–692. ISSN: 00063444.

- [123] C. E Shannon. “A mathematical theory of communication”. eng. In: *The Bell System Technical Journal* 27.4 (1948), pp. 623–656. ISSN: 0005-8580.
- [124] W. N. Venables and B. D. Ripley. *Modern Applied Statistics with S*. Fourth. ISBN 0-387-95457-0. New York: Springer, 2002. URL: <http://www.stats.ox.ac.uk/pub/MASS4>.
- [125] Michael C Neale and Lon R Cardon. *Methodology for genetic studies of twins and families*. eng. NATO ASI series. Series D, Behavioural and social sciences ; no. 67. Dordrecht ; Boston: Kluwer Academic Publishers, 2013. ISBN: 0792318749.
- [126] Kenneth Kendler et al. “A test of the equal-environment assumption in twin studies of psychiatric illness”. eng. In: *Behavior Genetics* 23.1 (1993), pp. 21–27. ISSN: 0001-8244.
- [127] Kenneth S Kendler et al. “Parental treatment and the equal environment assumption in twin studies of psychiatric illness”. In: *Psychological medicine* 24.3 (1994), pp. 579–590.
- [128] Robert Plomin, Lee Willerman, and John Loehlin. “Resemblance in appearance and the equal environments assumption in twin studies of personality traits”. eng. In: *Behavior Genetics* 6.1 (1976), pp. 43–52. ISSN: 0001-8244.
- [129] John Hettema, Michael Neale, and Kenneth Kendler. “Physical similarity and the equal-environment assumption in twin studies of psychiatric disorders”. eng. In: *Behavior Genetics* 25.4 (1995), pp. 327–335. ISSN: 0001-8244.
- [130] Kelly Klump et al. “Physical Similarity and Twin Resemblance for Eating Attitudes and Behaviors: A Test of the Equal Environments Assumption”. eng. In: *Behavior Genetics* 30.1 (2000), pp. 51–58. ISSN: 0001-8244.

- [131] Roar Efosse, Jay EJoseph, and Ken Erichardson. “A critical assessment of the equal environment assumption of the twin method for schizophrenia”. eng. In: *Frontiers in Psychiatry* 6 (2015). ISSN: 1664-0640.
- [132] Levente Littvay. “Do Heritability Estimates of Political Phenotypes Suffer From an Equal Environment Assumption Violation? Evidence From an Empirical Study”. In: *Twin Research and Human Genetics* 15.1 (2012), pp. 6–14. ISSN: 1832-4274.
- [133] Jacob Felson. “What can we learn from twin studies? A comprehensive evaluation of the equal environments assumption”. eng. In: *Social Science Research* 43 (2014), pp. 184–199. ISSN: 0049-089X.
- [134] Lindon Eaves, Debra Foley, and Judy Silberg. “Has the “equal environments” assumption been tested in twin studies?” In: *Twin Research and Human Genetics* 6.6 (2003), pp. 486–489.
- [135] Michael D Hunter. “State Space Modeling in an Open Source, Modular, Structural Equation Modeling Environment”. eng. In: *Structural Equation Modeling: A Multidisciplinary Journal* 25.2 (2018), pp. 307–324. ISSN: 1070-5511. URL: <http://www.tandfonline.com/doi/abs/10.1080/10705511.2017.1369354>.
- [136] Michael C Neale et al. “OpenMx 2.0: Extended Structural Equation and Statistical Modeling”. eng. In: *Psychometrika* 81.2 (2016), p. 535. ISSN: 00333123.
- [137] Constantino Tsallis and Daniel A. Stariolo. “Generalized simulated annealing”. eng. In: *Physica A: Statistical Mechanics and its Applications* 233.1-2 (1996), pp. 395–406. ISSN: 0378-4371.

- [138] Kelly L Klump et al. “The interactive effects of estrogen and progesterone on changes in emotional eating across the menstrual cycle.” In: *Journal of abnormal psychology* 122.1 (2013), p. 131.
- [139] S Alexandra Burt and Kelly L Klump. “The Michigan state university twin registry (MSUTR): an update”. In: *Twin Research and Human Genetics* 16.1 (2013), pp. 344–350.
- [140] Kelly L Klump and S Alexandra Burt. “The Michigan State University Twin Registry (MSUTR): Genetic, environmental and neurobiological influences on behavior across development”. In: *Twin Research and Human Genetics* 9.6 (2006), pp. 971–977.
- [141] S Alexandra Burt and Kelly L Klump. “The Michigan State University Twin Registry (MSUTR): 15 Years of Twin and Family Research”. In: *Twin Research and Human Genetics* (2019), pp. 1–5.
- [142] James Steiger, Alexander Shapiro, and Michael Browne. “On the multivariate asymptotic distribution of sequential Chi-square statistics”. eng. In: *Psychometrika* 50.3 (1985), pp. 253–263. ISSN: 0033-3123.
- [143] Conor V Dolan et al. “GE covariance through phenotype to environment transmission: an assessment in longitudinal twin data and application to childhood anxiety”. eng. In: *Behavior genetics* 44.3 (2014), p. 240. ISSN: 0001-8244.
- [144] Christopher Beam et al. “How Nonshared Environmental Factors Come to Correlate with Heredity”. In: (2020).
- [145] James A. Russell and James M. Carroll. “The Phoenix of Bipolarity: Reply to Watson and Tellegen (1999)”. eng. In: *Psychological Bulletin* 125.5 (Sept. 1999), pp. 611–617. ISSN: 0033-2909.

- [146] Susan E Embretson. “Item response theory for psychologists”. eng. In: *Multivariate applications book series* (2000).
- [147] Youngjo Lee. *Generalized linear models with random effects : unified analysis via h-likelihood*. eng. Second edition.. Monographs on statistics and applied probability (Series) ; 153. 2017. ISBN: 9781498720618.
- [148] Zita Oravecz, Francis Tuerlinckx, and Joachim Vandekerckhove. “A Hierarchical Ornstein–Uhlenbeck Model for Continuous Repeated Measurement Data”. eng. In: *Psychometrika* 74.3 (2009), pp. 395–418. ISSN: 0033-3123.
- [149] Richard McElreath. *Statistical rethinking : a Bayesian course with examples in R and Stan*. eng. Texts in statistical science. 2016. ISBN: 9781482253443.
- [150] Roxann Roberson-Nay et al. “Temporal stability of multiple response systems to 7.5% carbon dioxide challenge”. eng. In: *Biological Psychology* 124 (2017), pp. 111–118. ISSN: 0301-0511.
- [151] Rensis Likert. “A technique for the measurement of attitudes”. eng. In: *Archives of psychology* ; no. 140 (1978).
- [152] E.C Poulton. “Biases in quantitative judgements”. eng. In: *Applied Ergonomics* 13.1 (1982), pp. 31–42. ISSN: 0003-6870.
- [153] Karen E Jacowitz and Daniel Kahneman. “Measures of Anchoring in Estimation Tasks”. eng. In: *Personality and Social Psychology Bulletin* 21.11 (1995), pp. 1161–1166. ISSN: 0146-1672.
- [154] E. C Poulton. *Bias in quantifying judgements*. eng. Hove: Erlbaum, 1989. ISBN: 086377105X.
- [155] E. Christopher Poulton. “Models for biases in judging sensory magnitude”. eng. In: *Psychological Bulletin* 86.4 (1979), pp. 777–803. ISSN: 0033-2909.

- [156] K. S Kendler. “DSM disorders and their criteria: how should they interrelate?” In: 47.12 (2017), pp. 2054–2060. ISSN: 0033-2917.
- [157] David Watson and Lee Anna Clark. “Measurement and Mismeasurement of Mood: Recurrent and Emergent issues”. eng. In: *Journal of Personality Assessment* 68.2 (1997), pp. 267–296. ISSN: 0022-3891. URL: http://www.tandfonline.com/doi/abs/10.1207/s15327752jpa6802_4.
- [158] James A. Russell and James M. Carroll. “On the Bipolarity of Positive and Negative Affect”. eng. In: *Psychological Bulletin* 125.1 (1999), pp. 3–30. ISSN: 0033-2909.
- [159] Michael C Neale. *Methodology for genetic studies of twins and families*. eng. NATO ASI series. Series D, Behavioural and social sciences ; no. 67. Dordrecht ; Boston: Kluwer Academic Publishers, 1992. ISBN: 0792318749.
- [160] Kenneth S Kendler et al. “The structure of genetic and environmental risk factors for DSM-IV personality disorders: a multivariate twin study”. In: *Archives of General Psychiatry* 65.12 (2008), pp. 1438–1446.
- [161] Kristian Tambs et al. “Structure of genetic and environmental risk factors for dimensional representations of DSM-IV anxiety disorders”. In: *The British Journal of Psychiatry* 195.4 (2009), pp. 301–307.

Appendix A

AR(1) ACE HIERARCHICAL LIKELIHOOD MODEL AND SIMULATION IN OPENMX

The following R code uses package `OpenMx` to specify a hierarchical model that estimates the biometrical genetic components of the parameters of twin-pair specific state space model. The simulation is set up to generate the data for each twin while building the complete model, which is then fit using a custom compute plan.

```
PART=1 #For running multiple simulation files at once

nCores<-4
nTrials<-60

p<-1 #Number of indicators per factor
q<-2 #Number of factors (2, ie. twin 1 and 2)
t<-45 #Occasions of measurement per twin
N<-150 #Number of twin pairs

VA<- .6
VC<- .3
VE<-1-(VA+VC)

meanBeta<- .5
varBeta<- .1^2

exactSigma<-FALSE
exactTheta<-FALSE

outputFile<-paste0("sPFX_",t,"xN",N,"_part",PART, ".RDS")

library(OpenMx)
library(MASS)
library(foreach)
library(parallel)
```

```

mxOption(NULL, 'Number of Threads', parallel::detectCores()) #now

cl<-makeCluster(nCores)
library(doSNOW)
registerDoSNOW(cl)
clusterEvalQ(cl, library(OpenMx))

#Make sure random data from OpenMx is not too exact by taking a center
  portion
genDat<-function(model, exact=F){
  if(exact)return(mxGenerateData(model))
  nObs<-model$data$numObs
  sInd<-sample(1:(nObs*3-nObs), 1)
  randDat<-mxGenerateData(model, nrows=nObs*3)[sInd:(sInd+nObs-1),]
  return(randDat)
}

# Build model -----
varnames <- c(paste0("T1y",1:p),paste0("T2y",1:p))
latentnames<-paste0("x",1:q)

Amat<-matrix(c(.7,0,0,.7),2,2)
cLab<-rbind(cbind(paste0("C1_", 1:p),NA), cbind(NA, paste0("C1_", 1:p)))
rLab<-rep(paste0("r",1:p),2)
qLab<-c("q11","q12","q11")

ssModel <- list(
  mxMatrix("Full", q, q, free=c(T,F,F,T), Amat, labels=c(paste0("a",row(
    Amat),col(Amat))), name="A"),
  mxMatrix("Zero", q, 1, name="B"),
  mxMatrix("Full", 2*p, q, free=F, values=diag(q), labels=cLab, name="C",
    dimnames=list(varnames, latentnames )),
  mxMatrix("Zero", 2*p, 1, name="D"),
  mxMatrix("Symm", q, q, free=c(T,F,T), values=c(1,0,1), name="Q", lbound=c
    (1e-8,-.95,1e-8), ubound=c(NA,.95,NA)),
  mxMatrix("Diag", 2*p, 2*p, FALSE, 0.00, labels=rLab, name="R", lbound=1e
    -8),
  mxMatrix("Full", q, 1, FALSE, labels="x",values=c(0,0), name="x0"),
  mxMatrix("Diag", q, q, FALSE, 1, labels="px", name="P0", lbound=1e-8),
  mxMatrix("Zero", 1, 1, name="u"),

  mxData(observed=matrix(NA, t, p), type="raw"),#fewer rows = fast
  mxExpectationStateSpace("A", "B", "C", "D", "Q", "R", "x0", "P0", "u"),
  mxFitFunctionML()
)

```

```

###START ITERATIONS
output<-NULL
for(trial in 1:nTrials){

  # Simulate data
  -----

  rBeta<-matrix(c(
    VA+VC+VE, VA+VC, 0, 0,
    VA+VC, VA+VC+VE, 0, 0,
    0, 0, VA+VC+VE, .5*VA+VC,
    0, 0, .5*VA+VC, VA+VC+VE
  ),4,4,byrow=T)

  betas<-mvrnorm(N, mu=rep(meanBeta, 2*q), Sigma = rBeta*varBeta, empirical
    =exactSigma)

  clusterExport(cl, c("ssModel","betas", "genDat"))

  # Create MZ models and data
  -----

  MZ.models<-foreach(i = 1:N, .inorder=T)%dopar%{
    current.MZ<-mxModel(name=paste0("MZ",i,"ssm"), ssModel)
    current.MZ<-omxSetParameters(current.MZ, labels=c("a11","a22"), values=
      betas[i,1:2], newlabels=paste0("MZb",1:2,"_",i) )
    MZsimdat<-genDat(current.MZ, exact=exactTheta)
    current.MZ<-mxModel(current.MZ, mxData(MZsimdat, type="raw"),
      mxAlgebra( log(det(modelACE.bCovExpMZ)) + 2*log(2*pi)
        + (cbind(A[1,1],A[2,2])-mean_beta)%*%solve(
          modelACE.bCovExpMZ)%*%t(cbind(A[1,1],A[2,2])-
            mean_beta), name="ACEm2LL" ))
    diag(current.MZ$A$values)<-.2
    current.MZ.shell<-mxModel(name=paste0("MZ",i), list(current.MZ),
      mxMatrix("Full",1,1,values=t,name="t"),
      mxAlgebraFromString(paste0("MZ",i,"ssm.ACEm2LL +
        MZ",i,"ssm.fitfunction"), name="ffc"),
      mxFitFunctionAlgebra("ffc"))
    return(current.MZ.shell)
  }

  # Create DZ models and data
  -----

  DZ.models<-foreach(i = 1:N, .inorder=T)%dopar%{

```

```

current.DZ<-mxModel(name=paste0("DZ",i,"ssm"), ssModel)
current.DZ<-omxSetParameters(current.DZ, labels=c("a11","a22"), values=
  betas[i,3:4], newlabels=paste0("DZb",1:2,"_",i) )
DZsimdat<-genDat(current.DZ, exact=exactTheta)
current.DZ<-mxModel(current.DZ, mxData(DZsimdat, type="raw"),
  mxAlgebra( log(det(modelACE.bCovExpDZ)) + 2*log(2*pi)
    + (cbind(A[1,1],A[2,2])-mean_beta)%*%solve(
      modelACE.bCovExpDZ)%*%t(cbind(A[1,1],A[2,2])-
        mean_beta), name="ACEm2LL" ))
diag(current.DZ$A$values)<- .2
current.DZ.shell<-mxModel(name=paste0("DZ",i), list(current.DZ),
  mxMatrix("Full",1,1,values=t,name="t"),
  mxAlgebraFromString(paste0("DZ",i,"ssm.ACEm2LL +
    DZ",i,"ssm.fitfunction"), name="ffc"),
  mxFitFunctionAlgebra("ffc"))
return(current.DZ.shell)
}

```

```

names(MZ.models)<-unlist(lapply(MZ.models, function(x) x$name))
names(DZ.models)<-unlist(lapply(DZ.models, function(x) x$name))

```

```

pairModels<-list("MZ"=MZ.models, "DZ"=DZ.models)
pairNames<-c(names(pairModels$MZ),names(pairModels$DZ))

```

```

# Set up compute sequence and ACE model
-----

```

```

bigSeq<-list()
for(h in pairNames){
  bigSeq<-c(bigSeq, mxComputeGradientDescent(fitfunction=paste0(h,".
    fitfunction"), freeSet = c(paste0(h,"ssm.A"),paste0(h,"ssm.Q"))) )
}

```

```

mgSSM<-mxModel("modelACE", pairModels[["MZ"]], pairModels[["DZ"]],

```

```

  #ACE expected covariance:

```

```

  mxMatrix("Full",nrow=1,ncol=3, labels=c("VA", "VC", "VE"),
    values=c(.01, .01, .1), free=T, lbound=1e-8, name="ACE")

```

```

  ,
  mxMatrix("Full",1,6, labels=c("VUMZ1","VUDZ1","VUMZ2","VUDZ2",
    "CUMZ", "CUDZ"), values=0,free=F, name="rfxSE"),

```

```

  mxAlgebra( rbind(
    cbind(VA+VC+VE+VUMZ1,          VA+VC+CUMZ ),

```

```

        cbind(VA+VC+CUMZ,          VA+VC+VE+VUMZ2)
    ), name="bCovExpMZ"),

    mxAlgebra( rbind(
        cbind( VA+VC+VE+VUDZ1,      .5*VA+VC+CUZ),
        cbind( .5*VA+VC+CUZ,        VA+VC+VE+VUDZ2)
    ), name="bCovExpDZ"),

    #Observed covariance:
    mxMatrix("Full", 1, 1, values=.5, free=T, labels="mean_beta
    ", name="meanMatExp"),
    mxFitFunctionMultigroup(pairNames),
    mxComputeIterate(
        steps=list(mxComputeSequence(c(bigSeq,
                                        mxComputeGradientDescent(
                                            freeSet=c("ACE", "
                                            meanMatExp") ))))
        ,maxIter = 3) ###SET OPTIMIZATION RESTRICTIONS HERE

    )

mgSSM<-mxRun(mgSSM)
ests<-coef(mgSSM)[c("VA", "VC", "VE")]/sum(coef(mgSSM)[c("VA", "VC", "VE")])

cat("Runtime:",mgSSM$output$cpuTime[[1]]/60, "minutes\n")
print(ests)

output<-rbind(output, ests)
saveRDS(output, outputFile)
}

```

Appendix B

AR(1) ACE BAYESIAN HIERARCHICAL MODEL IN STAN

The following model may be loaded with R package `rstan` to fit an ACE model to the parameter of simple AR(1) processes in simulated twin pairs.

```
data {
  int<lower=0> N;           // num individuals
  int<lower=0> T;           // num individuals
  matrix[T, N] MZ1;       // MZ Twin 1 series
  matrix[T, N] MZ2;       // MZ Twin 2 series
  matrix[T, N] DZ1;       // DZ Twin 1 series
  matrix[T, N] DZ2;       // DZ Twin 2 series
}
parameters {
  vector<lower = -1, upper = 1>[2] betaMZ[N];
  vector<lower = -1, upper = 1>[2] betaDZ[N];

  real <lower=-1, upper=1> betaMu;
  real <lower=0, upper=1> q;

  real<lower=0, upper=1> a;
  real<lower=0, upper=1> c;
  real<lower=0, upper=1> e;
}
model {
  matrix[2,2] SigMZ;
  matrix[2,2] SigDZ;
  vector[2] betaMuVec = rep_vector(betaMu, 2);
  vector[T*N*4] err;
  real nu;
  int u = 0;

  SigMZ[1,1] = a^2+c^2+e^2;
  SigMZ[2,2] = a^2+c^2+e^2;
  SigMZ[1,2] = a^2+c^2;
  SigMZ[2,1] = a^2+c^2;
}
```

```

SigDZ[1,1] = a^2+c^2+e^2;
SigDZ[2,2] = a^2+c^2+e^2;
SigDZ[1,2] = .5*a^2+c^2;
SigDZ[2,1] = .5*a^2+c^2;

for(i in 1:N){
    nu = 0;
    u+=1;
    err[u] = MZ1[1,i] - nu; //needs to be
    for (t in 2:T) {
        u+=1;
        nu = betaMZ[i,1] * MZ1[t-1,i];
        err[u] = MZ1[t,i] - nu;
    }
    u+=1;
    nu = 0;
    err[u] = MZ2[1,i] - nu;
    for (t in 2:T) {
        u+=1;
        nu = betaMZ[i,2] * MZ2[t-1,i];
        err[u] = MZ2[t,i] - nu;
    }
    u+=1;
    nu = 0;
    err[u] = DZ1[1,i] - nu;
    for (t in 2:T) {
        u+=1;
        nu = betaDZ[i,1] * DZ1[t-1,i];
        err[u] = DZ1[t,i] - nu;
    }
    u+=1;
    nu = 0;
    err[u] = DZ2[1,i] - nu;
    for (t in 2:T) {
        u+=1;
        nu = betaDZ[i,2] * DZ2[t-1,i];
        err[u] = DZ2[t,i] - nu;
    }
}

err ~ normal(0,q);
betaMZ ~ multi_normal(betaMuVec, SigMZ);
betaDZ ~ multi_normal(betaMuVec, SigDZ);

```



```
betaMu ~ normal(.1,.3);  
q ~ normal(.5, 1) T[0, ];  
}
```

Appendix C

SIMULATION SCRIPT FOR BAYESIAN AR(1) ACE MODEL

The following code simulates AR(1) data in twin pairs and uses R package `rstan` to fit the model specified in Appendix B.

```
library(rstan)
library(MASS)

#Rapidly generate random AR1 processes using convolution
rAR<-function(N, b, q){
  f<-exp(log(b)*1:N)
  g<-rnorm(N,0,q)
  return(convolve(f,g))
}

#Set up hierarchical AR parameters
pars<-list(
  "q" = 0.75,
  "a"=.6,
  "c"=.3,
  "e"=.1,
  "bMu"=.5,
  "bSig"= .1
)

#Sample dimensions
N<-150
TT <- 45

nTrial<-60
output<-NULL
for(i in 1:nTrial){

  z<-with(pars,{
    Sig.MZ<-matrix(c(a+c+e,a+c,a+c,a+c+e),2,2)
    Sig.DZ<-matrix(c(a+c+e,.5*a+c,.5*a+c,a+c+e),2,2)
    betas.MZ<-mvrnorm(N, rep(bMu,2), Sig.MZ*bSig^2, empirical=F)
    betas.DZ<-mvrnorm(N, rep(bMu,2), Sig.DZ*bSig^2, empirical=F)
```

```

t1mz<-vapply(betas.MZ[,1], function(x) rAR(TT, x, q), rep(0,TT))
t2mz<-vapply(betas.MZ[,2], function(x) rAR(TT, x, q), rep(0,TT))
t1dz<-vapply(betas.DZ[,1], function(x) rAR(TT, x, q), rep(0,TT))
t2dz<-vapply(betas.DZ[,2], function(x) rAR(TT, x, q), rep(0,TT))

betas.est<-
  cbind(apply(t1mz, 2, function(x)ar(x,order.max=1,aic=F)$ar),
        apply(t2mz, 2, function(x)ar(x,order.max=1,aic=F)$ar),
        apply(t1dz, 2, function(x)ar(x,order.max=1,aic=F)$ar),
        apply(t2dz, 2, function(x)ar(x,order.max=1,aic=F)$ar))

  return(list("MZ1"=t1mz,"MZ2"=t2mz,"DZ1"=t1dz, "DZ2"=t2dz))
})

dat<-c(list("N"=N, "T"=TT), z)

fit <- stan(file = "ar_ACE.stan",
  data = dat,
  warmup = 200,
  iter = 500,
  chains = 1,
  cores = 1,
  thin = 2,
  init=.3,
  control=list("adapt_delta"=.95, "max_treedepth"=10))

res<-extract(fit)
res.mu<- unlist(lapply(res, function(x) mean(x^2) ))
ACE<-res.mu[c("a","c","e")]
print(rbind("Raw"=ACE, "Std"=ACE/sum(ACE)))
print(nrow(output))

output<-rbind(output, ACE/sum(ACE))
}

```

VITA

Kevin McKee

EDUCATION

Virginia Commonwealth University, *2008 - 2012*

Department of Psychology

B.S., Psychology

PEER-REVIEWED PUBLICATIONS

- **McKee, K. L.**, Klump, K., Burt, A., & Neale, M. C. (2020). Results and Considerations for Dynamical Phenotypes from Experience Sampling of Twin Pairs (in review)
- **McKee, K. L.**, Russell, M., Mennis, J., Mason, M., & Neale, M. C. (2020). Emotion Regulation Dynamics Predict Substance Use in High-Risk Adolescents. Addictive Behaviors
- **McKee, K. L.**, & Neale, M. C. (2019). Direct estimation of the parameters of a delayed, intermittent activation feedback model of postural sway during quiet standing. PloS one, 14(9), e0222664.
- **McKee, K. L.**, Hunter, M. D., & Neale, M. C. (2019). A Method of Correcting Estimation Failure in Latent Differential Equations with Comparisons to Kalman Filtering. Multivariate behavioral research, 1-20.
- **McKee, K. L.**, Rappaport, L. M., Boker, S. M., Moskowitz, D. S., & Neale, M. C. (2018). Adaptive Equilibrium Regulation: Modeling Individual Dynamics

on Multiple Timescales. *Structural Equation Modeling: A Multidisciplinary Journal*, 1-18.

- Moscati, A., Verhulst, B., **McKee, K. L.**, Silberg, J., & Eaves, L. (2018). Cross-Lagged Analysis of Interplay Between Differential Traits in Sibling Pairs: Validation and Application to Parenting Behavior and ADHD Symptomatology. *Behavior genetics*, 48(1), 22-33.

CONFERENCE PRESENTATIONS

- **McKee, K.L.**, Boker, S.M., Neale, M.C., Adaptive Equilibrium Regulation: Modeling Individual Dynamics on Multiple Time Scales. Richmond, Virginia, Advanced Statistical Epidemiology Workshop, October 23 - 27, 2017. Presented as a talk.
- **McKee, K.L.**, Neale, M.C., Boker, S. M., Modeling Psychological Dynamics with Random Events. Oslo, Norway, Behavioral Genetics Association, June 28-July 3, 2017. Presented as a poster.
- Hillhouse TM, **McKee KL**, Joseph BL, Spindle TR, Steele FF, Negus SS, Porter JH. (2013) Differentiating the antidepressant and abuse-related effects of the N-Methyl-D-aspartate non-competitive antagonists ketamine and MK-801. Presented at 25th Annual Symp. Central Virginia Chapter of the Society for Neuroscience, Roanoke, VA, March 2013. Presented as a poster.
- Hillhouse TM, **McKee KL**, Joseph BL, Spindle TR, Porter JH. (2012) Ketamine, but not MK-801, produces antidepressant-like effects in rats responding on differential-reinforcement-of-low-rate (DRL) 72 second operant schedule.

24th Ann. Symp. Central Virginia Chapter of the Society for Neuroscience ,
Richmond, VA, December 2012. Presented as a poster.

ACKNOWLEDGEMENTS

- Hillhouse, Todd M; Porter, Joseph H (2014) Ketamine, but not MK-801, produces antidepressant-like effects in rats responding on differential-reinforcement-of-low-rate (DRL) 72 second operant schedule. *Behavioral Pharmacology*, Vol. 25(1) 80-91. (For assistance with data collection)
- Hillhouse, Todd M; Porter, Joseph H (2015) A Brief History of Antidepressants: From Monoamines to Glutamate. *Experimental and Clinical Psychopharmacology*, Vol. 23(1) 1-21. (For graphics and illustration)
- Meredith, M. A., Clemo, H. R., Corley, S. B., Chabot, N., & Lomber, S. G. (2016). Cortical and thalamic connectivity of the auditory anterior ectosylvian cortex of early-deaf cats: Implications for neural mechanisms of crossmodal plasticity. *Hearing research*, 333, 25-36. (For static and animated illustrations)